Fall 2007

Terahertz data processing for standoff detection of improvised explosive devices

Amit Bipin Shah

Follow this and additional works at: https://scholarsmine.mst.edu/masters_theses

Part of the Computer Engineering Commons

Department:

Recommended Citation

TERAHERTZ DATA PROCESSING FOR STANDOFF

DETECTION OF

IMPROVISED EXPLOSIVE DEVICES

by

AMIT BIPIN SHAH

A THESIS

Presented to the Faculty of the Graduate School of the

UNIVERSITY OF MISSOURI-ROLLA

In Partial Fulfillment of the Requirements for the Degree

MASTER OF SCIENCE IN COMPUTER ENGINEERING

2007

Approved by

_____   _____
Dr. Vittal Rao, Co-advisor   Dr. Jagannathan Sarangapani, Co-advisor

_____
Dr. Scott Smith

ABSTRACT

Improvised Explosive Devices (IEDs) are homemade, non-conventional explosive devices, which are used to destruct and incapacitate individuals and property. IEDs are becoming a popular weapon of attack among terrorists and insurgents due to their easy of making and capability to cause major damage. Hence, is has become necessary to develop efficient systems for detecting and disarming these devices. The Terahertz technology which uses electromagnetic radiations between 0.3 THz to 10 THz for imaging is one of the most recently developed detection techniques and is ideally suitable for detection of IEDs and similar devices.

Although a lot of work has been done for developing a standoff detection system for detecting IEDs using terahertz imaging, it is still needed to develop advanced techniques for processing of the THz data. In this thesis, efficient signal processing techniques are developed for standoff, real time and wide area detection of IEDs. The signal processing algorithm is a two stage algorithm where the first stage is a preprocessing stage. In this stage, THz data from a large field is given to the correlation filters which detect hotspots in the field where an IED could be present. This stage avoids the computational burden of processing data from the entire field in the second stage. In the second stage, THz data from the hotspots of stage one are unmixed to find the individual explosive materials in each data point/pixel. The unmixing is done using a variant of the Independent Component Analysis algorithm which separates only the required component. Once the components are separated, they are analyzed to see if any of them matches an explosive. Thus, the presence of an IED or explosive can be accurately determined within the field.

ACKNOWLEDGMENTS

I would like to thank my advisor Dr. Vittal Rao for his guidance, support and encouragement throughout the course of my research and graduate study. I would also, like to thank him for having patience with me and understanding my problems from time to time. I would like to express my gratitude to Dr. Jagannathan Sarangapani for his support and assistance. Finally, I would like to thank Dr. Scott Smith for agreeing to serve on my committee.

I wish to thank my parents Bipin Shah and Sandhya Shah, who have always stood by me, and my dear friend Vasudha, who has put up with me through everything. Finally, I thank my friends Shubhika, Pravin and Gerard for their constant encouragement and help.

TABLE OF CONTENTS

LIST OF ILLUSTRATIONS

LIST OF TABLES

1: INTRODUCTION

Improvised Explosive Devices (IEDs) have become a popular weapon of destruction for terrorists and insurgents. What makes these devices so popular is their simplicity of design and deployment, ability to remotely detonate it with some remote control device and above all their ability to cause major damage. As a result, IEDs have been responsible for numerous civilian and army deaths in the recent past. Hence, an efficient system for standoff and wide-area detection and diffusing the threat must be developed. Present day systems include ground penetrating radars, IR imaging, millimeter wave imaging, X-ray imaging, etc. These systems do not have a standoff capability and require the inspection team to go very near to the threat which can be fatal. Also, these systems have significant false negatives and require large amount of time for processing the data and detecting the threat.

Terahertz (THz) technique is a fairly new imaging technique and is an excellent candidate for developing an efficient IED detection system. Terahertz waves can penetrate materials like cloth, paper, etc which are generally used to hide explosives. Also, these waves are non-ionizing and produce a characteristic signature for most of the materials including commonly used explosives. In this thesis, efficient signal processing techniques are proposed for standoff and wide area surveillance of IEDs using terahertz technology. The spectra from a THz imaging system are used as inputs to the signal processing algorithms where they are processed to detect the presence of any explosive spectra. These algorithms are designed for fast and accurate detection at a standoff range and for surveillance of a large area. A brief introduction to IEDs and the terahertz technology is given below.

1.1 IMPROVISED EXPLOSIVE DEVICES

Improvised Explosive Devices (IEDs) are homemade, non-conventional explosive devices, which are used to destruct and incapacitate individuals and property. IEDs are made with commercial or military explosives like Trinitrotoluene (TNT), dynamite, HMTD (Hexamethylenetriperoxidediamine), TATP (Triacetonetriperoxide), Ammonium nitrate and Cyclotrimethylenetrinitramine (RDX). An important property of an IED

which separate it from landmines is its capacity of remote detonation. IEDs are detonated by using a simple triggering mechanism which may include a cell phone, a garage door opener, or a radio-controlled toy, or may be as simple as running over a rubber hose to produce enough air pressure to activate a detonating switch. IEDs are becoming very popular among terrorists and insurgents due to their ease of making and capacity to induce maximum damage. Between October 2001 and August 2005, IEDs have been responsible for more than 2,000 combat deaths in Iraq, and 178 combat deaths in Afghanistan [3]. There are no specialized techniques for detection of IEDs. The only available techniques are traditional techniques like X-Ray imaging, Infrared imaging, chemical mapping, biosensors, millimeter wave imaging, etc. None of these techniques have a low false negative and false positive rate for detection of a threat from a standoff distance. For standoff detection of IEDs it is required to utilize several technologies. In addition to detecting the explosives in an IED, the RF radiations from the electronic circuitry in an IED should be explored for minimizing the false negatives in the detection system.

1.2 DETECTION OF IEDs USING TERAHERTZ TECHNOLOGY

Terahertz (THz) radiation encompasses electromagnetic radiation that falls within an approximate frequency range of 0.3 THz to 10 THz (Figure 1.1). This corresponds to wavelengths between 1mm (at 0.3 THz) and 30 μ m (at 10 THz).
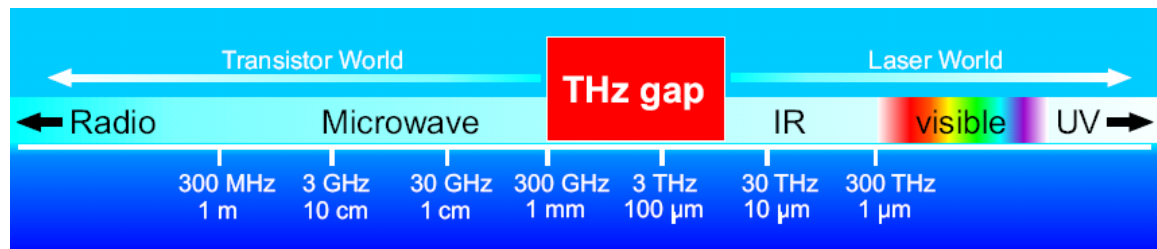
Figure 2.1 The THz gap in the electromagnetic spectrum [15]

In the electromagnetic spectrum, the THz regime is sandwiched between microwaves at lower frequencies and infrared light at higher frequencies as shown in Figure 1.1. Due to the difficulty of producing strong and dependable sources and efficient detectors in this exotic band of radiation, the THz regime has for many decades been the last part of the electromagnetic spectrum which has not been intensely used for research and technological applications. It is, therefore, referred to as the THz gap.

However, due to recent advances in the generation and detection of T-rays, THz radiation has increasingly gained importance. One of the key features of THz radiation is its spectral distinctiveness. Typical photon energies of THz radiation are on the order of a few meV. Since many molecules exhibit activation energies for vibrations and rotations which are also on the order of a few meV, these molecules feature a specific spectroscopic fingerprint in this frequency region thus making chemical recognition possible [1]. Furthermore, THz radiation penetrates many materials, which are impervious to visible light, such as paper, textiles and various plastics. With its low photon energy, THz radiation is considered to be non-ionising and is therefore suited for nondestructive, noninvasive inspection of materials for security applications.

Thus, the THz technology is an excellent candidate for developing an efficient IED detection system. Several efforts have been made for developing THz imaging systems that assist in the standoff and real time detection of explosive threats. Most of the research efforts have been in the development of efficient transmitters and detectors for terahertz radiations and capturing the THz images. However, the analysis of the THz spectra received by the THz detectors has not been fully developed in the literature. There is a lot of potential to develop signal processing algorithms for efficient detection of IEDs. In this thesis efficient signal processing techniques are developed for detection of IEDs and similar threats. The signal processing techniques aim at developing a system with low probability of error for standoff detection of IEDs with a real time processing capability to reduce the detection time.

The thesis is organized as follows. Section 2 provides a literature review of the existing IED problem and developments made in generation and detection of THz waves. It also reviews various terahertz imaging modalities. Section 3 discusses the development in THz technology for standoff detection of IEDs. It covers the various issues related to

standoff detection and techniques that aid in standoff detection. Section 4 details the proposed signal processing techniques that have been developed during the course of this research and thesis. A two stage processing technique is proposed which aims at real time detection by reducing the computational burden without compromising accuracy in the first stage and accurate detection of the location of an IED or similar threat in the second stage. In Section 5 and Section 6 provide simulations of the proposed signal processing techniques. In Section 5 simulations of the algorithm are performed using THz data of explosives and in Section 6 using mineral data. Finally, the conclusions and suggestions for future work are mentioned in the Section 7. The appendix A provides theory of optimization and appendix B provides the MATLAB codes used for the developed signal processing algorithms.

2: LITERATURE REVIEW

2.1 IMPROVISED EXPLOSIVE DEVICES (IEDs)

Explosives in the hands of terrorists continue to pose a significant threat. "According to the FBI Bomb Data Center, approximately 70% of all terrorist incidents involve the use of explosives and incendiary agents" [2]. During the past decade, the world has witnessed an increase in the use of Improvised Explosive Devices. Between October 2001 and August 2005, Improvised Explosive Devices (IEDs or roadside bombs) have been responsible for more than 2,000 combat deaths in Iraq, and 178 combat deaths in Afghanistan [3]. Improvised Explosive Devices (Figure 2.1) are homemade, non-conventional explosive devices, which are used to destruct and incapacitate individuals or property. IEDs are hidden beneath soil and vegetation, under roadside debris, or inside animal carcasses, and encounters with these bombs are becoming more numerous and deadly in both Iraq and Afghanistan. The threat includes vehicle-borne IEDs, in which extremists drive cars laden with explosives directly into a target. IEDs can utilize commercial or military explosives, and often are constructed in a home using materials at hand [4]. Triggering methods include using a cell phone, a garage door opener, or a child's radio-controlled toy, or may be as simple as running over a rubber hose to produce enough air pressure to activate a detonating switch.
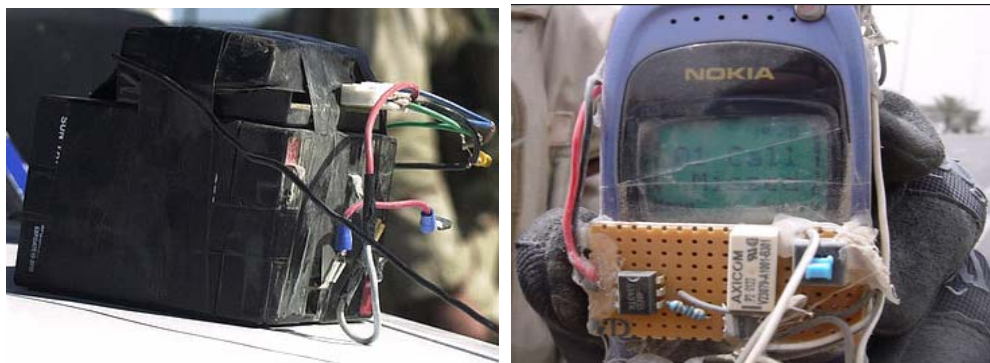
Figure 2.1: Pictures of IED found in Iraq that failed to detonate [5]

IEDs generally consist of five components viz power source, initiator, explosive, shrapnel and a switch.

- Power sources: Majority of IEDs contains an electronic initiator and require a power source. Batteries (a common power source) are manufactured in numerous shapes and sizes. In some cases, they can be cut and shaped to make detection more difficult. Most commercially available batteries can reliably cause an initiator to function. Mechanical action, such as a spring under pressure, can store sufficient energy to cause the functioning of a non-electric initiator.

- Initiators: They are blasting caps or flame-producing components like fuse igniters for a length of time fuse. Improvised initiators causing low explosives or highly sensitive explosives to detonate can easily be made. Examples of improvised initiators include a modified flash bulb, a percussion primer, or even improvised hobby fuses that impart flame much as time fuse, only at an uncontrolled burn rate. Initiators can also be improvised for high explosives e.g. using Triacetone triperoxide (TATP) formulation to make an improvised initiators.

- Explosives: Commonly used explosives in IEDs are TNT, C4, dynamite, HMTD (Hexamethylenetriperoxidediamine), TATP (Triacetonetriperoxide), Ammonium nitrate and RDX.

- Switches: They are incorporated into a device as either an arming switch or a fuse. They can be simple or complex in nature. More than one switch can be used to create redundancy in the system. Many IED will incorporate both an arming switch and a fusing switch. The arming switch is a safety for the IED and works by disarming (electrically disengaging) the fusing switch. When the arming switch is armed the fusing switch becomes functional, however, the circuit is still closed. When the fusing switch is activated, the circuit becomes open and will connect battery power to the initiator (blasting cap) and detonation will occur. Switches are almost unlimited in design and constructed in such a way that any approach or action by its intended target or a first responder will result in detonation. Switches specifically for IEDs can take on any form and can appear quite innocent looking completely fitting into the environment.

- Fragmentation and shrapnel: They are a part of the IED, wherein materials are added to the device for inflicting maximum casualties. Examples include ball bearings and nails

2.2 TERAHERTZ TECHNOLOGIES

The terahertz frequency band, spanning from roughly 0.1 Thz through 10 THz, is often sited as the most scientifically rich, yet unexplored region of the electromagnetic spectrum. In the past, terahertz spectroscopy has been hindered by the low brightness of incoherent far-infrared sources and poor sensitivity of bolometric detectors. With an exception of free electron lasers that use relativistic electrons and are capable of reaching kilowatt level terahertz power [6], other THz sources generate milliwatt or microwatt power levels. The photon energy at a frequency of 1 THz is approximately 4 meV, compared to the thermal energy of 26 meV at room temperature. This clearly shows the difficulty of designing THz lasers relying on optical transitions and operating at room temperature. Also, acquisition of THz waveforms required lock-in detection and low-pass filtering with a 100–300-ms time constant per data point. With resulting acquisition times of a few minutes for a single THz waveform at each image point, imaging with THz transients has so far been impractical. However, because of many recent developments and applications in imaging, medicine, biology, space exploration, covert communications, compact radar ranges, industrial controls, terahertz microscopy, terahertz tomography, and homeland security there has been considerable research going on in the field of Terahertz technology. This has led to the development of efficient terahertz transmitters and detectors. This section provides an overview of various terahertz transmitters and detectors with their advantages and disadvantages.

2.2.1 Generation of THz Pulses. Several techniques exist to create radiation in the far-infrared region of the spectrum, each with its own advantages and disadvantages. Common to all these methods is an ultrafast change in polarization triggered by a femtosecond laser pulse. A femtosecond laser pulse is used as an excitation pulse that upon passing through the generation medium changes its polarization and creates an electromagnetic pulse whose electric field is related to the intensity envelope of the exciting pulse. The THz pulse generated contains just a few cycles of the electric field.

One approach is to get a fast polarization change by using nonlinear optical effects in crystals (optical rectification). A wide range of materials has been investigated for this purpose. The most widely used material is zinc telluride (ZnTe) at (100) orientation which has excellent phase matching properties [1]. Different methods for THz generation are, synchrotron radiation from a storage ring [7], free-electron lasers [8], light sources used in FIR Fourier transform spectroscopy [9], gas lasers (the most prominent being the CO2 laser [10]), quantum cascade lasers [11] and ultrafast modelocked optical lasers used either with second order non-linear optical materials [12] or with photoconductive switches made of semiconductors [13]. Two main THz generation methods viz generation by photoconductive antennas and by optical rectification are discussed below.

> **Generation by Photoconductive Antennas:** This technique was introduced by Auston [13] and is referred to as Auston-switch (Figure 2.2). Two parallel metal lines, which are usually separated by 20 - 50 μm, are deposited on a semiconductor material.
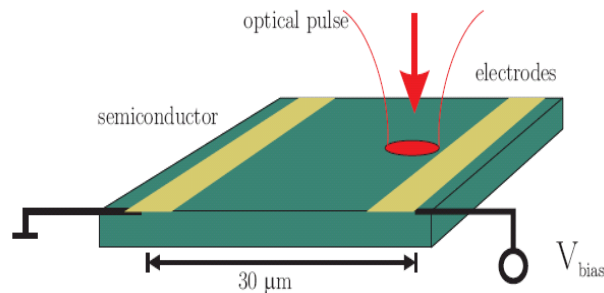
Figure 2.2 The Auston 0073witch [13]

---

[1] In this case, the term "phase matching" refers to the propagation of radiation at optical and THz frequencies in the material. The generation process requires the co-propagation of the optical and THz signals through the crystal i.e. matching of the group refractive index of the optical pulse with the phase refractive index of the THz signal.

These electrodes are biased with a voltage on the order of 10-50 V. Above bandgap laser pulses, usually from femtosecond lasers with pulse lengths under 100 fs, are focused in between the metal lines creating electron-hole pairs. These charge carriers are accelerated by the bias field resulting in production of pulses in the terahertz frequency range.

➢ **Generation by Optical Rectification:** This generation method is capable of producing a THz pulse whose spectrum peaks in the THz region and can contain useful power upto 70 THz [14]. The THz pulse is generated through optical rectification in a crystal of $\langle 110 \rangle$ ZnTe. Optical rectification is a difference frequency mixing and occurs in media with large second order susceptibility, $\chi^{(2)}$. That is, a polarization is induced in the crystal that is the *difference* of the individual frequencies instead of their sum. Thus, light of a given frequency passing through a nonlinear medium will generate the same amount of both sum and difference frequencies, corresponding to second harmonic and dc. For ultrashort laser pulses that have large bandwidth the frequency components are differenced with each other to produce bandwidth from 0 to several THz (Figure 2.3).
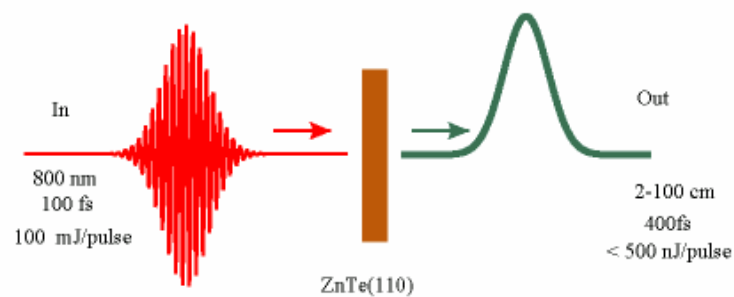
Figure 2.3 Generated THz pulse

2.2.2 Detection of THz Pulses. Two methods for detection of THz pulses are widely used, the photoconductive detection and the electro-optic detection. A brief description of these methods is given below.

➤ **Photoconductive Detection:** The principle of the photoconductive method is very similar to the generation of Terahertz by photoconductive effect discussed in Section 2.2.1. The fs-laser generates carriers in a semiconductor like GaAs. If the THz pulse arrives during the lifetime of the carriers they are accelerated towards the electrodes. This produces a measurable average current of the order of several hundred pico-amperes up to tens of nano-amperes. The current is measured at the detector with a lock-in amplifier.

➤ **Detection by Electro-Optic Sampling:** Until 1995, either photoconductive antennas or helium cooled bolometers were usually used to detect THz pulses. Important phase information is lost with the bolometers limiting their application and the superior photoconductive (PC) antennas were limited due to their carrier lifetime and resonant behavior. The first demonstration of free-space Electro-Optic Sampling (EOS) was performed in 1995 by Wu and Zhang [15]. The electro-optic sampling works on the principle of Pockels effect. The THz pulse propagates through free space towards the electro-optic sampling crystal. A gate or probe pulse is made collinear with the THz pulse after being sent through a variable delay line. This allows scanning of the gate beam to sample different parts of the terahertz field. The electric field of the THz pulse will change the refractive index along one axis of the Electro-optic-sampling crystal (n_e in Figure 2.4) i.e. the THz field creates birefringence in the crystal. The value of n_e will change by an amount dependent on both the strength and direction of the THz field. The angle between the THz pulse polarization and the n_e axis depends on the crystal used and is 45° for ZnTe. The quarter-wave plate and the polarizing beam splitter resolve the changes of polarization of the gate beam.
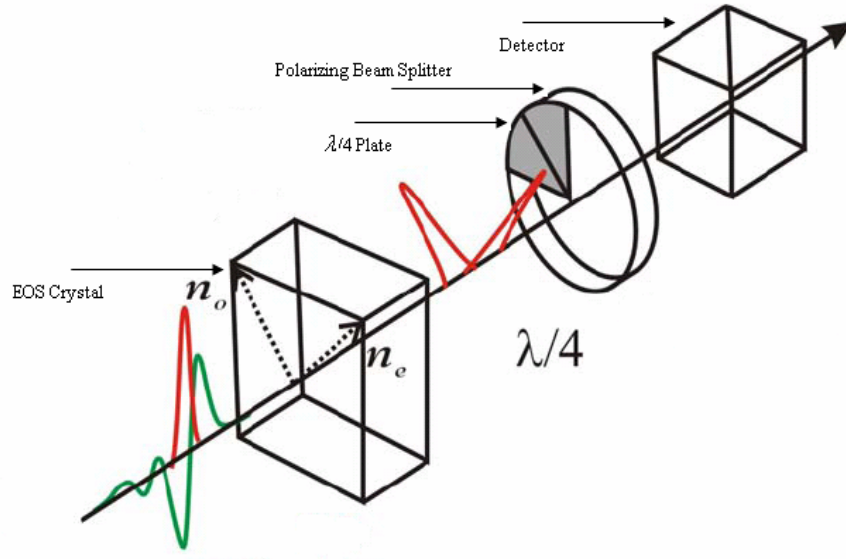
Figure 2.4 Detection of THz by electro-optic sampling [15]

The beams from the polarizing beam splitter are incident on the balanced diodes (detector). The diodes are wired such that the produce zero output when the signals on each are same and positive/negative output when the signals are different. The total phase change caused by the change in refractive index n_e of the ZnTe $\langle 110 \rangle$ crystal can be expressed as a function of the THz electric field in Equation 2.2.1 [16].

$$\Gamma_{ZnTe} = \frac{2\pi}{\lambda} \ln_0^3 r_{41} E \qquad (2.2.1)$$

In the above equation E is the electric field induced by the THz waves. The total phase change is linearly dependent on length l of the EO crystal, refractive index of gate beam n_0, electro-optic coefficient r_{41} at wavelength of λ. Thus, the THz electric field can be calculated from the equation 2.2.1.

2.3 THZ IMAGING TECHNIQUES

Terahertz (THz) imaging systems are a recent addition to the wide array of available imaging modalities like X-rays, microwaves and infrared. THz sensing and imaging techniques have several advantages over other sensing and inspection techniques. While these techniques provide only density pictures, THz imaging also provides spectroscopic information about the material within the THz frequency range. In addition THz waves easily penetrate and image inside many dielectric materials which are opaque to visible light and have low contrast to X-rays. The primary measures of quality of an imaging system are its resolution, acquisition speed and its signal to noise ratio (SNR). The performance of a THz imaging system is quantified under these criteria. This section gives a description of various imaging techniques used for generating images using THz radiations. The section begins by introducing THz imaging systems and discussion of prominent challenges in this field. Three main imaging techniques that are widely used for THz imaging are discussed in detail with the advantages and disadvantages of each. Several methods that are used to improve SNR and speed of THz imaging are also presented.

2.3.1 Passive THz Imaging. Radiation is emitted by all objects in the universe with a temperature above 0 Kelvin. This radiation is emitted as a result of vibrations of molecules and is broadband, covering a broad range of the electromagnetic spectrum. The distribution of radiation with frequency is temperature dependent and is governed by Plank's Law given in equation 2.3.1,

$$M_\lambda = \frac{2\pi hc^2}{\lambda^5}\left(\frac{1}{\exp\left[\dfrac{hc}{\lambda kT}\right]-1}\right) \tag{2.3.1}$$

where M_λ is the spectral radiation intensity of the body at a temperature T as a function of λ, $h = 6.626\times10^{-34}\,Js$ is Planck's constant, $k = 1.3805\times10^{-23}\,J/K$ is the Boltzmann constant and $c = 3\times10^{8}\,m/\sec$ is the speed of light. Cool interstellar dust (around 30

Kelvin) emits radiation with peak wavelength in the THz range, while objects at room temperature (around 300 K) emit mostly in the infrared region. Passive THz has been used to determine existence of water on distant planets [17-20].

  2.3.2 Active THz Imaging. Active imaging refers to the technique of illuminating the target with a source of radiation and then measuring the reflected or transmitted radiation. Active imaging systems can have pulsed or continuous wave (CW) illumination. Early THz systems used CW gas THz lasers to illuminate the target and thermal detectors [21-22] or pyroelectric cameras [23]. Generally pulsed systems are preferred as they use much lower average illumination power and have power higher than the background thermal noise power at the same time. For pulsed systems the illumination power is compressed into short pulses with a width of few picoseconds (10^{-12} s). this results in a high illumination power with a low average value. Pulsed THz imaging systems or 'T-ray Imaging' was first demonstrated by Hu and Nuss [24] from Bell Laboratories in 1995. Since then a number of variations and alternatives have been developed to this technique. Some of the developed techniques are two dimensional electro-optic sampling [25-26], chirped probe beam imaging [27], quasi-optical THz imaging [28], Synthetic phase array methods [29] to name a few.

➢ **Traditional Scanning THz Imaging (T-ray Imaging):** This technique was first proposed by Nuss et all [30] and involves measuring entire terahertz waveform at each pixel of the image. Figure 2.5 shows an experimental setup of the imaging system. It consists of a femtosecond laser, a computer-controlled optical delay line, an optically gated terahertz transmitter, a set of off-axis parabolic mirrors for collimating and focusing the terahertz beam, the sample to be imaged, an optically-gated terahertz receiver and a lock in amplifier. The femtosecond laser generates near-infrared pulses (802 nm) with a pulse duration of 130 fs. Pulse energy is $700\,\mu$J at a repetition rate of 1 KHz providing 0.7W average power. The polarization of the laser pulses is rotated using a half wave plate (HWP) to determine the relative proportion of pump beam and probe beam. The pump beam is directed onto two mirrors (M3 and M4) mounted on a translational stage that allow the propagation

distance of the pump beam to be modified. The pump beam is amplitude modulated using a mechanical chopper and incident on a THz emitter.
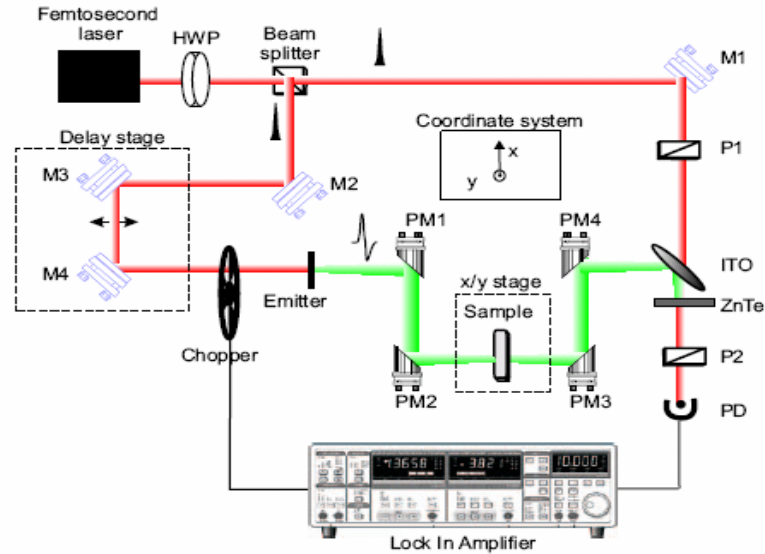
Figure 2.5 Experimental setup of traditional scanning technique [30]

Free-space electro-optic sampling [25] is used for detection of the THz field. The THz radiations are reflected by an indium tin oxide (ITO) beamsplitter and propagates collinearly through a polished 4mm thick $\langle 110 \rangle$ ZnTe crystal. The birefringence of ZnTe is modified by the external THz electric field and the probe beam polarization is rotated as a result of EO or Pockel's effect [25]. This signal is detected using a photodetector PD and digitized by the Lock in Amplifier (LIA) to get the instantaneous THz electric field. By iteratively reducing the pump path length using the delay translation stage, the electric field at later times is measured and the temporal THz pulse profile is recorded. To acquire an image these measurements are repeated as the target is raster scanned using x and y translational stages.

This imaging technique is slow but acquires images with a very high SNR. Using a LIA time constant of 10ms and averaging of 30ms for each sample, the system SNR is over 1000 but for a 50×50 pixel image with 100 temporal samples acquisition time is approximately 2 hours.

➢ **Two Dimensional Free Space EO Sampling:** This imaging technique offers a dramatic improvement in acquisition speed using Two Dimensional Electro-optic detection of THz pulses [26]. This technique provides a parallel detection capability and removes the need to scan the target. It has a spatial resolution limited by the diffraction limit of the THz beam, femtosecond temporal resolution, THz frequency bandwidth, mV/cm field sensitivity, and signal to noise ratio (SNR) better than 10000. Figure 2.6 shows the experimental setup for two dimensional electro-optic THz imaging.
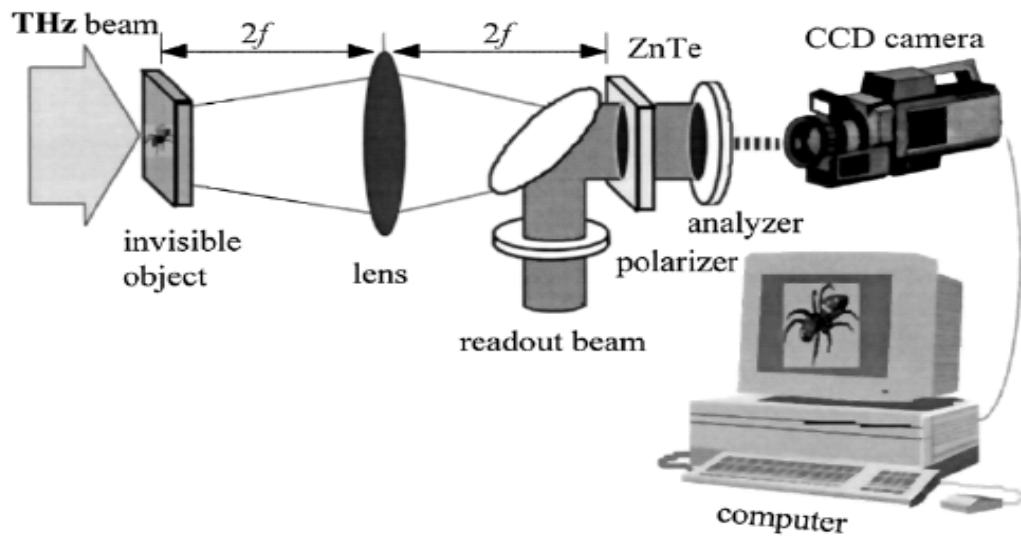
Figure 2.6 Experimental setup for two dimensional electro-optic imaging. [26]

The basic operating principle of electro-optic sampling is given in Section 2.2. This system is based on the linear Pockel's effect in electro-optic crystals where a pulsed microwave signal acts as a transient bias to induce a transient polarization in the sensor crystal. This polarization induces a birefringence that is then probed by a synchronously pulsed laser beam, and finally converted to an optical amplitude modulation via optical polarization analysis. The laser source is a Ti sapphire laser with pulse duration less than 50 fs, and an unbiased GaAs wafer is used to generate pulsed electromagnetic radiation. Parabolic mirrors were used to focus the THz radiation on a 0.9 mm thick, 6×8 mm $\langle 110 \rangle$ oriented ZnTe crystal. An optical readout beam with a diameter larger than that of the THz beam probes the electric field distribution within the crystal via the Pockels effect. The 2D field distribution in the sensor crystal is converted into a 2D optical intensity distribution after the readout beam passes through a crossed polarizer, and the optical image is then recorded by a digital CCD camera.

➢ **THz Imaging with a Chirped Probe Pulse:** This imaging technique has the highest theoretical acquisition rate as compared to traditional scanning technique and two dimensional electro-optic sampling. The two dimensional electro-optic imaging technique has limited temporal resolution as for each time delay between the THz signal and a synchronized optical probe pulse only a small portion of the temporal signal is measured. The entire waveform is reassembled by sequentially plotting the signal versus the time delay. Electro-optic detection of a terahertz pulse using chirped probe pulse [31] allows the full terahertz waveform to be measured simultaneously rather than the using the delay stage to scan the temporal profile. The chirped probe pulse is obtained by using a diffraction grating as shown in Figure 2.7. The different wavelength components of the incident pulse traverse different path lengths due to variations in first order diffraction angle with wavelength λ. The output from the grating is a pulse with longer pulse duration and a wavelength that varies linearly with time.
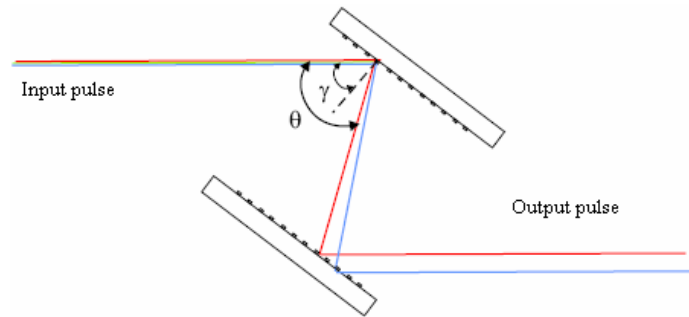
Figure 2.7 Generation of chirped probe pulse

The experimental setup of electro-optic sampling with chirped probe beam is shown in Figure 2.8.
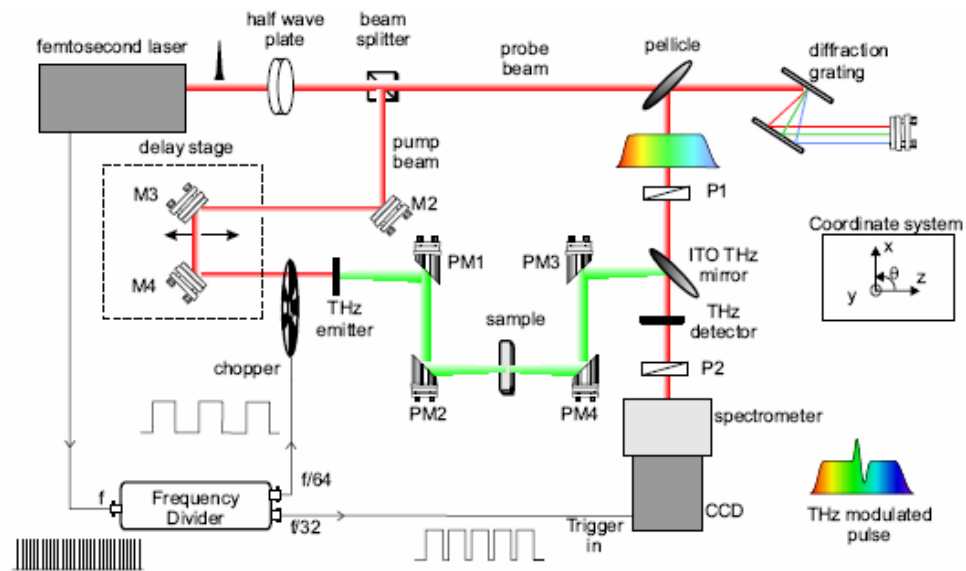
Figure 2.8 Experimental setup of electro-optic sampling with chirped probe beam [31]

The chirped optical probe pulse and the THz pulse co-propagate in the ZnTe crystal. During this time the polarization of the wavelength components of the optical pulse are modulated differently, depending on the temporal profile of the THz pulse. The temporal THz pulse is recovered by detecting the spectrum of the modulated pulse using a spectrometer grating and the digital CCD camera.This method offers a high acquisition rate due to the reduction in time for acquiring the temporal profile but it causes reduction in the temporal resolution. The temporal resolution is governed by the pulse width of the chirp probe pulse [32]. A shorter original probe pulse or equivalently broader spectrum is more desirable. In principle, a wider bandwidth can support shorter pulse duration. However the trade-off is that for the probe beam a large bandwidth could have large group velocity mismatch and reduce the temporal resolution.

➢ **Other THz Imaging Techniques:** There are several other techniques for THz imaging, many of which are improvements over the above mentioned techniques. Hu and Nuss [24] suggested construction of an array of photoconductive antennas for 2D detection of spatial THz field. An eight element photoconductive antenna detector array is used [33] for simultaneously recording sets of eight time domain THz waveforms. An efficient electronic circuit replaces the lock in amplifier to detect and read THz signals. The Quasi-Optic synthetic phase array imaging technique [34] allows 3-D THz imaging of objects. It uses a spherical imaging mirror that has a large collection aperture making it possible to image small or weakly reflecting objects without a detrimental loss of SNR. Additionally, the large extent of the mirror enables it to form an image automatically with good resolution. The system also performs simultaneous range and transverse (cross range) imaging, thus obtaining 3-D data.

3: TERAHERTZ BASED DETECTION OF IEDS

During the past decade, the world has witnessed an increase in the use of Improvised Explosive Devices (IEDs). In wake of these events it is necessary to have an efficient system for detection and neutralization of these threats. This system must detect presence of IEDs from a standoff distance with maximum accuracy so that the IEDs can be neutralized. The existing standoff detection techniques are ground penetrating radar (GPR), X-Ray imaging, thermal neutron activation, microwave imaging, thermal radiation detection and optical chemical sensors [35]. X-rays and thermal neutrons are potentially harmful to humans and suffer from severe signal degradation over long distances hence are not suitable for standoff detection. Microwave imaging and thermal radiation cannot deal with the traces of targeted chemicals and also do not they provide enough spatial resolution. Recently, sensing of explosives at a distance of 50 m using Raman spectroscopy (optical sensors) has been reported [36]. However, a significant drawback of optical technique is its inability to detect threats concealed under covers. Terahertz (THz) imaging and sensing technologies are bridging technique between microwave and infrared sensing modalities. Three key properties of THz waves make it a potentially powerful technique for standoff detection of IEDs.

- Materials reflect and absorb differently at THz wavelengths. All the explosive substances used in IEDs have characteristic signatures in the THz frequency range. THz waves are transparent to many materials like clothing, paper and plastics which might be used to conceal IEDs.

- The extremely short femtosecond pulses used in pulsed Terahertz techniques enable 3-D imaging. This helps in imaging beneath soil and other covering materials.

- THz radiations are non-ionizing and can be used at very low power levels in the microwatt range. They are not as harmful as X-rays and can be used to screen individuals for presence of concealed IEDs and explosives.

Thus, THz imaging holds a significant potential for detection of IEDs. This section discusses issues concerning standoff detection of IEDs using THz waves, THz imaging and THz spectroscopy for standoff detection of IEDs are discussed.

3.1 STANDOFF DETECTION OF IEDS

As described in Section 2.1 improvised explosive devices are homemade, non-conventional explosive devices which use common explosives like TNT, RDX and PETN. For successful detection of IEDs, THz waves are used to illuminate the target area and the reflected THz waves from the target location are analyzed. Successful standoff detection of IED involves detection of a weak signal in a noisy environment. The speed with which the detection is performed is also a crucial factor when a potential threat is rapidly approaching. Finally, the detection technique must generate minimum false positive (false alarms) and must have zero false negatives i.e. must not miss a potential IED threat. Factors to be considered for standoff detection of IEDs are the standoff range, acquisition time and the imaging modality to be used.

3.1.1 Estimation of Stand-Off Range. In determining ranges for THz stand-off detection, a detailed analysis of the transmitted THz power, received THz power, and noise sources of the detector, background THz radiation, and detection method are required. The received THz power can be estimated for a transmission geometry as shown in Figure 3.1.
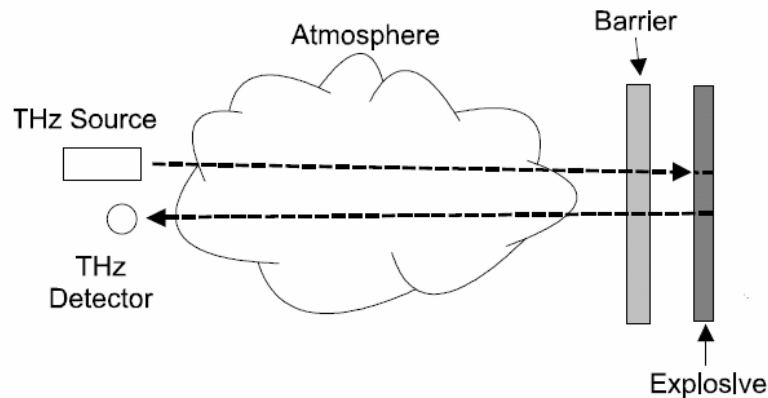
Figure 3.1 Determination of standoff distance

A bright THz source illuminates the area under investigation. The THz radiation is assumed to travel a distance D through the atmosphere. The THz radiation passes through a barrier material (eg. wood, cardboard, clothing), and through the explosive material and then reflect from the explosive material. The reflected light must pass back through the barrier material and atmosphere before being sensed with a THz receiver. The power received by the detector can be written as,

$$P_r = A_r \left[\frac{P_0}{\Theta(2D)^2} \right] e^{-2\alpha_b L_b} e^{-2\alpha_a D} e^{-2\alpha_e L_e} \qquad (3.1.1)$$

where P_0 is the transmitter power, Θ is the solid angle in which the transmitted power is directed, A_r is the effective area of the receiver, L_b and L_e are the thickness of the barrier and explosive layers, α_b, α_a and α_e are the attenuation coefficients of the barrier material, atmosphere and explosive, respectively. Equation (3.3.1) accounts for the geometric expansion of the illuminating THz beam, and the attenuation of the barrier, explosive materials and atmosphere. The factor of 2 in the exponents results from a double pass through the attenuating mediums. To estimate the effective range of a THz stand-off detector, the received THz power as a function of distance is calculated from Eqn (3.1.1).

3.1.2 Requirements of Imaging Modalities for Standoff Detection. The simplest method of THz imaging is to use a single transmitter and detector - i.e. line-of-sight detection. An image is obtained on a point-by-point basis by scanning the transmitter/detector pair over the sample under test and recording the THz phase and amplitude at each point. Using this method, THz images of macroscopic objects have been obtained [37] and extended to THz tomography [38] and synthetic phased-array techniques [39-40]. The imaging modalities that have potential for standoff imaging are focal plane array and interferometric imaging. A focal plane array is similar to a standard digital camera, for which detector denotes a pixel in the image. Interferometric imaging, unlike the focal plane array approach, uses intensity and phase information between pairs of detectors. The distance between each pair is referred to as a baseline, and the image quality is strictly dependant on utilizing a wide range of unique baselines. For *N* detectors,

there are $N(N-1)/2$ detector pairs corresponding to $N(N-1)/2$ pixels in a reconstructed image. Consequently, fewer detectors and faster frame rates are needed for the interferometric approach as compared to the focal plane array approach. Interferometric Imaging [41-44] has been suggested as an imaging modality for stand-off detection of explosives, weapons, and other threats. The interferometric THz imaging array design does not require a particular coherent or incoherent source of THz. It is flexible enough to utilize an electronic THz source, a laser-based THz illuminating source, or incoherent ambient THz radiation that may be present. To perform imaging in real time, the basic technique of radio interferometry [45] is employed for which signals at two or more points in space (the aperture plane) are brought together with the proper delay and correlated both in phase and in quadrature to produce cosine and sine components of the brightness distribution. The imaging interferometer consists of an array of individual detectors. As a wavefront of THz radiation encounters the array, each pair of detectors measures one spatial Fourier component of the incoming THz radiation as determined by the separation of the detector pair. Each spatial Fourier component is represented by a point in the Fourier transform plane (called the u-v plane). In order to determine a spatial Fourier component and consequently the direction of the incoming THz wavefront, the delay in arrival time of the wavefront between a pair of antennas must be measured. Also, efficient u-v plane coverage with a small number of detectors may be achieved by rotating the array about a fixed axis.

Also, THz imaging approaches have typically used either short-pulsed laser or continuous wave (CW) difference frequency THz generation and detection. Pulsed sources seem to be more favorable (in particular for close proximity applications) because they can be used for acquiring depth information. The advantages of pulsed THz Time-Domain Spectroscopy is that broad spectral information (0.1-3THz) can be acquired from a single picosecond THz pulse as well as the depth information from the difference in arrival times of the short pulses. CW imaging systems have the advantage of higher THz power at a distinct THz frequency. A further advantage of CW THz spectroscopy over pulse THz time-domain spectroscopy is that narrow spectral features are easier to measure using CW techniques due to the inherently spectrally narrow CW THz radiation and due to the lack of a long scanning delay line that would be required for

high spectral resolution using a time-domain system. For standoff detection, a dominating issue in choosing a short-pulsed or continuous wave source is the need to propagate through the atmosphere. Only certain bands of THz frequencies are appropriate transmission windows for remote detection applications. For THz time-domain pulses that are generated by short-pulse laser systems (eg. mode-locked Ti:Sapphire laser), the THz spectrum of the pulse spreads over several transmission bands. However, the THz power which is outside of the transmission bands is highly absorbed. Consequently, the amount of usable THz power in the pulse can be drastically reduced. In addition, the time duration of the picosecond pulses is considerably lengthened due to water absorption rendering pulsed time-of-flight detection impossible. For propagation of THz pulses through 2.4m of a humid atmosphere, a 1ps pulse is broadened to a time duration in excess of 30ps. After 100m, the pulse duration is well beyond 100ps in duration [46]. Thus, CW techniques are more suitable for standoff detection over longer distances.

The next two sections discuss the results of the various THz imaging and spectroscopy techniques used for detection of IEDs and explosives.

3.2 THZ IMAGING FOR DETECTION OF IEDs

THz imaging refers to imaging techniques utilizing picosecond pulses of broadband radiation in the frequency range of 0.1 THz to 10 THz. THz technologies help in producing a 2-D or 3-D image of an object. THz imaging can be particularly useful for IED detection if the IED or explosive has been covered by a metallic covering from which THz waves are reflected. In such cases the image of the object can hold vital information and aid in the detection. A THz image is acquired by analyzing the peak amplitude information of the THz pulse in the time domain at each pixel. The THz band is advantageous since it includes short wavelengths and therefore has a high resolution compared to traditional electromagnetic tomography at radio frequencies. It has significantly less scattering than infrared light, which allows for improved reconstruction fidelity compared to infrared tomography techniques. A number of imaging modalities implementing THz pulsed radiation have emerged, involving point-by-point scanning[47], computer tomography[48], ranging measurements[49], multi-static reflection imaging

[50], and so on. Described below are various THz systems developed for imaging of explosives, IEDs and other threats.

3.2.1 The 1.56 THz Trans-receiver Imaging System. This THz imaging system uses a 1.56 THz transreceiver system with two carbon dioxide lasers paired individually with two far-infrared lasers [51]. The system has transmitter beam power of 100 milliwatts and heterodyne receivers with sensitivity of approximately 10^{-19} W/Hz. The output power, over 100 milliwatts, in the transmitter laser beam allows sufficient power to easily transmit through the nearly 80 foot round trip distance to and from the targeted subject. An azimuth/elevation (Az/El) technique is used where a full beam illumination of the target helps in acquiring high resolution images by viewing the target through a 2D angular aperture similar to synthetic aperture radar [52]. The target in this case was clothed mannequin with a concealed weapon. The images gathered from this imaging system are shown in Figure 3.2.

Figure 3.2 A clothed mannequin with a concealed weapon "gun" (inset) [51]

The Figure 3.2 shows the image taken at 1.56 THz. The hidden gun is easily visible. To capture image of the six foot tall mannequin took 7 minutes with a standoff

distance of 2 meters. The acquisition time in this case does not allow real time imaging of subjects with concealed weapons or IEDs.

3.2.2 THz Imaging for Detection of Buried Objects. IEDs are many times buried under the soil or hidden under some covering material like paper, cloth and even in dead animals. Under such circumstances it is important to have information provided by a THz image to detect presence of an explosive material or a potential IED threat. Zhang et al have conducted an experiment [53] to detect the presence of metallic and nonmetallic objects buried in soil. A 2D electro-optic imaging system was used with a beam waist of 6 mm at the focusing point. The details of the 2D electro-optic imaging setup are explained in Section 2.3. The peak amplitude of the THz pulse corresponding to each pixel is tracked and plotted. Various metallic and nonmetallic objects buried under varying thickness of sand are imaged using this system. Figure 3.3 and Figure 3.4 show the actual photograph and the THz image of a metallic object buried under varying thickness of sand, respectively.

Figure 3.3. Photo of the aluminum block

Figure 3.4. THz image of aluminum block. From left to right, the average thicknesses of the sands are 0.5 mm, 10 mm, and 20 mm, respectively.
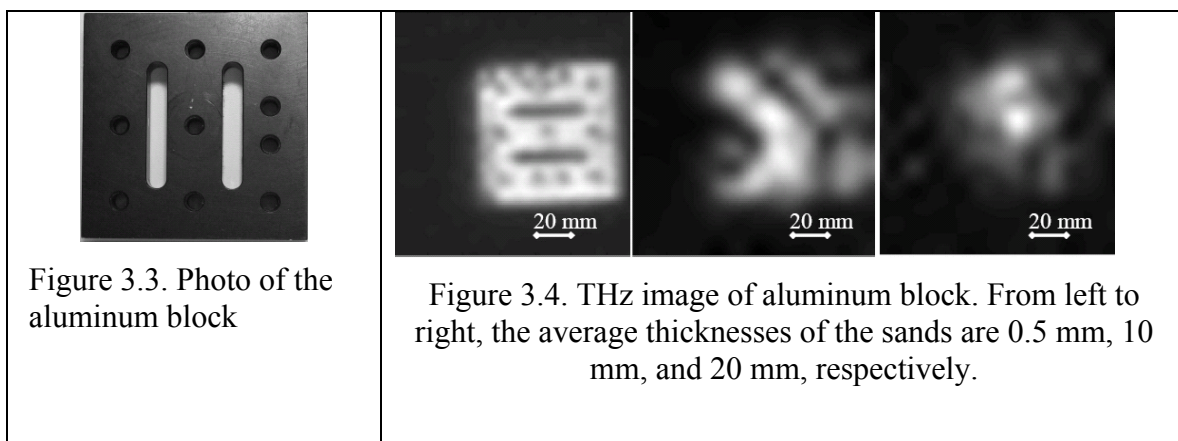
Thus, with the help of a THz image, valuable information can be obtained about a buried object which might be concealing an IED.

3.2.3 Terahertz Hand-Held Wand. A prototype for a THz hand-held detection and identification wand has been developed by Iconal Technology Ltd and Teraview Ltd [54-56]. This system can detect and identify hidden metallic, non-metallic objects and explosives. This system is aimed for detection of explosives and non-metallic weapons on individuals on airports and other strategic locations. A schematic diagram of this wand system is shown in Figure (3.5)
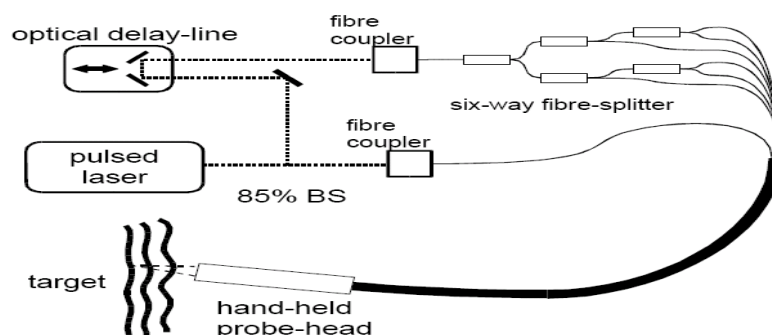
Figure 3.5. THz hand-held probe [54]

The six photoconductive THz detectors are incorporated in the head unit, and surround the emitter, each with a silicon lens to capture the reflected and scattered THz signal in multiple directions from the target. The signals from each detector can be analysed independently to form both spatial and spectroscopic information of the target. The THz wand prototype was used to image a number of test objects consisting of pieces of plastic explosive and other plastic-like objects such as polythene and Blu-Tak (an inert powder filled mastic material similar in physical appearance to plastic explosive) hidden beneath cloth. A typical measured B-scan for a series of targets is shown in Figure 3.6. From this figure it is difficult to differentiate and identify the objects hidden beneath the cloth.
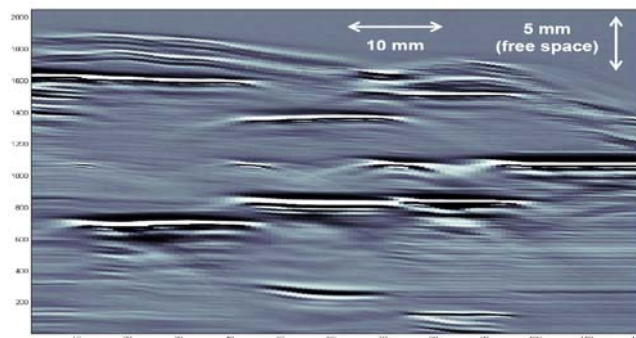
Figure 3.6 Grey scale image of plastic objects beneath two layers of cotton [56]

In order to enhance the readability of the above figure it is passed through a series of filters, separating the low, medium and high-frequency components of the image, which have then been mapped on to the red, green and blue channels of a color plot. The result of this processing is seen in Figure 3.7.
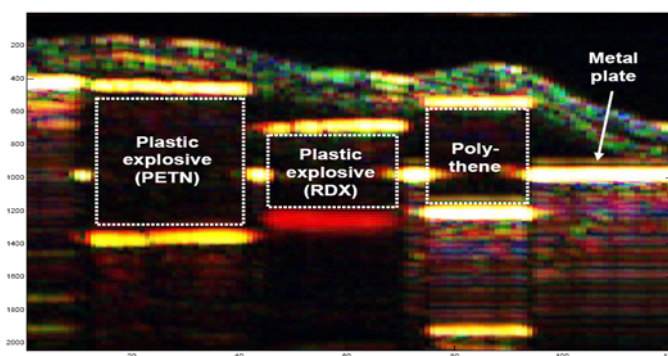
Figure 3.7 Hyperspectral image of plastic objects beneath two layers of cotton [56]

The various colors help in the easy identification of different objects which reflect (and/or absorb) different THz frequencies as seen in the Figure 3.7.

Thus, it is seen from this section the importance of THz imaging for detection of IEDs or other harmful threats. THz image of a target gives an idea about the shape, size, depth and nature of an object hidden under some covering material. Although these images give vital information, they are not used in the signal processing algorithms developed in this thesis. The reason for this is that terahertz spectroscopy described in the next section provides better information about the nature of the material present in the scene rather than only its shape. Nevertheless, the THz images can be used in conjunction to the signal processing of spectroscopic information for better detection of IEDs.

3.3 THZ SPECTROSCOPY AND SIGNAL PROCESSING TECHNIQUES

3.3.1 THz Spectroscopy. THz spectroscopy involves analyzing a spectrum of a target object or area to detect presence of an IED or explosive material. THz waves are capable of easily propagating through most of dielectric materials (clothing, packaging, plastics). However, the THz radiation is reflected from metals, solid objects and human bodies. When an object is illuminated with the THz radiation, the transmitted or reflected intensity of the THz rays depends on the composition of the material encountered, yielding characteristic signatures. Also, most of the explosives used in IEDs have characteristic THZ spectra which help in their identification and detection. The ability of THz light to interact differently with benign and threat materials as a function of THz frequency yields a highly flexible foundation for THz imaging screening based on spectroscopy. In general, non-polar, non-metallic solids such as plastics and ceramics are at least partially transparent and reflective in the 0.2-5 THz range. Non-polar liquids are transparent as well, whereas polar liquids, such as water, are highly absorptive.

Many commonly-used solid-state explosives and related compounds including RDX (hexahydro-1,3,5-trinitro-1,3,5-triazine), TNT (2,4,6-trinitrotoluene), HMX (tetramethylene tetranitramine), PETN (pentaerythritol tetranitrate), and DNT (dinitrotoluene), have spectral fingerprints in the range of 0.1-2.0 THz [57-60]. The experimental setup used for THz spectroscopy is similar to the imaging setup discussed in Section 2.3 with the Spectroscopy measurement is carried out in reflection geometry. The time domain THz signal is captured by the detector and a Fourier Transform of this

signal gives the THz spectrum. The signal in time and frequency domain is shown in Figure 3.8.
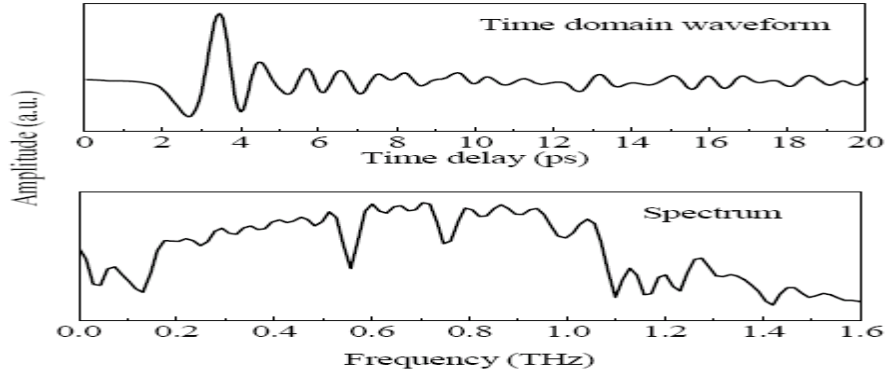
Figure 3.8. THz signal in time and frequency domain

The principle of THz time domain reflection spectroscopy is based upon Fresnel equations of reflections which help in calculation of the reflection coefficient. At normal incidence, the reflection coefficient r is given by the relation between the amplitudes of the reflected beam E2 and the incident beam E1, and can be expressed through the complex refractive index of the material $\tilde{n} = n + ik$ as follows,

$$r = \frac{E_1}{E_2} = \frac{\tilde{n}-1}{\tilde{n}+1} = \frac{(n-1)+ik}{(n+1)+ik} = \sqrt{R}e^{i\phi} \qquad (3.3.1)$$

If the phase shift φ between E1 and E2, and the reflectance R is determined, then the refractive index n and the absorption coefficient k can be retrieved from the equations,

$$n = \frac{1+R}{1+R-2\sqrt{R}\cos\phi} \ ; \ k = \frac{2\sqrt{R}\sin\phi}{1+R-2\sqrt{R}\cos\phi} \qquad (3.3.2)$$

Knowing the absorption coefficient k, the absorptivity α is given by,

$$\alpha = \frac{4\pi vk}{c} \qquad\qquad (3.3.3)$$

Where v is the frequency, c is the speed of light and k is the absorption coefficient.

Experimental data that has appeared in the literature suggests that many materials that are relevant to security applications have characteristic THz reflection or transmission spectra. Table 3.1 lists the commonly used explosives with the center frequencies of their characteristics absorption bands [61].

Table 3.1. Various explosives with feature band frequencies

Explosive	Feature band centre position frequency (THz)	Reference
Semtex-H	0.72, 1.29, 1.73, 1.88, 2.15, 2.45, 2.57	[61]
PE4	0.72, 1.29, 1.73, 1.94, 2.21, 2.48, 2.69	[61]
RDX/C4	0.72, 1.26, 1.73	[61]
PETN(pellets)	1.73, 2.51	[61]
PETN(compressed pellets)	2.01	[62]
HMX(pellets)	1.58, 1.91, 2.21, 2.57	[61]
HMX(compressed pellets)	1.84	[62]
TNT(pellets)	1.44, 1.91	[62]
TNT(compressed pellets)	1.7	[62]
TNT	5.6, 8.2, 9.1, 9.9	[63,64]
NH_4NO_3	4, 7	[62]

A dominant feature of the THz spectra is the sharp absorption peaks caused by phonon modes directly related to the crystalline structure [62]. This is due to the molecular vibrational modes and intramolecular vibrations associated, for example, with RDX [65]. Consequently, vibrational modes are unique and distinctive feature of the crystalline explosive materials. The presence of broad features might be caused by scattering from a structure with dimensions comparable to the THz wavelength. This usually occurs in materials that contain fibers or grains [66]. Figure 3.9 shows spectra for the raw explosives trinitrotoluene (TNT), tetranitro-tetracyclooctane (HMX), pentaerythritol tetranitrate (PETN), and trinitrotriazcyclohexane (RDX) together with spectra for the compound explosives PE4 and Semtex H. PE4 consists of RDX mixed with a plasticiser while Semtex H is a mixture of RDX, PETN, and plasticiser. All the raw explosives have distinctive spectra with several absorbance peaks in the measurement range while the compound explosives have peaks arising from their constituents.
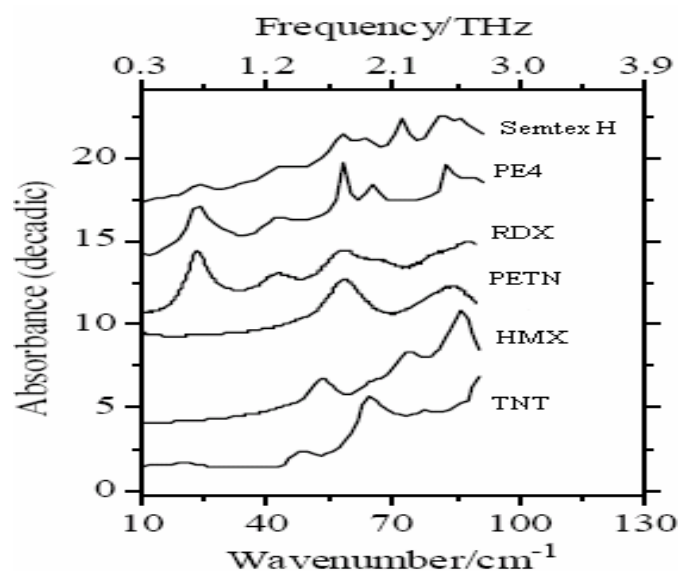
Figure 3.9 THz Signatures of various explosive materials [61]

A study of diffuse reflection spectroscopy was performed to explore the THz spectra of various explosives and related compounds [67]. According to the authors, when THz waves illuminate a flat sample surface, the reflected THz beam with a reflection angle the same as the incident angle can be theoretically treated using the Fresnel equations and it is called specular Fresnel reflection. But in a real world scenario, the targets are usually not flat and not aligned normal to the THz beam. Thus, the direction of the specular reflection is hard to determine and it is more feasible to detect the diffusely reflected THz waves. Accordingly the diffuse reflection spectra of various explosive materials like TNT, RDX, 2,4-DNT, 2,6-DNT, 1,3-DNB, 1,3,5-TNB, 2-amino-4,6-DNT and 4-amino-4,6-DNT were measured. Figure 3.10 shows the diffuse reflection and transmission spectra of these substances from approximately 1.5 THz to 21 THz (wave number 50cm^{-1}- 700cm^{-1}).

3.3.2. Signal Processing Techniques. The field of signal processing of terahertz signals is relatively unexplored. There have been some efforts in developing optimal techniques for denoising THz data [68], extracting material constants [69] and material classification using spectroscopic information [70]. Most of these techniques use well known image processing algorithms like pattern recognition, feature extraction and classification. Hence, these techniques rely more on analyzing the terahertz images to determine the nature of substances present in the scene. One such technique does an analysis of the terahertz images using a three stage algorithm [71]. The first stage is preprocessing by wavelet denoising and wiener filters. This stage removes the unwanted noise from the image. The second stage is of feature extraction. In this stage the features relevant to the target are extracted using principal component analysis and linear discriminant analysis. The last stage is of feature selection and classification which identifies the required features using genetic algorithms.

For the purpose of IED or explosive detection, terahertz spectroscopy holds the key because all commonly found explosives have a characteristic terahertz spectra. The signal processing algorithm must use this information to analyze data to detect the presence of IEDs. The algorithm must take into consideration that an IED can be present anywhere, in presence of lot of other substances like soil, vegetation, garbage, etc.
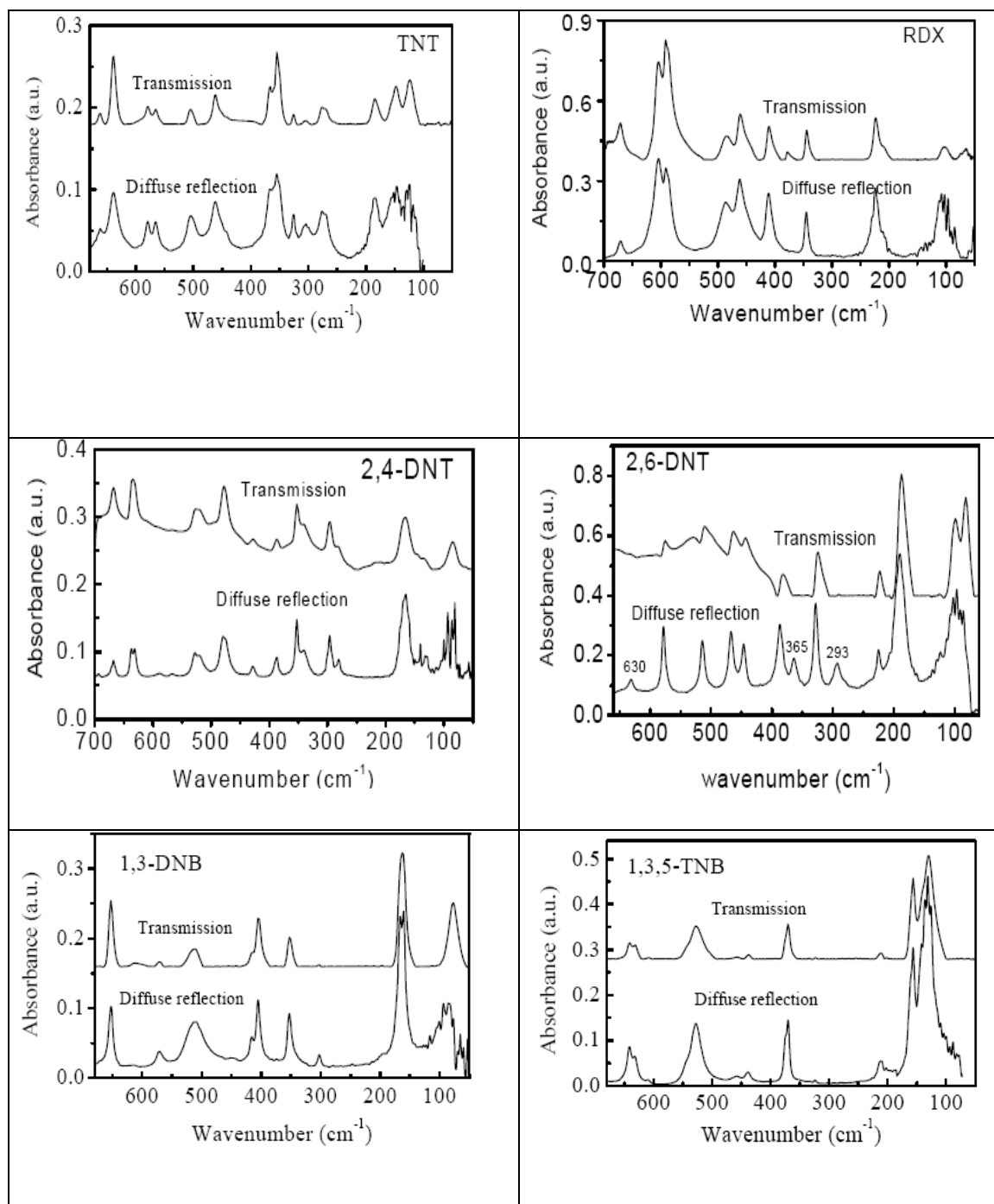
Figure 3.10 THz spectra of various explosives [67]

The received THz image or spectra in this case will be a combination of all the substances present within the range of the THz beam. The algorithm must be capable to

detect and identify the target spectra among this mixture. Other important issues to be considered for development of an efficient algorithm are standoff range and real time detection capability over a wide area. The standoff range is determined by the terahertz equipment, imaging modality used but an efficient algorithm can be developed to detect weak signals at a long distance. The algorithm must be fast enough to aid real time detection over a wide area. For this purpose, it must separate the scene into hotspots where IEDs could be present and safe-spots where there is no chance of a threat to be present. Only the hot-spots can be further probed of detection of IEDs.

Thus, in this section several issues relating standoff detection of IEDs and some existing signal processing techniques for terahertz waves have been discussed. With the help of THz imaging and spectroscopy and efficient signal processing algorithms, IEDs can be identified and detected at a standoff distance. Although some signal processing algorithms have already been developed, they have not fully utilized the spectroscopic information provided by terahertz imaging. In this thesis, an effort has been made to address the shortcomings of the existing algorithms and develop efficient algorithms that aid in standoff and real-time detection of IEDs. The next section details the development of these algorithms.

4: SIGNAL PROCESSING OF THZ DATA FOR DETECTION OF IEDS

The previous section discusses the existing signal processing techniques developed for analyzing captured THz images. Most of the developed techniques focus on using existing image processing techniques. There exists a lot of scope for developing efficient signal processing algorithms for analyzing the captured THz spectra. The signal processing algorithms developed during the course of this thesis for standoff and rapid detection of IEDs and similar threats are presented in this section. The developed algorithm comprises of two stages as shown in Figure 4.1.
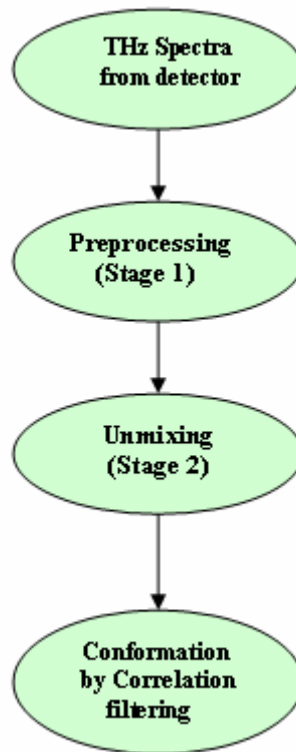
Figure 4.1 Flow chart of the detection algorithm

The THz spectra from the detectors are given to the preprocessing stage. This stage consists of correlation filters and is designed to select data/spectra which have significant probability of any explosive or threat present in it. All data/spectra which does not have a significant probability of explosive content is discarded. Thus, this stage results in significant reduction in computational burden on the further processing stages due to reduction in amount of data/spectra passed to the next stage. The selected data/pixels from the preprocessing stage are given to the unmixing stage which uses a variant of the Independent Component Analysis (ICA) algorithm to extract the explosive spectra if present in the data. If any explosive spectra are present they are separated out and if not some random spectra are separated. Hence, a final conformation stage is required to decide if the separated spectrum is of an explosive or not. This stage also uses correlation filters to decide whether a given spectrum is of an explosive or not.

Thus, the proposed algorithm ensures accurate and fast detection of IEDs. High accuracy is accomplished by unmixing explosive spectra. Fast detection is ensured by selecting data/pixels in the preprocessing stage and separating only the required spectra in the unmixing stage. The details of the proposed algorithm are provided in this section.

4.1 PRE-PROCESSING OF THZ DATA BY CORRELATION FILTERING

The 2D Electro optic imaging technique [25-27] is used for THz imaging and gives the THz spectra of the sample or scene under consideration. This technique has a limited temporal and spatial resolution mainly due to the laser pulse duration and diffraction limit of the THz beam, respectively. It can cover only a small area at a time and for a wide area surveillance application it will generate a very large number of data points called pixels analogous to pixels in an image. Each pixel is a spectrum which is combination of spectra of all materials present within it. In order to determine if an area contains any IEDs, the spectral information in the pixels in that area should be analyzed. For this detection, it is necessary to separate the individual spectra within a pixel using spectral un-mixing techniques like Independent Component Analysis (ICA) [74-79] described in the next section. But before performing spectral unmixing, it is necessary to reduce the amount of data to be processed. For wide area surveillance, it is very ineffective if ICA is performed for all data points covering the entire area as an IED

might be present in only a small area within it. Hence, it is proposed to perform preprocessing on the received THz data to reduce the number of data points or pixels. The correlation filters are proposed for preprocessing purposes and are presented in this section. Correlation filtering separates out data/pixels which have a significant probability of explosive spectra present in them. Such data/pixels are further investigated to accurately determine presence of IEDs in them. The section begins by explaining the general idea of correlation and correlation output. Then the design of correlation filters is proposed by computing the threshold for a correlation peak depending desired accuracy and probability of error.

4.1.1 Correlation. Correlation indicates the strength and direction of a linear relationship between two random processes. Correlation is also defined as the degree of similarity between two variables. In this preprocessing stage, correlation gives a measure of how similar or different a received spectrum is from a spectrum available in the spectral library called the target spectrum. There are two ways to compute correlation. One way is to perform repetitive multiplications and additions and another is to compute correlation by the FFT method. For the proposed correlation filters, the repetitive multiplication and addition method is used but both of the methods are described below.

Correlation by Multiplication and Addition: A THz transmitter-receiver gets the THz signal in time domain after which a FFT of this signal is computed to give the THz spectrum of that signal. Let r[n] be the received spectrum containing n frequency points and s[n] is the target spectrum with n frequency points. The target spectrum s[n] is available in the THz library containing the spectra of commonly occurring explosives in IEDs. The received spectrum r[n] can be a combination of the target spectrum s[n], spectra of other materials s_j and random noise $\omega(n)$. i.e.

$$r[n] = s[n] + \sum_{j=1}^{k} s_j(n) + \omega(n) \tag{4.1}$$

Or the received spectrum r[n] might not contain the target spectrum in which case it is

$$r[n] = \sum_{j=1}^{k} s_j(n) + \omega(n) \tag{4.2}$$

Mathematically correlation between r[n] and s[n] can be expressed as follows,

$$c[m] = \sum_{k=1}^{2n-1} s[k]r[k-n]$$ (4.3)

Correlation in Eqn (4.1.1) proceeds as follows. The two spectra are multiplied and the values in the resulting product array are summed to obtain the correlation value of the spectrum r[n] with s[n] for that relative location between the two. This calculation of correlation values is then repeated by shifting the spectra r[n] to all possible centerings with respect to spectra s[n]. The resulting correlation output is of size m = (2n-1). The above method of correlation can be used if the spectra are available in frequency domain. But if the signals are in time domain correlation by FFT would be more effective.

Digital correlation via FFT: The FFT method can be used when the signals are in time domain. FFT gives a more efficient method for computing cross-correlation. Correlation is performed by following three steps:

- Compute S[k] and R[k], the N point DFTs of the available signal and received signal, respectively. N must be at least as large as N = (2n-1).
- Multiply S[k] by R^*[k] to obtain C[k].
- Perform a N inverse DFT of C[k] to obtain cross correlation output c[m].

This method reduces the number of multiplications and additions needed as compared to the direct method. Although digital correlation by FFT is effective as compared to the direct correlation, the method of repetitive multiplication and addition correlation is used for the correlation filters as the received signal is available in frequency domain and the spectra in the spectral library are also in the frequency domain. Only in the case when both the received signal and the signals in spectral library are in time domain it would be more beneficial to use the FFT method.

4.1.2 Detection Strategy for the Correlation Filters. For the detection of IEDs it is important to detect the characteristic feature of the target spectrum s[n] and the frequency at which it occurs in the received spectrum r[n]. Hence, it is proposed to use two methods for the development of correlation filters of the preprocessing stage.

Method 1: In this method, the correlation filters use the entire frequency range of the target spectrum i.e. the filters try to correlate all the features within the entire frequency range. These filters will be beneficial if the target does not have specific features in a certain frequency range like a dominant peak or valley in its spectrum. In such a case using the entire frequency range would provide accurate results as it would use multiple smaller features and correlate them to the received spectrum.

Method 2: In this method, the correlation filters use a characteristic feature of the target spectrum like a peak or valley occurring in a narrow frequency range. Only this feature is correlated with the received spectrum. These filters are suitable for targets that have dominant peaks in certain frequency ranges like the absorption peak of RDX around 0.8 THz.

Also, it is important to understand the features of the correlation filter and its output. The correlation filters produce an output with significant peaks when the target spectrum is present in the received spectra and the peaks are insignificant when the target spectrum is absent. The received spectrum can be a combination of the target spectrum s[n] (present or absent), spectra of other materials present in the pixel and additive random noise shown in equation (4.1.1) and equation (4.1.2). Maximum signal to noise ratio (SNR) or discernable peaks in the correlation output can be achieved by correlating r[m] with s[n] to produce the output c[m]. This correlation output is searched for its peak and if the peak exceeds a pre-chosen threshold then it can be concluded that the target or known spectrum s[n] is present in the received spectrum. The computation of the threshold for peak selection discussed in the next section is important from the point of view of accuracy of the detector. Also, by adjusting the threshold the accuracy of the algorithm can be controlled.

Correlation filters have an important property of shift invariance meaning the correlation peak will shift by same amount as the shift of target spectrum in the received spectra. This means that if there is a characteristic feature of the target spectra in the received spectra but at a different frequency as compared to the target spectra it can be detected at that frequency. Thus, not only occurrence of a characteristic feature but also the frequency at which it occurs can be predicted.

4.1.3 Threshold of the Correlation Peak. If the received spectrum r[n] is similar to the target spectrum s[n] from the spectral library, then the correlation of r[n] with s[n] produces an output with a significant peak. If the received spectrum r[n] is affected by noise or other signals then the peak/peaks in the correlation are of lesser magnitude. Also, if the received spectrum is not same as the target spectrum but has some similarities to the target spectrum, it can still produce a correlation output with some peaks in it. Hence, a threshold must be set for the correlation peak and only select spectrums which produce peaks that exceed the threshold and reject ones that have peaks lesser than the threshold. The peak selection function is computed by the following analysis taking in to consideration the probability of error of the detection.

<u>Probability of error</u>

Let s[n] denote the target spectrum, r[n] denote the received signal and $\omega(n)$ denote additive noise. The following two cases arise.

$$H0 : r[n] = \sum_{j=1}^{k} s_j(n) + \omega(n)$$

$$H1 : r[n] = s[n] + \sum_{j=1}^{k} s_j(n) + \omega(n)$$

(4.4)

H0 is a hypothesis that the received spectrum r[n] does not contain the target spectrum s[n] but contains k different spectra of other materials and noise. H1 is a hypothesis that the received spectrum r[n] contains the target spectrum s[n] along with k spectra of other materials and noise. To determine the detection method yielding the smallest probability of error, first note that the detection error can occur in two different ways. If hypotheses H_0 is true, but H_1 gets selected, that error is called false positive, since the detection method falsely indicates the presence of the target. On the other hand, if H_1 is true but H_0 gets chosen, there is a false negative since the detector missed the target. Let P_0 and P_1 denote the a-priori probability of the two hypotheses H0 and H1, respectively. The probability of error P_e is obtained by weighting the probability of false positive (P_{FP}) and the probability of false negative (P_{FN}) by the corresponding a-priori probabilities P_0 and P_1 and adding them up.

$$Pe = P_0 P_{FP} + P_1 P_{FN}$$

(4.5)

where $P_{FN} = P\ (H_0/H_1)$ i.e. detector selects H_0 when H_1 is true.

and $P_{FP} = P\ (H_1/H_0)$.

Based on these two hypotheses a peak selection function is computed which will decide the peak selection threshold.

Statistical peak selection function

The detection scheme must minimize the probability of error defined in equation (4.1.5) by choosing a proper threshold for the correlation peaks. In the case of IEDs it is beneficial to assign different costs to the two types of errors i.e. P_{FP} and P_{FN} in order to increase accuracy of the system. One would assign a P_{FP} greater than a P_{FN} as it would be acceptable to get more false positives (false alarm about the presence of an IED) rather than false negatives (i.e. miss the IED completely). Also, this is a preprocessing stage which aims at reducing the data hence can tolerate some false positives samples but not any false negatives.

Taking the above discussion into consideration, a function is proposed for peak detection. Let r[n] be the received spectra containing n data points and s[n] is the spectra to be detected present in an available spectral library containing n data points. Let c[m] be the correlation function of r[n] and s[n]. σ is the variance of c[m]. So the probability density function of c[m] is,

$$f(c[m]) = \frac{1}{\sqrt{2\pi\sigma^2}} \exp[-\frac{c^2[m]}{2\sigma^2}] \qquad (4.6)$$

One of many possible statistical peak-selection functions is,

$$\breve{c}[m] = 1 - \exp[-\frac{c^2[m]}{2\sigma^2}] \quad \text{if} \quad c[m] > R_0 \qquad (4.7)$$

and is zero if $c[m] < R_0$

The peak selection function has values from zero for small peaks and one for large peaks. R_0 is chosen by specifying the probability that the selected peak is due to noise. The probability that a noisy peak exceeds R_0 is,

$$P(\breve{c}[m] \geq R_0) = 2erfc(\sqrt{-2\ln(1-R_0)}) \qquad (4.8)$$

where the complimentary error function is,

$$erfc(x) = \frac{1}{\sqrt{2\pi}} \int_x^\infty \exp(-t^2/2)dt$$

Given $P(\breve{c}[m] \geq R_0)$, R_0 is found numerically.

Thus, knowing the probability of error the threshold value R_0 can be calculated for that particular probability of error. Once R_0 is computed then the correlation output c[m] is searched for peaks exceeding R_0 and all pixels that produce a correlation with peaks exceeding R0 can be said to have presence of the target spectrum with a significant probability. All such pixels are selected and given to the next stage of spectral unmixing for further processing to ascertain the presence of IEDs in them.

Thus, it is seen that this preprocessing stage can considerably reduce the burden on the further processing stages that more accurately ascertain the presence of IEDs. Consider a field as shown in the Figure 4.2, 100 meter square large containing vegetation, sand, metal junk, trace explosives and IEDs. The 2-D electro-optic imaging technique generates a beam width of maximum 10mm square. This means that it generates 10,000 data points or pixels to be probed for the presence of IEDs. Without the preprocessing stage it is necessary to perform spectral unmixing (stage 2) for the 10000 data points, then analyze the spectra contained in each, compare each extracted spectrum with the library spectrum of explosives and then ascertain the presence of IEDs and the trace explosives in the field. This is very ineffective as it involves processing data from the areas which have no probability of any explosive. The preprocessing stage on the other hand reduces the data to only the hotspots as shown in the figure which have considerable probability of explosives to be present within them.
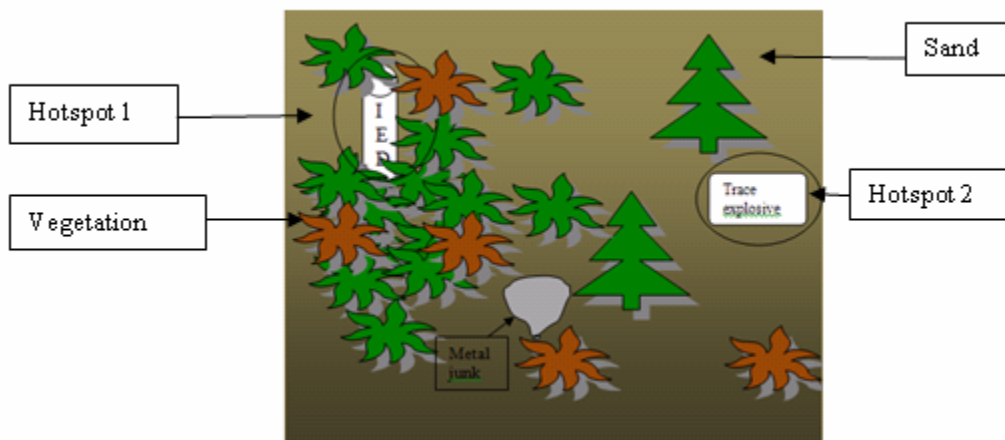
Figure 4.2 Field with IEDs and other materials

Thus, the 10000 data points are reduces to say 100 data points.Now the unmixing stage has to process only 100 data points instead of the 10000. Thus, this stage can reduce a considerable burden on the further stages, help in real time detection and in wide area surveillance.

4.2 UNMIXING OF COMPOSITE SPECTRA USING IMPROVED ICA

The stage of correlation filtering described in Section 4.1 filters out all the areas that have no probability of any explosive content and selects areas or hotspots which could contain some explosives hidden in them. All the pixels/data points in these areas are selected for further processing in stage 2. This section describes the stage 2 of the detection algorithm. This stage unmixes the pixels/data points selected in the preprocessing stage. It needs to be determined which explosives are present along with their precise location. A THz spectra received by the THz receiver from the field is a mixture of THz responses of all the substances present in the field. These substances may include rocks, soil, vegetation, plastic or leather covers and possible explosives. The explosive spectra (if present) needs to be separated out from the composite received spectrum in order to accurately detect presence of IEDs.

Spectral unmixing is the procedure by which the measured spectrum of a mixed pixel is decomposed into a collection of constituent spectra, or endmembers, and a set of corresponding fractions, or abundances, that indicate the proportion of each endmember present in the pixel. There are various algorithms for spectral unmixing. Some of the commonly used for the purpose are Least Square Methods [72], Principal Component Analysis [73], Independent Component Analysis (ICA) [74-79] and Kalman Filtering [80-81]. Out of these ICA is a very well developed algorithm for spectral unmixing. ICA finds a linear transform in which the transformed components are mutually independent or as independently as possible. Also, ICA blindly separates all the components in the mixture whether they are of interest or not. It would be very ineffective to analyze all of the separated spectra like that of soil and rocks and try to find out if there are any explosive spectra among them. Instead it would be better to separate out only the explosive spectra if present in a given pixel. Also, the THz spectra of the commonly found explosives are available from the THz spectral library. These explosive spectra can be used as a-priori information to the ICA algorithm so that it separates out only the explosive spectra if present in the pixel. Such an improved version of the ICA algorithm which separates out only the desired spectra from a composite mixture is discussed in this section. The section begins by explanation of the original ICA algorithm and then the improved version of ICA for detection of IEDs is discussed.

4.2.1 Independent Component Analysis. Independent component analysis, or ICA, is a statistical technique that represents a multidimensional random vector as a linear combination of nongaussian random variables ('independent components') that are as independent as possible.

Assume that n linear mixtures $x_1,...,x_n$ of n independent components,

$$x_j = a_{j1}s_1 + a_{j2}s_2 + ... + a_{jn}s_n \text{ for all j} \tag{4.9}$$

Using the vector-matrix notation, the above mixing model is written as,

$$x = As \tag{4.10}$$

The starting point for ICA is the very simple assumption that the components s_i are statistically independent and have nongaussian distributions. After estimating the matrix A, its inverse can be computed, say W, and obtain the independent component simply by:

$$s = Wx \qquad (4.11)$$

Here W is known as the unmixing matrix. W = [w_1 w_2 … w_n] contains n weight vectors w_j = (w_{j1} w_{j2} … w_{jn})^T which need to be learned in the algorithm.

Principles of ICA estimation:
1: ``Nongaussian is independent"

The key to estimating the ICA model is nongaussianity. The Central Limit Theorem, a classical result in probability theory, tells that the distribution of a sum of independent random variables tends toward a gaussian distribution, under certain conditions. Thus, a sum of two independent random variables usually has a distribution that is closer to gaussian than any of the two original random variables.

Assuming that the data vector x is distributed according to the ICA data model i.e. it is a mixture of independent components. For simplicity, assume that in this section that all the independent components have identical distributions. To estimate one of the independent components, a linear combination of the x_i is considered and is denoted by,

$$y = w^T x = \sum_i w_i x_i \qquad (4.12)$$

where w is a vector to be determined. If w were one of the rows of the inverse of A, this linear combination would actually equal one of the independent components. In practice, such a w cannot be determined exactly, because there is no knowledge of matrix A, but an estimator can be found that gives a good approximation.

Define $z = A^T w$. Then,

$$y = w^T x = w^T As = z^T s \qquad (4.13)$$

y is thus a linear combination of s_i, with weights given by z_i. Since a sum of even two independent random variables is more gaussian than the original variables, $z^T s$ is more gaussian than any of the s_i and becomes least gaussian when it in fact equals one of the s_i. In this case, obviously only one of the elements z_i of z is nonzero.

Therefore, taking w as a vector that maximizes the nongaussianity of $w^T x$. Such a vector would necessarily correspond (in the transformed coordinate system) to a z which has only one nonzero component. This means that $w^T x = z^T s$ equals one of the independent components.

2: Measure of Non-gaussianity

Kurtosis

The kurtosis of y is classically defined by,

$$kurt(y) = E\{y\} - 3(E\{y^2\})^2 \qquad\qquad (4.14)$$

Since it is assumed that y has unit variance,

$$kurt(y) = E\{y^4\} - 3 \qquad\qquad (4.15)$$

In practice, the algorithm would start from some weight vector w, compute the direction in which the kurtosis of $y = w^T x$ is growing most strongly (if kurtosis is positive) or decreasing most strongly (if kurtosis is negative) based on the available sample x(1),…,x(T) of mixture vector x, and use a gradient method or one of their extensions for finding a new vector w. The example can be generalized to arbitrary dimensions, showing that kurtosis can theoretically be used as an optimization criterion for the ICA problem.

Negentropy

Negentropy is based on the information-theoretic quantity of (differential) entropy. The entropy of a random variable can be interpreted as the degree of information that the observation of the variable gives. The more ``random'', i.e. unpredictable and

unstructured the variable is, the larger its entropy. Entropy H is defined for a discrete random variable Y as,

$$H(Y) = -\sum_i P(Y = a_i) \log P(Y = a_i) \tag{4.16}$$

where a_i are possible values of Y. A fundamental result of information theory is that a gaussian variable has the largest entropy among all random variables of equal variance is used in ICA. The term Negentropy J defined as,

$$J(y) = H(y_{gauss}) - H(y) \tag{4.17}$$

where y_{gauss} is a Gaussian random variable of the same covariance matrix as y. Negentropy is always non-negative, and it is zero if and only if y has a Gaussian distribution.

The fast ICA algorithm can be summarized as follows:
1. Center the data;

2. Whiten the data;

3. Choose an initial (e.g. random) weight vector w;

4. Update weight W by $\hat{W} = E(Xg(W'X)) - E(g'(W'X))W$

5. Normalize weight: $W = \hat{W} \Big/ \| \hat{W} \|$

6. If not converged, go back to step 4.

where g() is a nonquadratic function, e.g., $g_1(x) = \tanh(a_1 x)$, $g_2(x) = y\exp(-y^2/2)$

The above algorithm is for finding one component. To find multiple independent components, a deflation technique is needed after each step. After having searched p independent components, inserting the following step right after step 5 in the above algorithm:

1. Let $W_{p+1} = W_{p+1} - \sum_{j=1}^{p} W_{p+1}{}^T W_j W_j$

2. Let $W_{p+1} = \dfrac{W_{p+1}}{\| W_{p+1} \|}$

4.2.2 Improved ICA (ICA with Reference). The ICA algorithm described above separates out all the constituents in a given composite spectra. Theoretically it can extract components equal to the number of mixtures or observations given to it. For wide area surveillance of IEDs using the electro-optic imaging method [25-27] large number of data points/pixels are generated and these need to be analyzed for the presence of IEDs. Using the traditional ICA algorithm will require additional processing to identify the target spectra from the large number of separated spectra. Also, with so many separated components it is very easy to miss out on the target spectra. Thus, for the purpose of IED detection the traditional ICA algorithm leads to redundant components, requires large memory for estimating unnecessary signals and degrades the quality of recovered signals which can lead to increased error in detecting IEDs.

Hence, it is proposed to use a variant of the traditional ICA algorithm called ICA with reference [82] for the purpose of IED detection. The ICA with reference algorithm uses the framework of the constrained ICA algorithm [83-84]. The cICA incorporates additional requirements and prior information in the form of constraints in the ICA contrast function. Using this framework the ICA with reference algorithm is designed to extract a desired subset of ICs and discard the rest of the components as irrelevant signals. This algorithm has to be given a-priori information about the signals that need to be extracted from the composite mixture. These a-priori signals are known as reference signals. In the case of IED detection the THz spectra of commonly used explosives in IEDs are available from the THz spectral library. These can use this as a-priori information to the ICA algorithm so that it will separate out only the target spectra and ignore all other spectra. The fundamentals of the optimization theory used in this algorithm are given in the Appendix 1.

The cICA algorithm imposes constrains of the a-priori information on the ICA algorithm and solves this as a constrained optimization problem [85]. The method of Lagrange multipliers [86] is adopted to search for the optimal solution. The algorithm computes ICs that are subsets of ICs mixed in the input data and the estimated ICs are

closest to the corresponding reference signals given as a-priori information to the algorithm.

Computation of one IC: Suppose that the contrast function of ICA is given by the negentropy function $J(y)$ defined by equation (4.2.9) having m solutions $w_i (i = 1,...,m)$ corresponding to each independent source. The closeness between the estimated output y and the reference r is measured by a norm, $\varepsilon(y,r)$. Assuming that there is only one IC closest to the reference signal r, the inequality can be written as,

$$\varepsilon(w^{*T} x, r) < \varepsilon(w_1^T x, r) \leq ... \leq \varepsilon(w_{m-1}^T x, r) \tag{4.18}$$

where the optimum vector w^* corresponds to the desired output. A threshold ξ is defined such that the closeness $\varepsilon(y,r)$ is less than or equal to it. i.e. $g(w) = \varepsilon(y,r) - \xi \leq 0$, only when $y = w^{*T} x$ but not with any other weight matrix w. The negentropy in equation (4.2.9) can be written as,

$$L(w, \mu, \lambda) = J(y) - \frac{1}{2}[\max^2 \{\mu + \gamma g(w), 0\} - \mu^2] - \lambda h(w) - \frac{1}{2}\gamma \|h(w)\|^2 \tag{4.19}$$

where ρ is a positive constant, $G(\square)$ is a non-quadratic function and υ is a Gaussian variable having zero mean and unit variance. The constrained optimization problem is to maximize the equation (4.2.11) subject to the constraints

$$g(w) \leq 0, h(w) = E\{y^2\} - 1 = 0 \tag{4.20}$$

The equality constraint $h(w)$ ensures the contras function $J(y)$ and weight vector w are bounded. To convert the inequality constraint into an equality constraint a slack variable z is introduced to get,

$$g(w) + z^2 = 0 \tag{4.21}$$

Thus, the Lagrangian function $L(W, \mu, \lambda, z)$ is given by

$$L(W, \mu, \lambda, z) = J(y) + \mu^T \bar{g}(w) + \frac{1}{2}\gamma \| \bar{g}(w) \|^2 + \lambda^T h(w) + \frac{1}{2}\gamma \| h(w) \|^2 \quad (4.22)$$

where $\mu = (\mu_1, \mu_2, \dots, \mu_i)^T$ is the Lagrange multiplier for inequality constraint and $\lambda = (\lambda_1^T, \lambda_2^T, \dots, \lambda_i^T)^T$ is the Lagrange multiplier for equality constraint. The first derivative of the Lagrangian function in equation (4.2.14) with respect to w is given by,

$$L'_w = \bar{\rho}E\{xG'_y(y)\} - \frac{1}{2}\mu E\{xg'_y(w)\} - \lambda E\{xy\} \quad (4.23)$$

where $G'_y(y)$ and $g'_y(w)$ are first derivatives of $G(y)$ and $g(w)$ with respect to y as y is a function of w. The second derivative of the Lagrangian function is approximated as a product of a scalar value and input covariance,

$$L''_{w^2} = s(w)R_{xx} \quad (4.24)$$

Where the scalar $s(w)$ and covariance matrix R_{xx} are given by,

$$s(w) = \bar{\rho}E\{G''_{y^2}(y)\} - \frac{1}{2}\mu E\{g''_{y^2}(w)\} - \lambda \quad (4.25)$$

$$R_{xx} = E\{xx^T\} \quad (4.26)$$

The weight vector w is updated by the following formula,

$$w_{k+1} = w_k - \eta R_{xx}^{-1} L'_{w_k} / s(w_k) \quad (4.27)$$

The Lagrange multipliers are found iteratively by following equations.

$$\mu_{k+1} = \max\{0, \mu_k + \gamma g(w_k)\}$$
$$\lambda_{k+1} = \lambda_k + \gamma h(w_k) \quad (4.28)$$

Thus, the weight vector is updated and output is computed till it is close enough to the given reference.

Computation of multiple ICs: When more than one ICs are desired and a reference signal is available corresponding to each, the above algorithm can be easily extended for the same. The problem of multiple ICs is:

$$\text{Maximize} \qquad \sum_{i=1}^{l} J(y_i)$$

$$\text{subject to} \qquad g(W) \leq 0, h(W) = 0$$

where l is the desired number of ICs

The weight vector is updated in a similar way for each reference signal to compute the corresponding output.

Thus, the improved ICA algorithm can separate out one or many desired components and discards rest of the components. This algorithm will separates out components which are as close as possible to the references provided. In case the target spectrum is not present in the composite mixture, the algorithm still separates out a component. But, the separated component will be different as compared to the target spectra. Hence, to decide if the separated component is the target spectrum or not, the separated component is passed through a final correlation filtering stage similar to one discussed in Section 4.1. If the separated component is the target spectrum then the correlation filters produce an output with peaks greater than the threshold else the peaks are less than the threshold. Thus, it can be accurately detected if the target is present in a given composite spectra.

5: SIMULATION OF DETECTION ALGORITHM WITH EXPLOSIVE DATA

In this section the simulation of the detection algorithm is performed using explosive THz data of RDX and TNT. Due to lack of THz equipment actual data could not be obtained. Hence, the explosive spectra were taken from published papers [61, 67].

5.1 PRE-PROCESSING STAGE FOR RANDOM CONTENT OF RDX

As described in section 4.1, the preprocessing of THz data using correlation filters is done for rapid processing of data and reduction of computational time. Before doing the simulations it is necessary to set the threshold for the correlation filter depending on the desired accuracy.

5.1.1 Threshold for the Correlation Filters. As discussed in Section 4.2, the threshold of the correlation filters depends on the probability of error and is given by the following equation.

$$P(\check{c}[m,n] \geq R_0) = 2erfc(\sqrt{-2\ln(1-R_0)}) \qquad (5.1)$$

where R_0 is the threshold, $\check{c}[m,n]$ is the correlation peak magnitude, P is the error probability and erfc is the complimentary error function. Following simulations are done for an error probability of 0.2 for which the threshold R_0 can be computed to be 0.491. Thus, if the output of the correlation filters produce a positive peak exceeding R_0 then that pixel has a significant probability of the target to be present. Such pixels are chosen for further preprocessing to ascertain the presence of the target material.

Two methods of correlation filtering were proposed for the preprocessing stage in Section 4.1.2. In Method 1 the filters correlate the entire target spectrum covering the entire frequency range. In Method 2 a characteristic feature of the target spectrum like a peak or valley that occur at specific frequencies are correlated. To demonstrate these two methods of correlation filtering consider a field with 100 data points/pixels as shown in Figure 5.1. These data points/pixels are evenly spread in the field and are of three types as mentioned below.
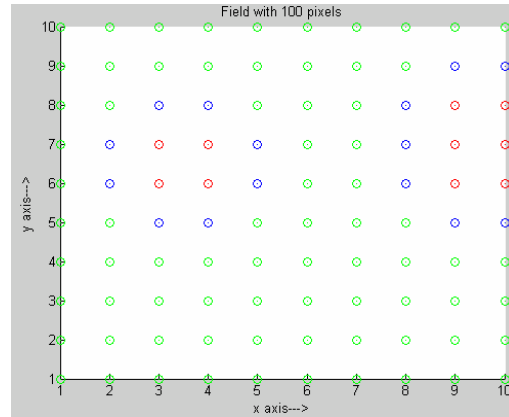
Figure 5.1. A field with 100 pixels

o: Type 1, o:Type2, o: Type3

Type 1: Pixels in red. These pixels contain a combination of varying proportion of RDX (target spectrum) and noise.

Type 2: Pixels in blue. These pixels contain a combination of RDX, and THz spectra of few other materials like calcite, etc mixed in varying proportions with noise. Also, the content of RDX in the type 1 and type 2 pixels is varied randomly for this set of experiments.

Type 3: Pixels in green. These pixels do not contain the target spectrum of RDX, instead it contains spectra of three other materials in varying combination with noise.

The objective of the preprocessing stage is to detect and select for further processing all type 1 and type 2 pixels which contain the RDX spectrum.

5.1.2 Method 1. Here the correlation filters are built to correlate the entire RDX spectrum covering its entire frequency range of 0.1 THz to 2.4 THz.

Results for Type 1 pixels

Figure 5.2 shows the spectrum of RDX (target spectrum) which has to be detected. The characteristic absorbance peak at 0.8 THz is clearly visible. Figure 5.3 shows the signal from the sample received by the THz detector.
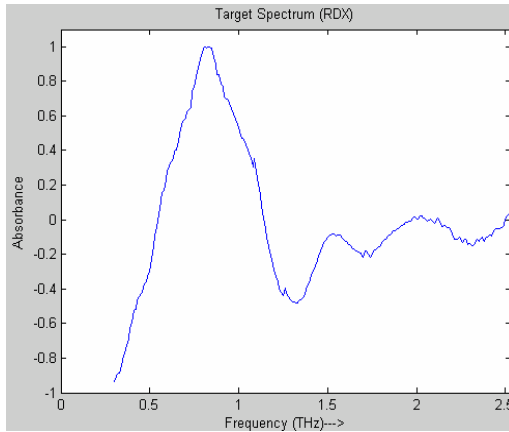
Figure 5.2. RDX spectrum   Figure 5.3. RDX spectrum affected by noise
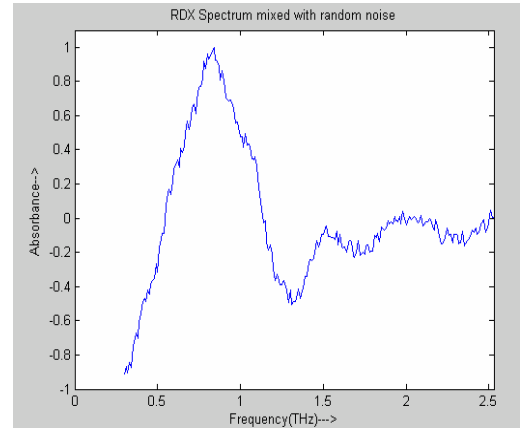
The noise added in the spectrum may be due to the environmental factors like moisture, dust, etc present in the air between the sample and the measuring equipment. The spectrum in Figure 5.3 is the input to the correlation filter. Figure 5.4 shows the output of the correlation filter. There is a positive correlation peak centered at the origin and it exceeds the threshold R_0. This indicates the presence of the target spectrum in the received signal.
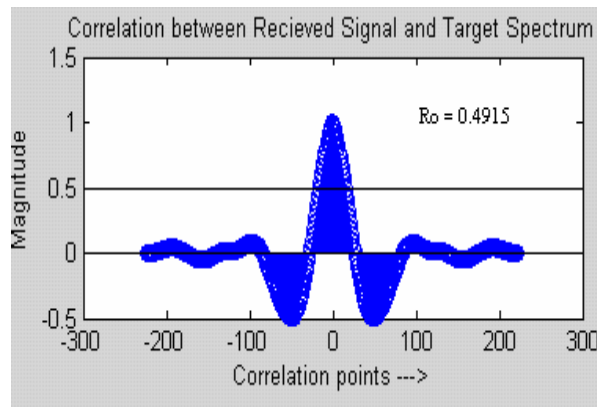
Figure 5.4. Correlation filter output

Results for Type-2 pixels

        These pixels contain a combination of the target spectrum i.e. RDX and spectra of few other substances mixed in a random proportion. Simulations for known proportions are also done later. Shown below are results for one such pixel. Figure 5.5 is the spectrum of RDX which is to be detected and Figure 5.6 is the spectrum from the type-2 pixel.
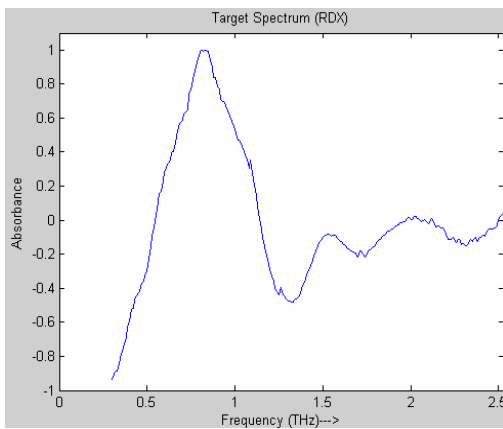
Figure 5.5. RDX spectrum
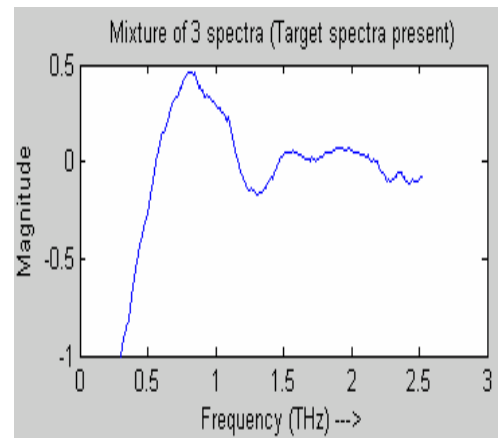
Figure 5.6. Spectrum from type-2 pixel

        Figure 5.7 shows effect of noise on the spectrum in Figure 5.6 as it travels from the sample to the detector. Figure 5.8 is the correlation filter output which shows a positive correlation peak at the origin with a magnitude of 0.6145 which exceeds the threshold R_0 indicating that the spectrum of RDX is present in the received composite spectrum.

        Thus, this type-2 pixel has a significant probability of RDX being present in it and is selected for further processing.
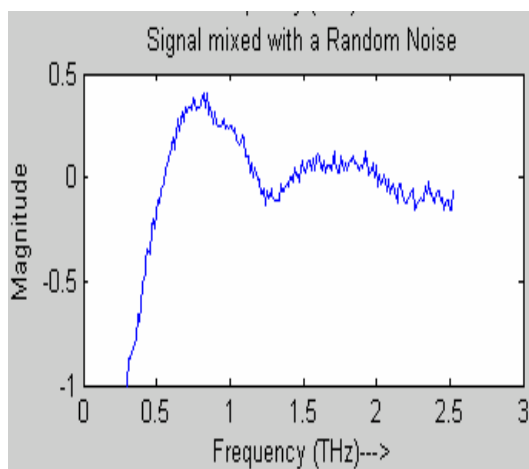
Figure 5.7. Spectrum affected by noise
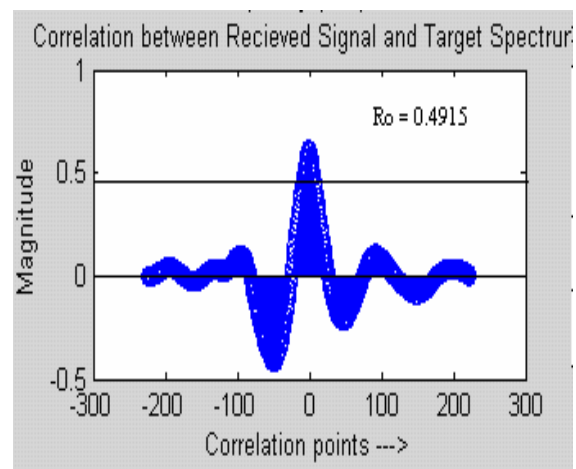
Figure 5.8. Correlation filter output

Type-3 pixel

These pixels do not contain the target spectrum i.e. RDX spectrum. Instead they contain spectra of three other substances in varying proportions and noise. Figure 5.9 shows a spectrum for a type-3 pixel and Figure 5.10 shows the spectrum affected by noise.
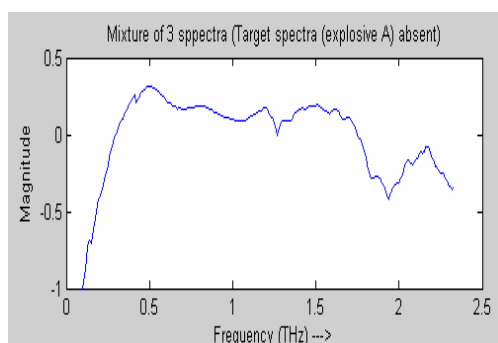
Figure 5.9. Spectrum from type-3 pixel
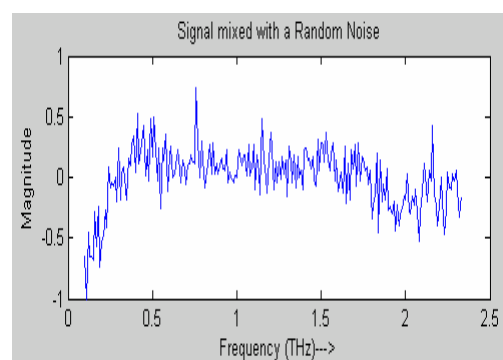
Figure 5.10. Spectrum affected by noise

Figure 5.11 shows the correlation filter output where it is seen that none of the positive correlation peaks exceeds the threshold R_0. Hence, it can be concluded that such pixels do not have any probability of explosive content and are discarded.
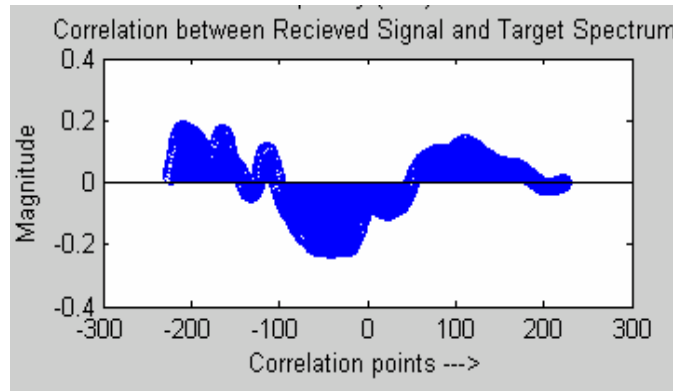
Figure 5.11. Correlation filter output

The above simulations were performed for each of the 100 pixels in Figure 5.1. Figure 5.12 shows the result of the simulations for an error probability of 0.2.
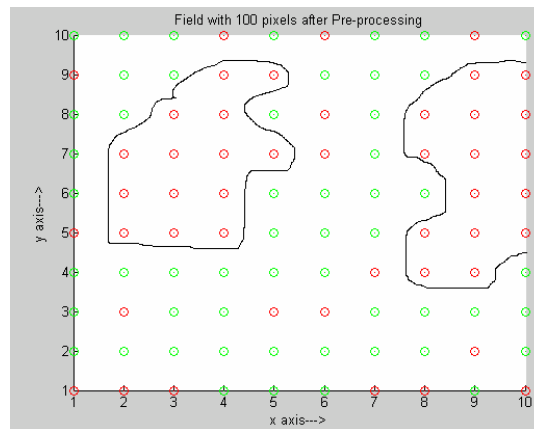
Figure 5.12. Field with selected pixels after preprocessing

Red dots indicate presence of RDX and green dot indicates its absence. Thus, the field reduces to hotspots where RDX could be present. There are a few false positives i.e. pixels which do not contain RDX but are still selected but most of the type-3 pixels are eliminated as they contain no RDX spectrum. Also, there are few false negatives i.e. pixels which have the target spectrum but are not selected but their number can be reduced by reducing the threshold R_0.

The error probability of the correlation filters is varied form 0.1 to 0.25 to observe the effects in number of pixels correctly detected and pixels missed. The results are summarized in Table 5.1 and plotted in Figure 5.13.

Table 5.1. Results of preprocessing stage (Method 1) for RDX spectrum

Error Prob	Threshold R_0	Pixels	Target present in	Target absent in	False positive	False Negative (Type-1 pixels)	False Negative (Type-2 pixels)
0.05	0.7152	100	25	75	0	0	7
0.10	0.6172	100	25	75	2	0	4
0.15	0.5473	100	25	75	14	0	3
0.20	0.4915	100	25	75	21	0	2
0.25	0.4448	100	25	75	30	0	1
0.30	0.4043	100	25	75	38	0	0
0.35	0.3687	100	25	75	42	0	0

Figure 5.13 shows the variation of false positives and false negatives with the error probability.
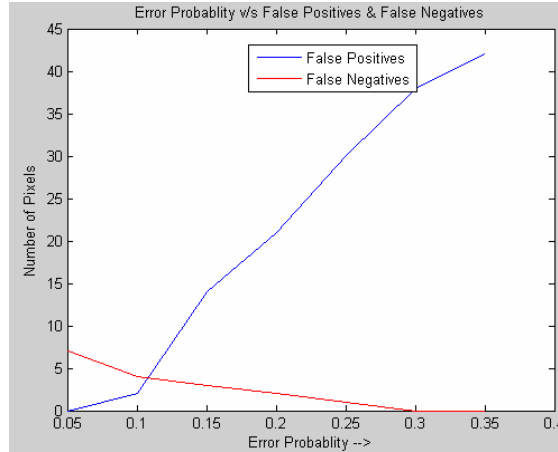
Figure 5.13 Variation of FP & FN with error probability

From Table 5.1 and Figure 5.13 it can be seen that as the error probability is increased i.e. threshold of the correlation filter decreases the number of false negative pixels decreases but at the same time the false positives increase sharply. Thus, depending on the desired accuracy the error probability of threshold can be predetermined.

5.1.3 Method 2. Each substance has a characteristic spectrum in the THz region and can be detected by the occurrence of its characteristic features in the received spectrum e.g. RDX shows a strong absorption peak at 0.8 THz. In this method target spectrum (RDX) is detected using its characteristic feature i.e. the dominant absorption peak occurring at 0.8 THz instead of detecting the entire spectrum. Figure 5.13 shows the spectrum of RDX and the characteristic peak at 0.8 THz spectrum is shown in detail in Figure 5.14. The occurrence of this peak at the same frequency in the received spectrum indicates the presence of RDX in the received spectrum. The algorithm checks the magnitude of the peak as well as the frequency at which it occurs. If the peak exceeds the pre chosen threshold R_0 and occurs around 0.8 THz then the pixel corresponding to that spectrum is selected for further processing.

a. Complete RDX spectrum | b. Dominant peak in RDX
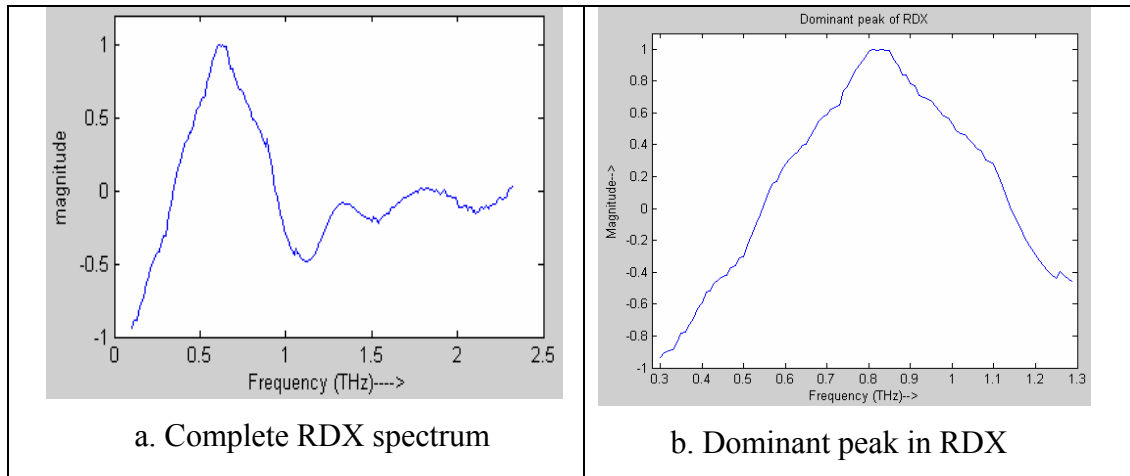
Figure 5.14. RDX spectrum

Similar to the first method, consider a field (Figure 5.15) with 100 data points with three types of pixels as before.
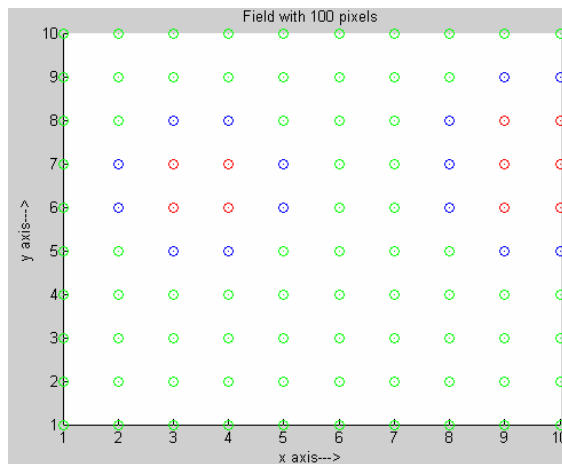
Figure 5.15. Field with 100 pixels

o: Type-1, o:Type-2, o: Type-3

Thus, the purpose of the algorithm is to detect as many type-1 and type-2 pixels and eliminate as many type-3 pixels as possible. Shown below are results for correlation filtering with an error probability of 0.2 for each type of pixel.

Results for Type-1 pixels

Figure 5.16 shows the spectrum from one of the type-1 pixels and Figure 5.17 shows the noise corrupted spectrum. Spectrum in Figure 5.17 is received by the THz detector.
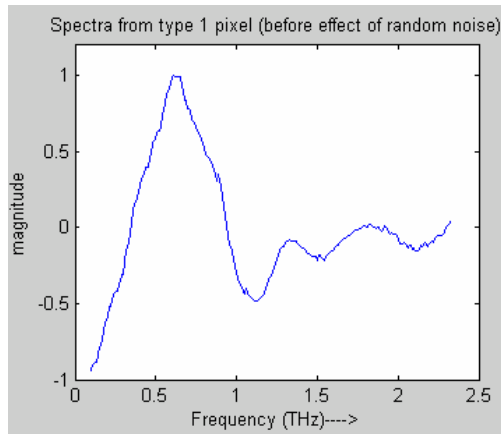
Figure 5.16. RDX spectrum   Fig 5.17. RDX spectrum affected by noise
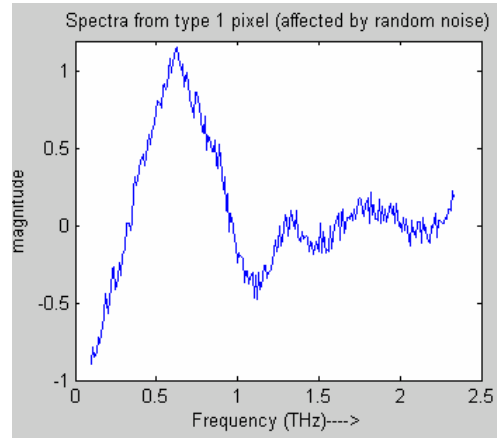
Figure 5.18 shows the output of the correlation filter when the spectrum in Figure 5.17 is the input. It is seen that there is a correlation peak that exceeds the threshold R_0 at exactly the same frequency as characteristic peak (Figure 5.14) occurs in the target spectrum (Figure 5.13) indicating the presence of the peak at that frequency. Thus this pixel is selected for further processing in the unmixing stage.
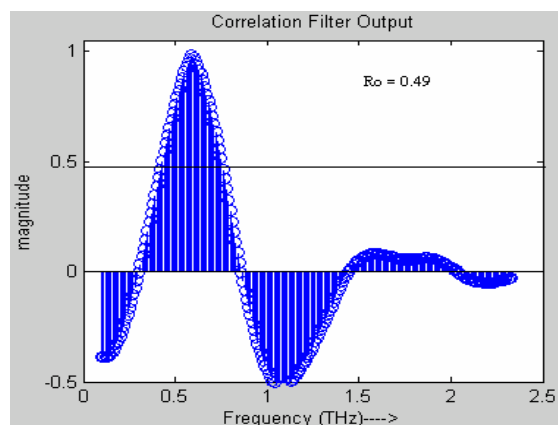
Figure 5.18. Correlation filter output

Type-2 pixels

Figure 5.19 shows the composite spectrum from the sample in the field. This is a mixture of RDX spectrum, and spectra of few other substances. Figure 5.20 shows the effect of noise on the received spectrum. This spectrum is the input to the correlation filter.
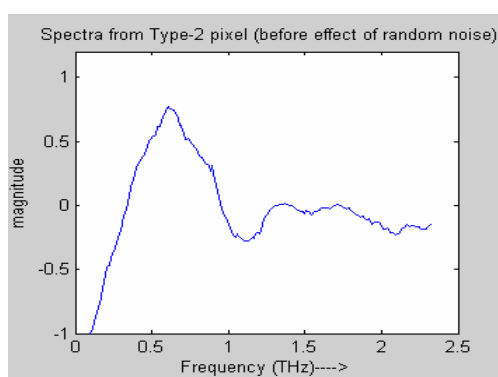
Figure 5.19. Spectrum from type-2 pixel
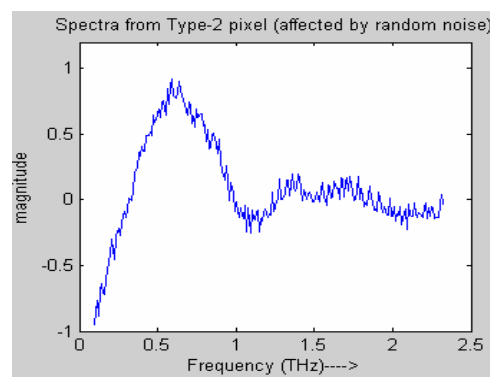
Figure 5.20. Spectrum with noise

Figure 5.21 shows the output of the correlation filter which shows a positive correlation peak that exceeds the threshold R_0 at a frequency of 0.8 THz. Hence, it can be concluded that the received composite spectrum contains a peak similar to the peak of RDX at a frequency of 0.8 THz.
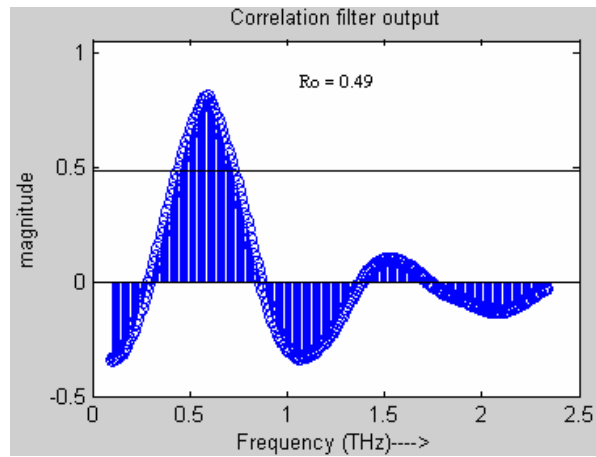
Figure 5.21. Correlation filter output

Type-3 pixel

Such pixels do not contain the target spectrum of RDX. One such pixel spectrum is shown in Figure 5.22 and this spectrum after being affected by noise in the environment is shown in Figure 5.23. Figure 5.24 shows the output of the correlation filter with the spectrum in Figure 5.23 at its input. From this figure it is seen that none of the positive correlation peaks exceed the threshold R_0. Hence, it can be concluded that the received spectrum does not contain a peak similar to the target spectrum at any frequency. Even if a type-3 pixel produces a output with a peak exceeding the threshold at some other frequency it is not selected as the preprocessing algorithm checks both the magnitude of peak and frequency at which it occurs. All Such pixels are discarded by the correlation filters thus reducing the computational burden in the second stage.
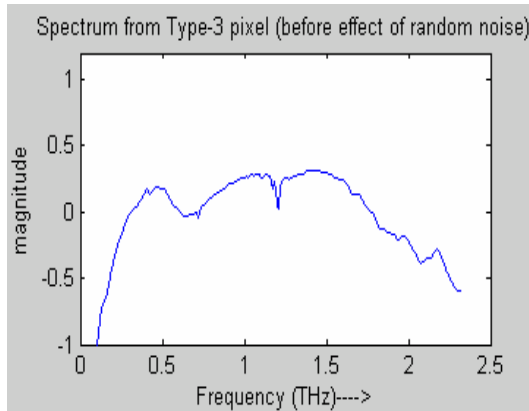
Figure 5.22. Spectrum from type-3 pixel
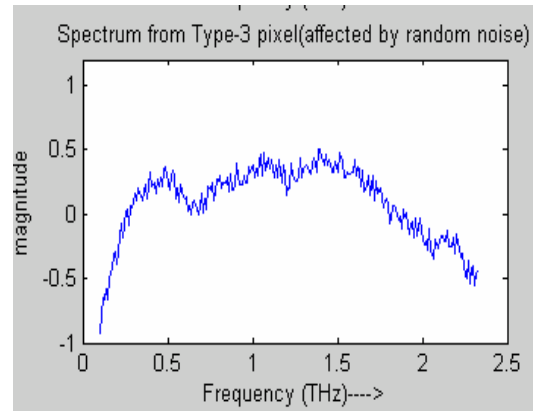
Figure 5.23. Spectrum with noise
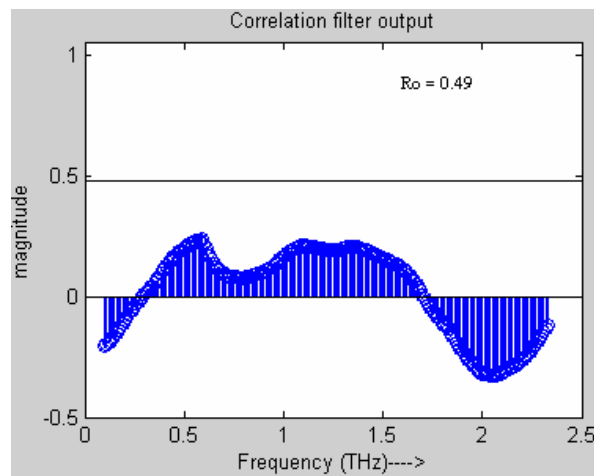
Figure 5.24. Correlation filter output

Thus, the above simulations were performed for each of the 100 pixels in Figure 5.15. Figure 5.25 shows the result of the simulations for correlation filters with an error probability of 0.2 corresponding to a threshold of $R_0 = 0.4915$. Red dots indicate presence of IED and green dot indicates its absence. The field reduces to hotspots (areas with red pixels) and all pixels within these areas have a significant probability of the target spectrum to be present. All selected pixels are given to the second stage for further

processing. From Figure 5.25 it can be seen that all of the type-1 pixels and most of the type-2 pixels are selected. Few type-2 pixels that are not selected are called false negatives and the type-3 pixels that are selected are called false positives.
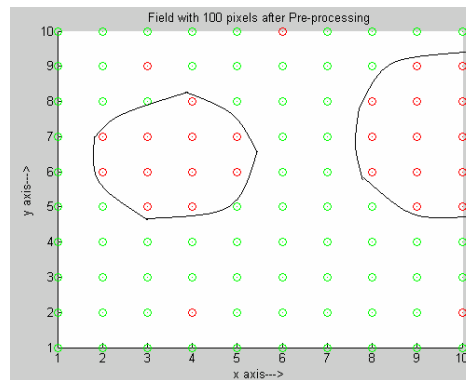
Figure 5.25. Field with selected pixels after preprocessing

The error probability of the correlation filters was varied from 0.1 to 0.25 to evaluate the performance of the preprocessing stage. The results are plotted in Figure 5.26 and summarized in Table 5.2.
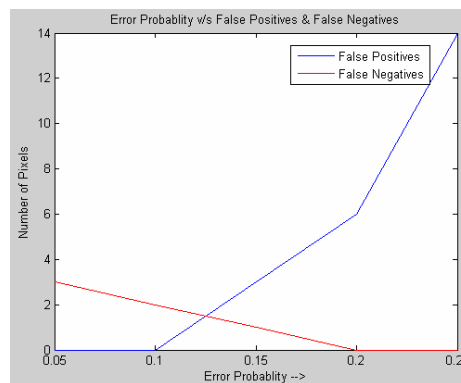
Figure 5.26. Variation of FP & FN with error probability

Table 5.2. Results of preprocessing stage (Method 2) for RDX spectrum

Error Prob	Pixels	Target present in	Target absent in	False positive	False Negative (Type 1 pixels)	False Negative (Type 2 pixels)
0.05	100	25	75	0	0	3
0.10	100	25	75	0	0	2
0.15	100	25	75	3	0	1
0.20	100	25	75	6	0	0
0.25	100	25	75	14	0	0

After the preprocessing stage with correlation filters having error probability 0.2, only 48 (all red dots) out of the 100 pixels are selected for further processing as they have some probability of the target spectrum being present. Table 5.2 along with Figure 5.26 shows the variation of the false positives and negatives with the error probability. It is seen that as the error probability increases the threshold for detection will decrease. Hence, the number of false negatives decreases but at the same time false positives increase sharply.

The correlation filters detect the presence of the target spectra or a characteristic peak in it. It is possible to vary the error probability hence the threshold of detection to reduce the number of false negatives at the cost of a few false positives. Also, the correlation filters have shift invariance due to which they detect the frequency at which a characteristic feature in a spectrum occurs. Based on these simulations, it is seen that if a given spectrum produces a correlation exceeding the threshold then it can be concluded that it contains the target spectrum. Once it is identified that a given pixel contains the target, it is chosen for further processing to determine its exact spectral content. Due to this stage, there is a reduction in the number of pixels or data points to be given to further processing stages. Thus, this stage avoids processing huge amount of data from the scene

at further stages in the detection process and reduces the area to hotspots where the target could be present.

5.2 UNMIXING STAGE FOR RANDOM CONTENT OF RDX

In Section 5.1 simulation of the preprocessing stage for random content of RDX in the pixels is presented. In this section unmixing of all the pixels selected by the preprocessing stage is performed. These pixels have a significant probability of RDX to be present within them. The stage of unmixing by the improved ICA algorithm is used to ascertain which pixels have the target present and which do not with maximum accuracy hence eliminating all the false positives. The unmixing algorithm used is the improved ICA algorithm discussed in Section 4.2 and it separates only the required spectra. The unmixing algorithm is performed for both types of filters of the preprocessing stage i.e. ones which use the entire target spectrum and ones which use a characteristic feature. The entire RDX spectrum or a characteristic feature is given as reference to the improved ICA algorithm. The improved ICA algorithm separates the spectrum of RDX if present in a pixel for each of the pixels selected by the preprocessing stage. The separated spectra form each of the pixels is given to a final correlation filtering stage designed to detect the target with maximum accuracy.

5.2.1 Unmixing of Data from Method 1 Filters. These filters discussed in Section 4.1.2 correlate the entire target spectrum. Figure 5.27 shows the actual location of the target i.e. type-1, type-2 and type-3 pixels within the field and Figure 5.28 shows the hotspots in the field separated by the pre-processing stage with filters that detect the entire target spectrum. These hotspots contain pixels that have significant probability of RDX to be present within them and spectrum from these pixels has to be unmixed in this stage. The unmixing algorithm takes the spectrum from each pixel as the input and computes a spectrum as close as possible to the RDX spectrum. A spectrum is computed by the unmixing algorithm irrespective of whether the input spectrum contains the RDX spectrum or not.

The RDX spectrum (Figure 5.29) acts as a reference input to the ICA algorithm and spectra from all the pixels marked in red in Figure 5.28 are given as an input to the improved ICA algorithm. Spectra from one pixel of each type are shown in Figure 5.30
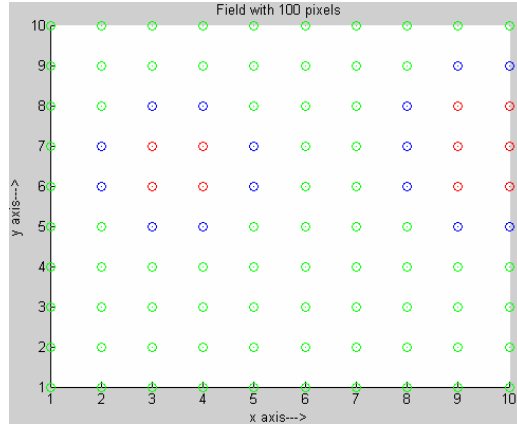
Figure 5.27. Field with 100 pixels   Figure 5.28. Field after preprocessing
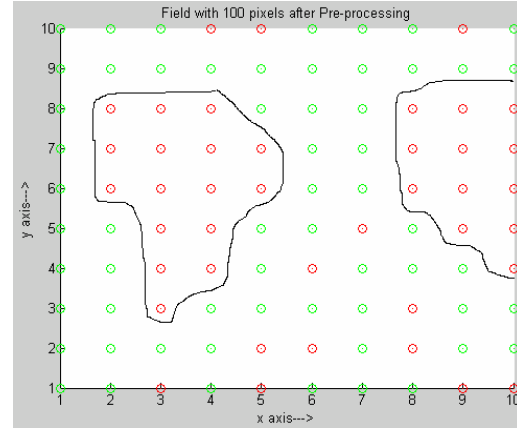
o: Type-1, o:Type-2, o: Type-3

The RDX spectrum (Figure 5.29) acts as a reference input to the ICA algorithm and spectra from all the pixels marked in red in Figure 5.28 are given as an input to the improved ICA algorithm. Spectra from one pixel of each type are shown in Figure 5.30 a, b, c.

Figure 5.29. RDX spectrum

a. Spectrum from Type-1 pixel b. Spectrum from Type-2 pixel

c. Spectrum from Type-3 pixel
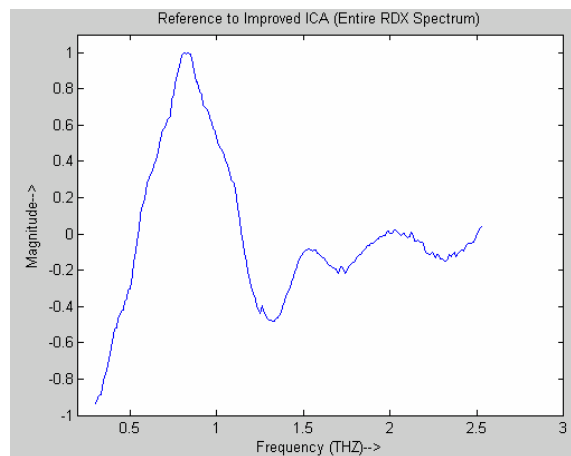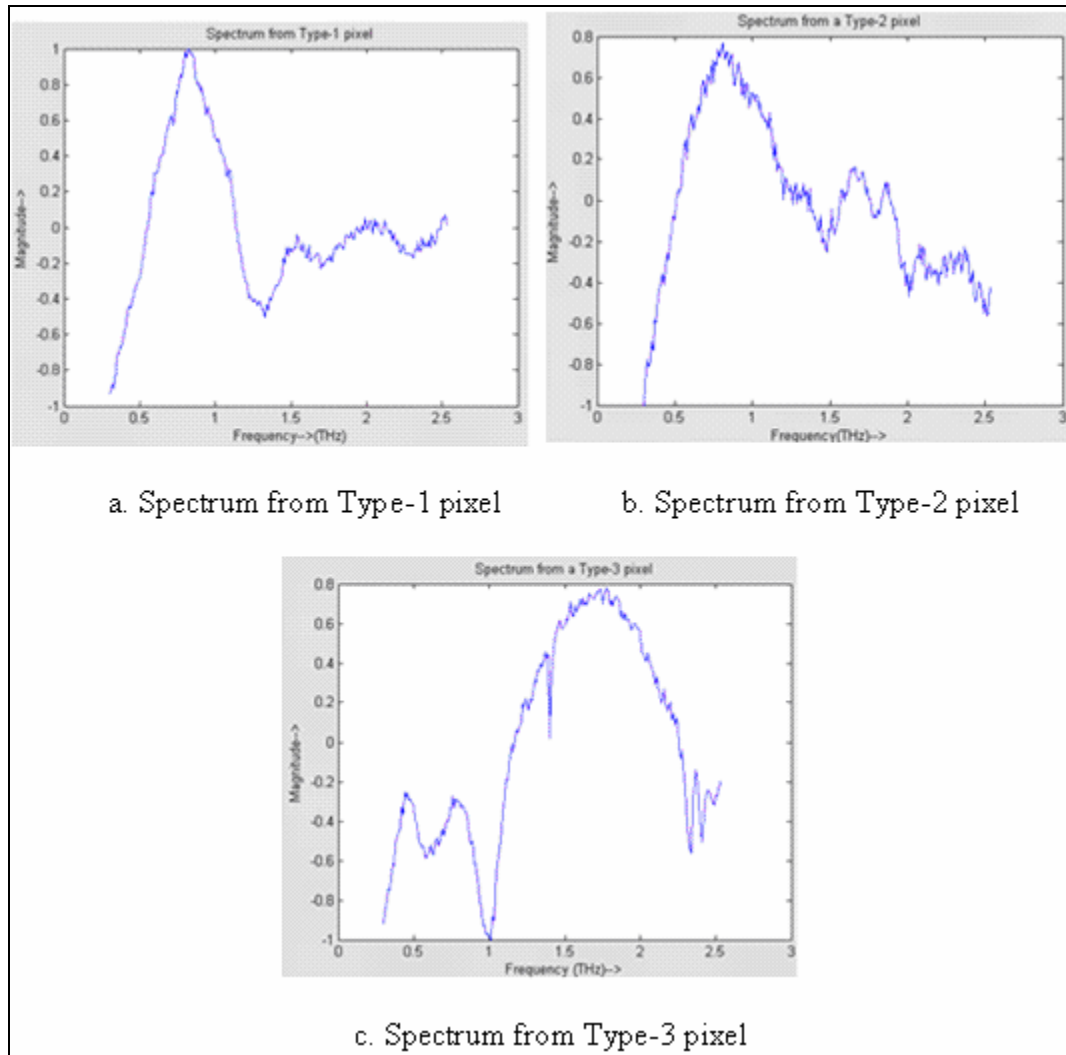
Figure 5.30. Inputs to improved ICA

For each composite spectrum given to it, the improved ICA algorithm separates outs a spectrum which is as close as possible to the RDX spectrum. The separated spectrum from each type of pixel is shown in Figure 5.31a, b, c. It can be seen from this figure that spectra from type-1 and type-2 pixels closely resembles the RDX spectrum while the separated spectrum from type-3 pixels is some arbitrary spectrum having no resemblance to the RDX spectrum.

a. Output from Type-1 pixel

b. Output from Type-2 pixel

c. Output from Type-3 pixel
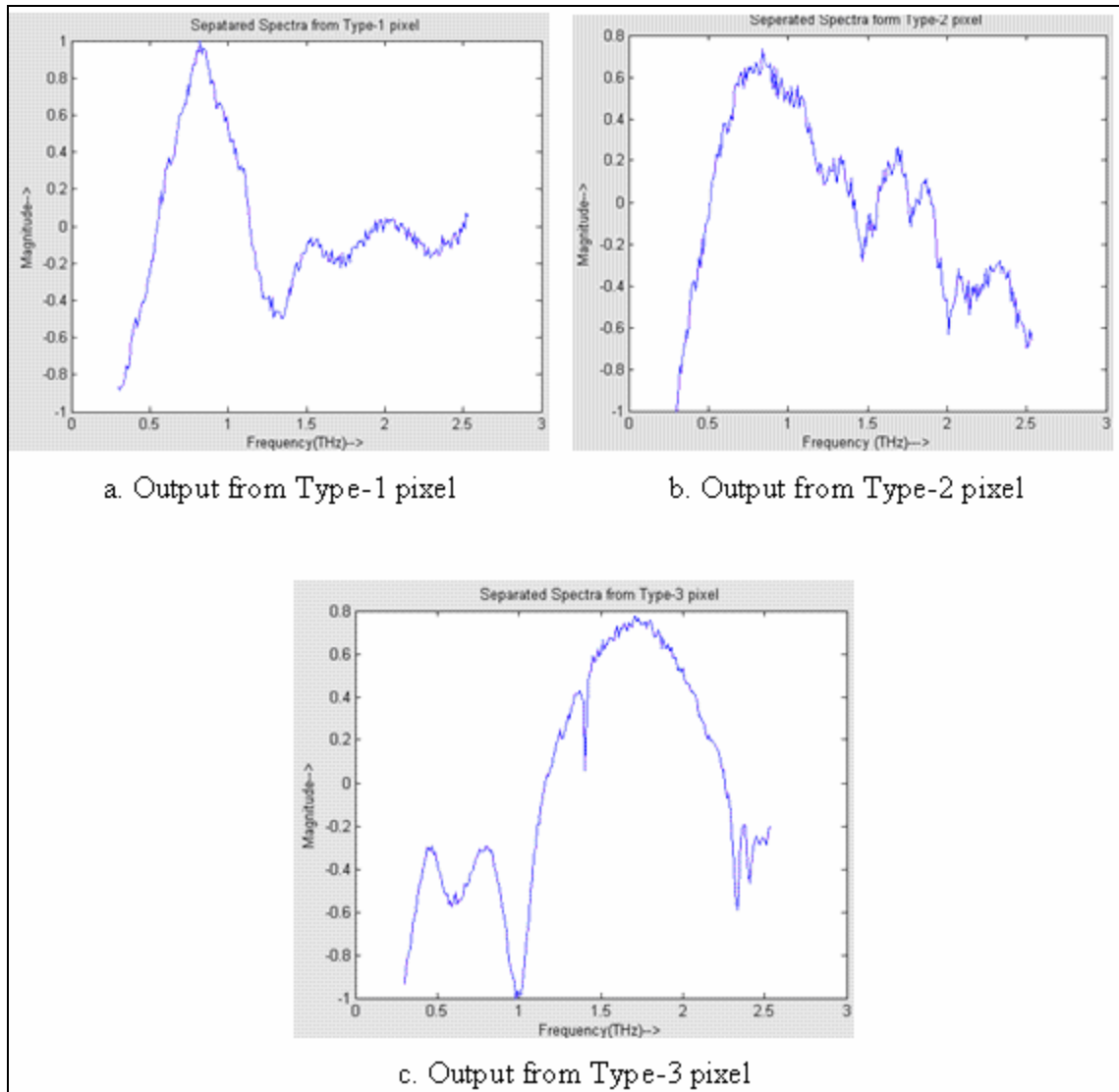
Figure 5.31. Outputs of improved ICA

To make a final decision about which pixels have the target and which do not, the separated spectrum from each pixel is given to a correlation filter designed to detect the RDX spectrum. Figure 5.32 shows the correlation filter output for each pixel type. It can be seen that type 1 and 2 pixels have a high correlation peak which is above the threshold for this filter while peaks of the type-3 pixels are below the threshold.
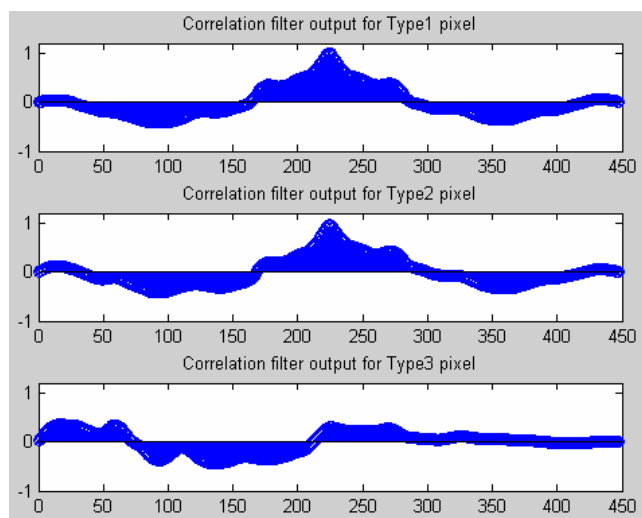
Figure 5.32. Correlation filter output

Figure 5.33 shows the field before and after unmixing. It can be seen that nearly all of the false positives have been eliminated and there are no additional false negatives.

| a Pixels after preprocessing | b Detected pixels containing the target |
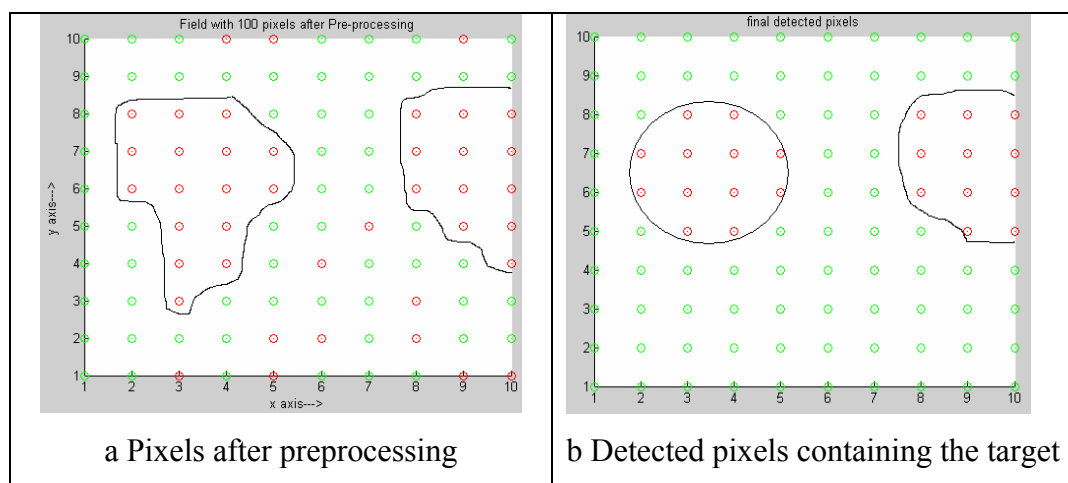
Figure 5.33. Field before and after unmixing

Thus, the unmixing algorithm gives an accurate detection of the RDX in the field. The accuracy of the algorithm can be adjusted by changing the error probability of the correlation filters.

5.2.2 Unmixing of Data from Method 2 Filters. This is the second type of filter of the preprocessing stage which correlates a characteristic feature of the target spectrum like a peak or valley. Performance of the unmixing algorithm for data from this type of filter is demonstrated here. Figure 5.34 shows the actual field and field with the hotspots after the preprocessing stage with this type of filters. For this type of filters the false positive rate is very low as they detect a characteristic feature and also check the frequency at which it occurs. From the figure it can be seen that there are no false positives.

| a Actual target locations | b. Selected pixels after preprocessing |
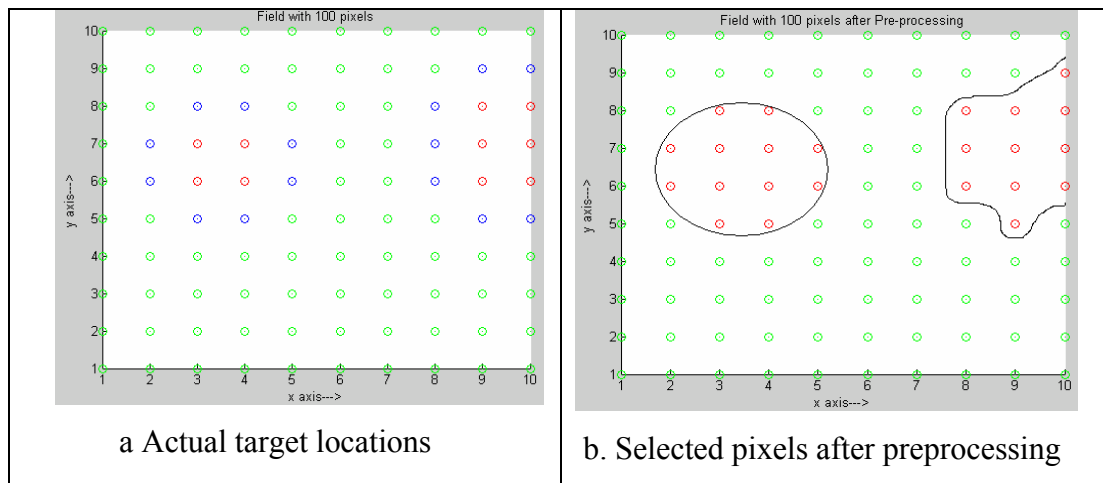
Figure 5.34. Field before and after preprocessing

Although it is seen that there are no false positives by this method, unmixing is performed so that it can be confirmed that all selected pixels have the target spectrum present within them. The unmixing stage performs a more accurate analysis as compared to the preprocessing stage, hence, it would be beneficial in a real life scenario where the

location of the targets is not known. Figure 5.35 shows actual target locations and the detected pixels after the unmixing and final correlation filtering.

| a Actual target locations | b Detected pixels after unmixing |
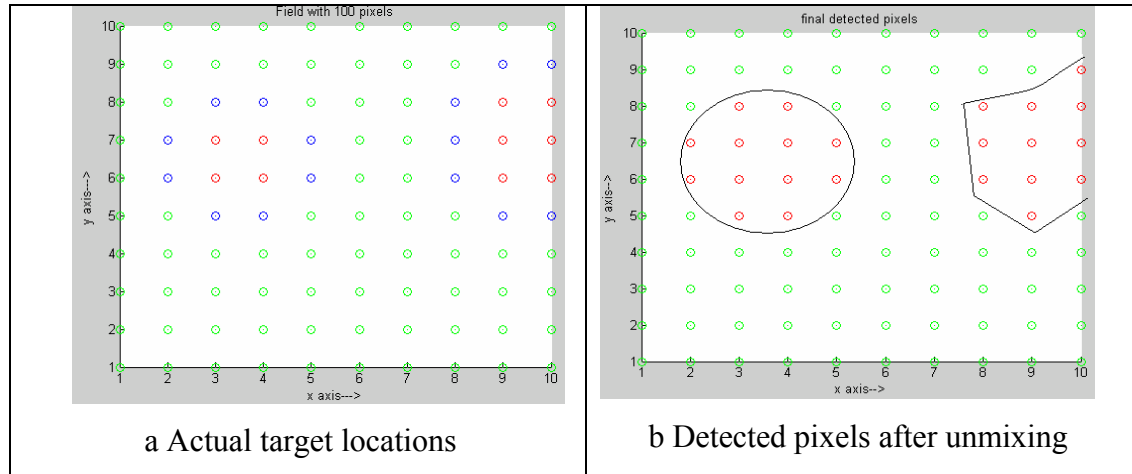
Figure 5.35. Original and final detected pixels

Thus, similar results are seen after the preprocessing stage and after unmixing by improved ICA for this type of filters. But after this stage it can be said with 100% surety that the selected pixels contain the target.

5.3 PREPROCESSING STAGE FOR DETERMINISTIC CONTENT OF RDX

In the simulations of Section 5.1 the content of RDX within a pixel is varied in a random fashion for the hundred pixels. To demonstrate the performance of the preprocessing correlation filters with a deterministic content of the target, the content of RDX in the type-2 pixels is varied from less than one percent to 50 percent. As the content of RDX is varied the threshold R_0 of the correlation filter has to be adjusted accordingly for efficient detection. Thus, the user can choose the threshold depending on the circumstance and desired accuracy of the system. For each chosen value of the threshold i.e. at each error probability value there is a minimum limit of RDX that can be

detected. Only the content of the type-2 pixels is made deterministic whereas the content of the type-1 and type-3 pixels is still varied randomly.

      5.3.1 Performance of Method 1. Consider a field similar to Figure 5.1 with 100 pixels of type-1, type-2 and type-3. The type-1 and type-3 pixels are same as described in section 5.1. The type-2 pixels contain a combination of RDX, and few other substances. The proportion of RDX is varied from less than one percent to 50 percent to determine the minimum detectable content of RDX for each value of threshold and corresponding error probability. Figure 5.36 shows the RDX spectrum which is to be detected.
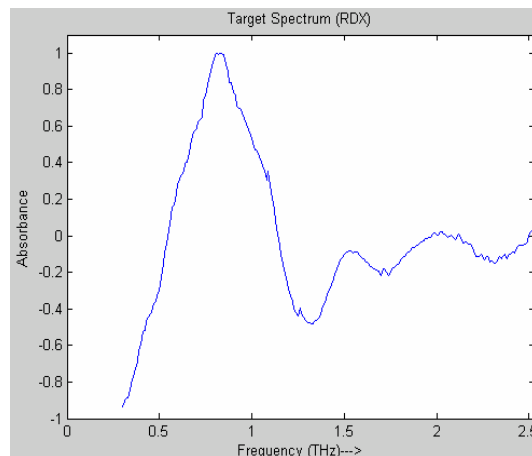
Figure 5.36 RDX spectrum

      Figures 5.37-5.41 show the spectrum from a type-2 pixel with decreasing content of the target on left and corresponding correlation filter output on the right. The content of the target is indicated below each figure. It can be seen that as the content of the target decreases the spectrum looks less like the target spectrum and needs a filter with a higher threshold to detect it. Also, in each case the other minerals present with RDX are randomly chosen to ensure that these minerals do not affect the detection and to simulate a real life scenario where any materials could be present with the target mineral.

a Type-2 pixel. RDX content 52%

b. Correlation filter output
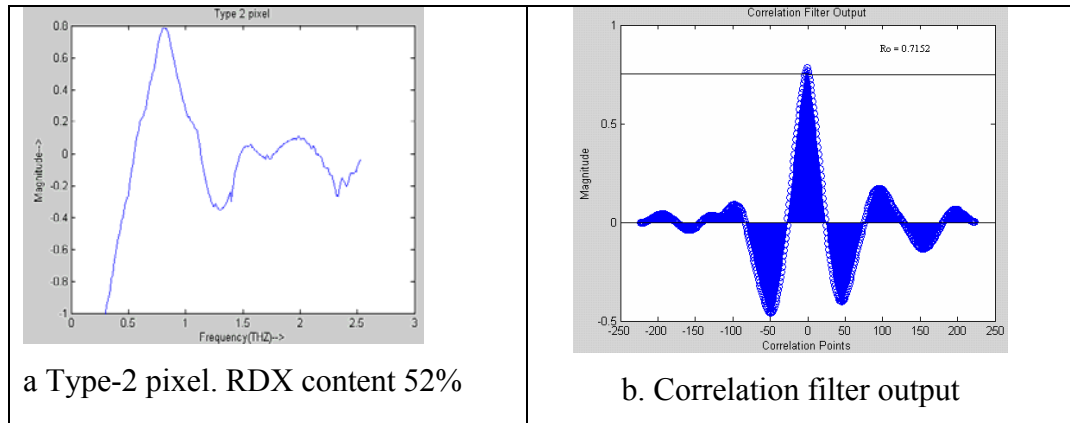
Figure 5.37. RDX spectrum (57%) and its filter output

a Type-2 pixel. RDX content = 40%

b. Correlation filter output
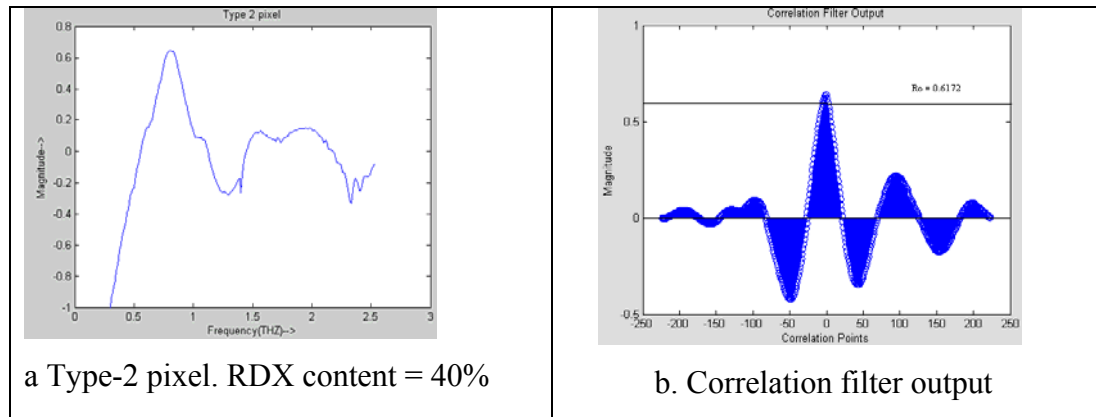
Figure 5.38. RDX spectrum (40%) and its filter output

a Type-2 pixel. RDX content = 29%

b. Correlation filter output
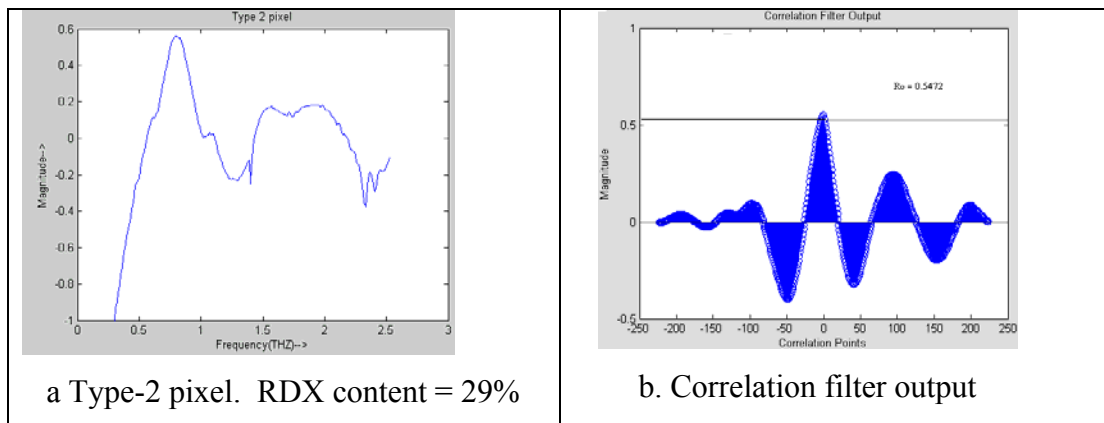
Figure 5.39. RDX spectrum (29%) and its filter output

a Type-2 pixel. RDX content = 22%

b. Correlation filter output
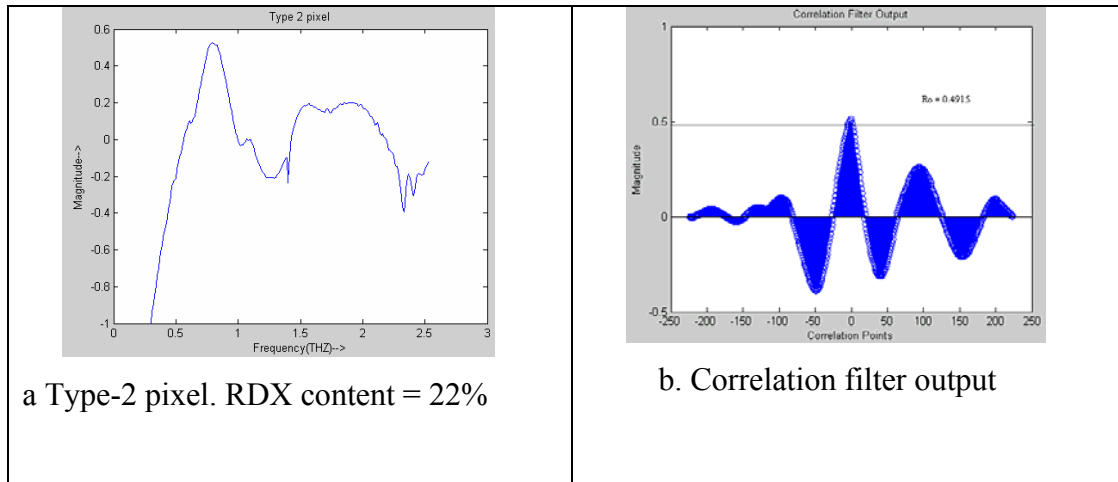
Figure 5.40. RDX spectrum (22%) and its filter output

a Type-2 pixel. RDX content = 14%

b. Correlation filter output
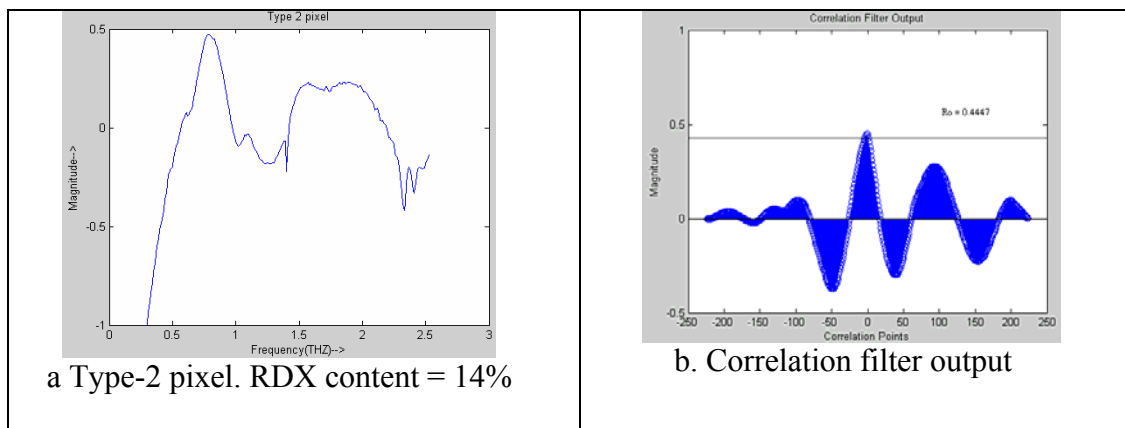
Figure 5.41. RDX spectrum (14%) and its filter output

The results are summarized in Table 5.3. It can be seen that as the percentage of the target reduces, a filter with a lower threshold and higher error probability is needed to detect it. Thus, the user can set the threshold depending on the desired accuracy. Also, as the error probability increases the number of false positives (pixels that do not contain the target but are detected) increase thus increasing the number of pixels selected for further processing.

Table 5.3: Results of preprocessing stage (Method 1) with deterministic content of RDX

Error Probability	Threshold R_0	Minimum % of RDX that can be detected	False Positives
0.01	0.8605	75	2
0.05	0.7152	52	12
0.1	0.6172	40	16
0.15	0.5472	29	20
0.2	0.4915	22	35
0.25	0.4447	14	40
0.3	0.4043	<5	45

5.3.2 Performance of Method 2. Similar simulations were performed for the method 2 where the filters correlate a characteristic feature in the target spectrum instead of the entire target spectrum. Figure 5.42 shows the RDX spectrum and its characteristic peak which is to be detected. This characteristic peak is correlated with the received spectrum. If the correlation filter output has a peak at the same frequency as the frequency in the RDX spectrum where the peak occurs then that pixel can be said to have the RDX pixel present. The percentage of RDX within the type-2 pixels is varied and the results observed.

a Complete RDX spectrum   b Characteristic peak at 0.8 THz
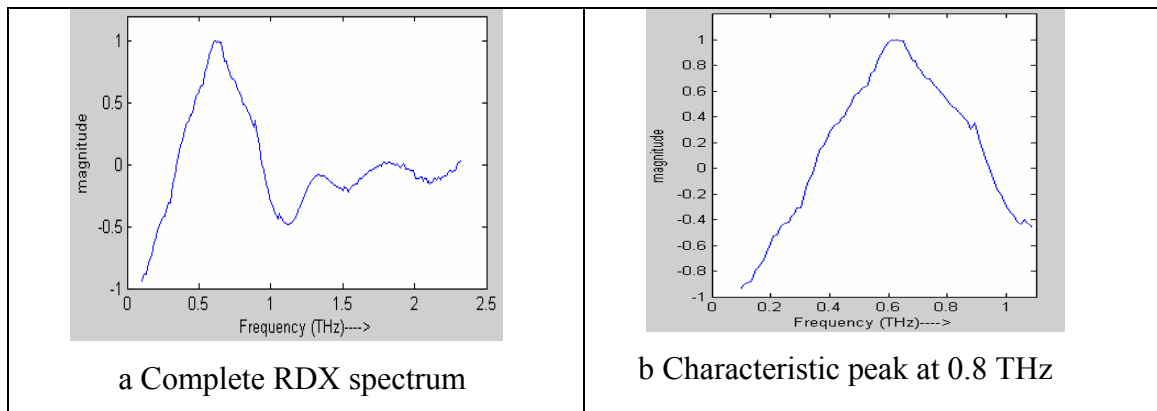
Figure 5.42. RDX spectrum

The results for this case are summarized in Table 5.4

Table 5.4.Results of preprocessing stage (Method 2) with deterministic content of RDX

Error Probability	Threshold R_0	Minimum % of RDX that can be detected	False positives
0.01	0.8605	50	0
0.05	0.7152	20	0
0.1	0.6172	15	0
0.15	0.5472	13	1
0.2	0.4915	10	0
0.25	0.4447	<5	0

Thus, from the above table it can be seen that the performance for feature (peak or valley) correlation is better as compared to the correlation of entire spectra. This kind of correlation filters can detect lesser percentage of RDX at a given threshold or error probability. The reason for this is that these filters look for the absorption peak of RDX around 0.8 THz thus leading to more accurate results. It can also be seen that there are nearly zero false positives for this type of filters. Thus, if the target spectra has prominent features occurring in certain frequency ranges it is recommended to use this type of filters.

5.4 UNMIXING STAGE FOR DETERMINISTIC CONTENT OF RDX

In Section 5.3 an evaluation of the pre-processing stage for deterministic content of RDX is done. It was found that for a given error probability or threshold value the filters can detect a sample data/pixel only if it contains a minimum percentage of RDX. In this section an evaluation of the unmixing stage is done with deterministic content of RDX. The percentage of RDX in the sample data/pixel is varied from 1 percent to 50 percent and the pixel is given to the unmixing algorithm. The unmixing algorithm i.e. the improved ICA algorithm finds a spectrum resembling the reference. The similarity of this spectrum to the reference depends on the content of RDX present in the sample. Thus, as the content of RDX reduces the threshold of the output correlation filters has to be lowered to detect the separated spectrum.

5.4.1 Unmixing of Data from Filters of Method 1. These filters discussed in Section 4.1.2 correlate the entire target spectrum with the spectrum from the sample/pixel. The composite spectra from the selected pixels are given to the unmixing stage where the improved ICA algorithm separates a spectrum similar to the reference provided to it. The RDX content in the composite spectra is varied from one percent to around 50 percent and the separated spectrum is observed. Also, the threshold or error probability of the output correlation filters is computed so that these filters can detect the separated spectrum as RDX spectrum. Figure 5.43 shows the RDX spectrum to be detected. This spectrum also forms the reference input to the improved ICA algorithm.
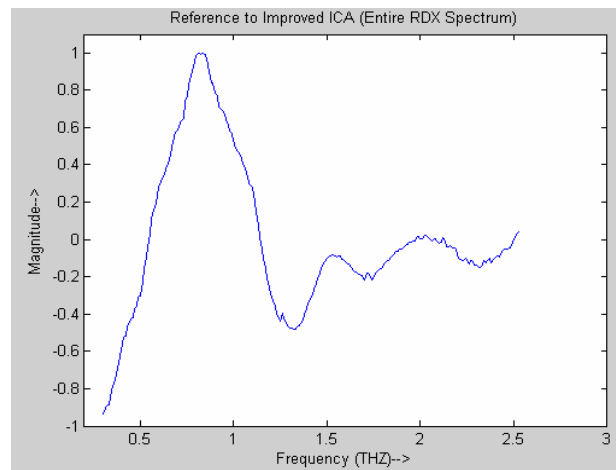
Figure 5.43. RDX spectrum

Table 5.5 shows the error probability of the final correlation filters depending on the percentage of target present in the composite spectra. It can be seen that as the percentage of the target increases the peak value of correlation output also increases and a filter with lower error probability can be used to detect the separated spectrum.

Table 5.5. Results of unmixing stage (Method 1) with deterministic content of RDX

RDX content (%)	Maximum value of Correlation peak of the output Correlation Filter	Error probability of the output Correlation filters
1	0.4432	0.2518
5	0.4376	0.2584
10	0.4706	0.2214
15	0.6482	0.0819
20	0.6774	0.0668
25	0.7553	0.0353
50	0.8783	0.0074

Figures below show the separated RDX spectra and the correlation output for each.

a Type-2 pixel   RDX content = 1%

b Final correlation output
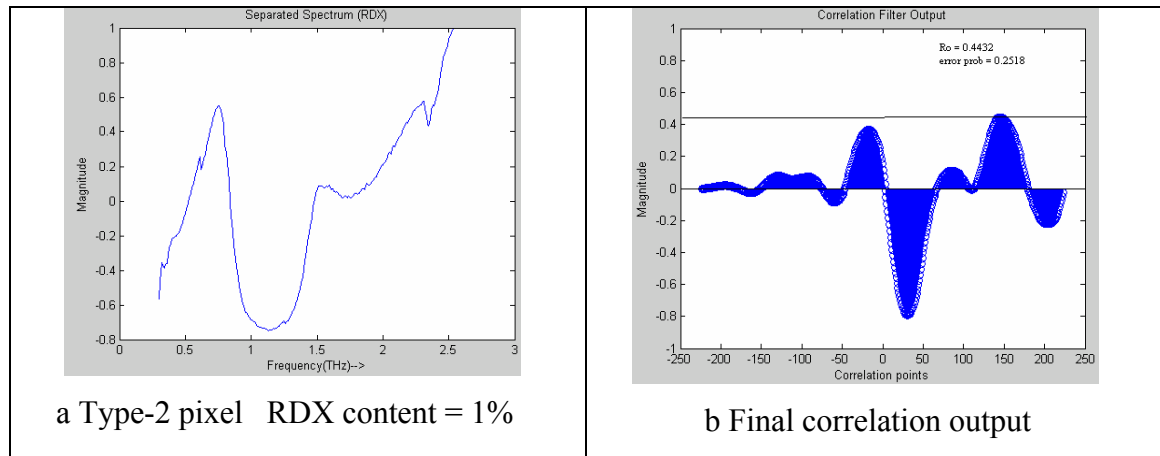
Figure 5.44. Unmixed RDX spectrum and filter output

a Type-2 pixel RDX content = 10% b Final correlation output
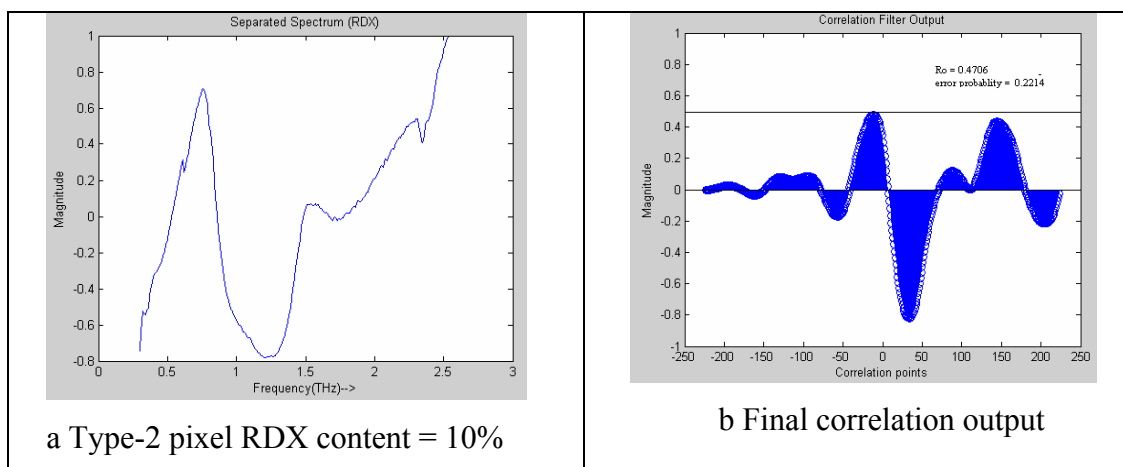
Figure 5.45. Unmixed RDX spectrum and filter output

a Type-2 pixel RDX content = 25% b Final correlation output
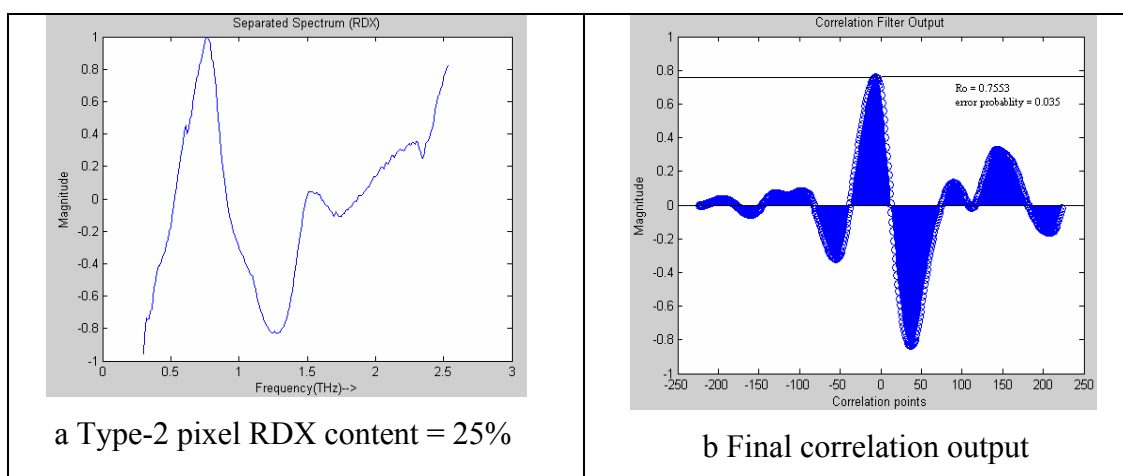
Figure 5.46. Unmixed RDX spectrum and filter output

a Type-2 pixel RDX content = 50% b Final correlation output
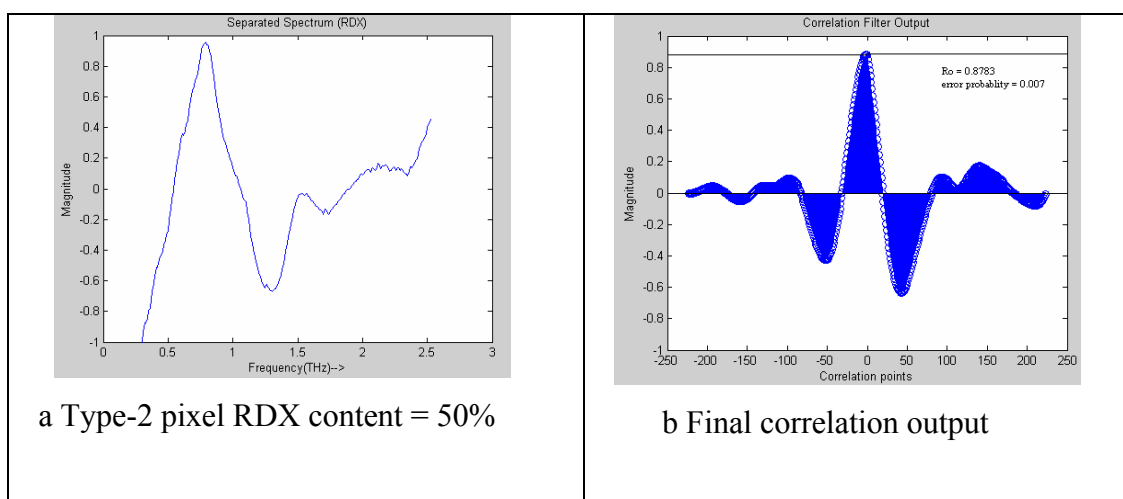
Figure 5.47. Unmixed RDX spectrum and filter output

From Figures 5.44 – 5.47 it can be seen that as the percentage of RDX content in the composite sample given to the unmixing stage increases the separated spectrum looks more and more similar to the RDX spectrum. Also, the final correlation filters which do a correlation of this separated spectrum with the RDX spectrum produces an output with higher peaks thus lowering the error probability of the correlation filters required to detect them.

5.4.2 Unmixing of Data from Filters of Method 2. These filters discussed in Section 4.1.2 correlate a characteristic feature of the target spectrum like the dominant peak of RDX around 0.8 THz with the received spectrum from the sample/pixel. Figure 5.48a shows the RDX spectrum and Figure 5.48b shows the dominant peak at 0.8 THz in detail.

| a. Complete RDX spectrum | b Characteristic peak in RDX |
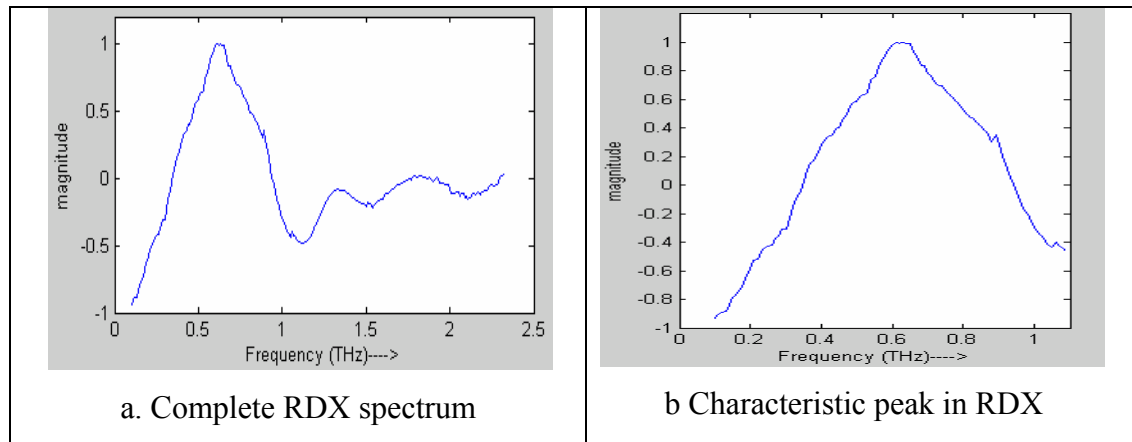
5.48. RDX spectrum

Similar simulations are performed wherein the percentage of RDX in the sample/pixel is varied from one percent to 50 percent and the unmixed RDX spectrum is computed by the improved ICA algorithm. This unmixed RDX spectrum has to be detected by the final correlation stage. The error probability of the final correlation filters is found so that they can accurately detect the unmixed RDX spectrum. Results are summarized in Table 5.6.

Table 5.6 Results of unmixing stage (Method 2) with deterministic content of RDX

RDX content (%)	Maximum value of Correlation peak of the output Correlation Filter	Error probability of the output Correlation filters
1	0.2753	0.5937
5	0.2847	0.4940
10	0.4207	0.2790
15	0.4775	0.2142
20	0.6313	0.0915
25	0.7141	0.0504
50	0.8723	0.0082

The results in the table show that as the percentage of RDX increases the maximum value of the correlation peak also increases. Hence, filters with lesser error probability are needed to detect the RDX spectra.

5.5 PREPROCESSING STAGE FOR A MIXTURE OF RDX AND TNT

In all previous simulations the detection algorithm assumed presence of only one target material to be present within the data samples/pixels. An IED can be made using more than one explosive material hence the performance of the detection algorithm when more than one target materials or explosives is present needs to be evaluated. In this section the performance of the preprocessing stage is evaluated when the data samples/pixels contain a combination of RDX and TNT in a random proportion. Consider a field (Figure 5.49) with 100 data samples/pixels spread evenly. The field contains three types of pixels as before.

Type-1: Pixels in red. These pixels contain a combination of RDX and TNT in randomly varying proportions.

Type-2: Pixels in blue. These pixels contain a combination of RDX, TNT and some other minerals which can be considered as impurities present in the field Again all the spectra are mixed randomly.

Type-3: Pixels in green. These pixels do not contain RDX or TNT but some random spectra of impurities that could be present within the field.
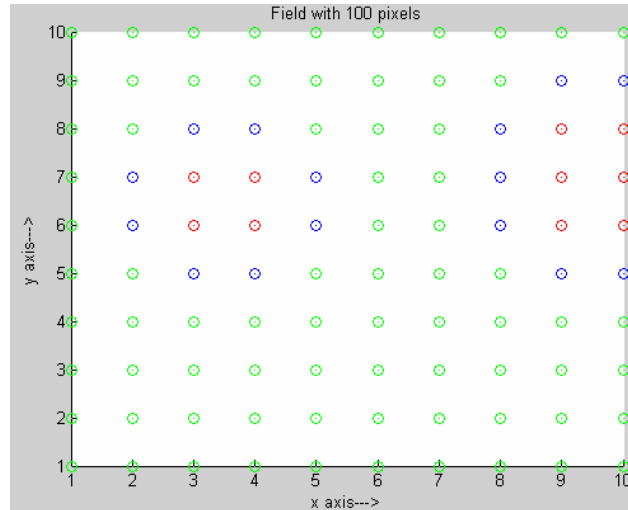
Figure 5.49. Field with 100 pixels

o: Type-1, o:Type-2, o: Type-3

The aim of the preprocessing stage is to select all data samples/pixels that have a significant probability of either RDX or TNT to be present. Hence, the correlation filters of the preprocessing stage are designed to correlate both the RDX and TNT spectrum with the received spectrum.

5.5.1 Performance of Method 1: In this method the entire spectrum of RDX and TNT is correlated sequentially with the received spectrum. If any of the spectrums produce a correlation exceeding the pre-chosen threshold then the data sample/pixel corresponding to it is selected for further processing in the unmixing stage.

Results for Type-1 pixels

These pixels contain only the target spectra affected by noise i.e. RDX and TNT spectra. Figure 5.50a and 5.50b show the spectrum of RDX and TNT, respectively. As the type-1 pixels contain these two spectra the composite spectra as seen in Figure 5.51 is received from these pixels. The spectrum in Figure 5.51 is given to two correlation filters, one for RDX and one for TNT to generate two correlation outputs shown in Figure 5.52a and 5.52b.

a RDX Spectrum | b. TNT Spectrum
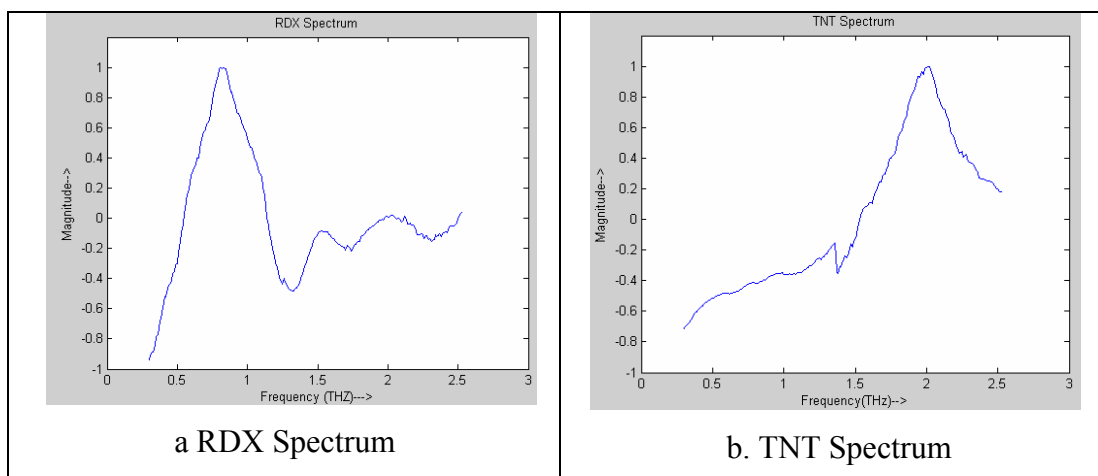
Figure 5.50 Different explosive spectra
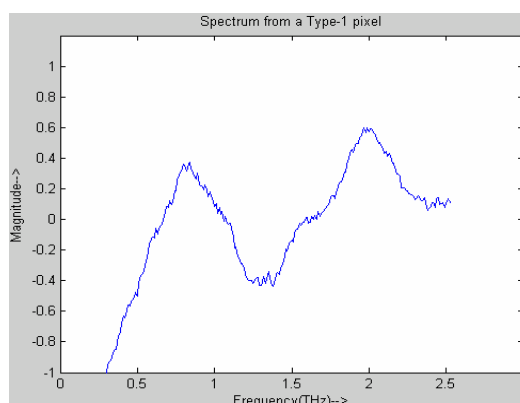
Figure 5.51. Mixture of RDX and TNT spectra

The error probability is chosen to be 0.2 for which the threshold R_0 is 0.4915. As seen in Figure 5.52 both of the correlation outputs produce peaks exceeding the threshold. Hence, this data point/pixel is selected for further processing. The algorithm checks if either one of the correlation outputs has peaks exceeding the threshold hence in this case if only one output had peak exceeding the threshold it would be selected.

Figure 5.52. Correlation filter output

Type-2 pixels

These pixels contain some other spectra along with the RDX and TNT spectra. Figure 5.53 shows a spectrum from a type-2 pixel.
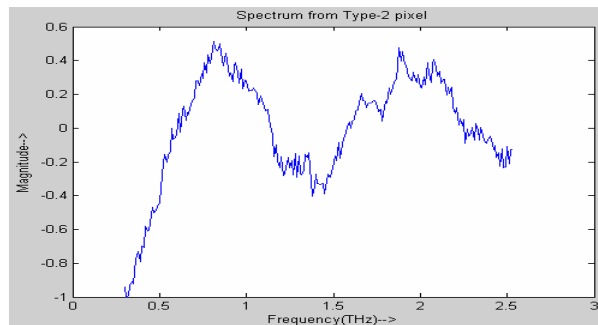
Figure 5.53. Type-2 pixel spectrum

The spectrum in Figure 5.53 is correlated with the RDX and TNT spectra to produce a correlation output for each shown in Figure 5.54.

a Correlation filter output (RDX) | b Correlation filter output (TNT)
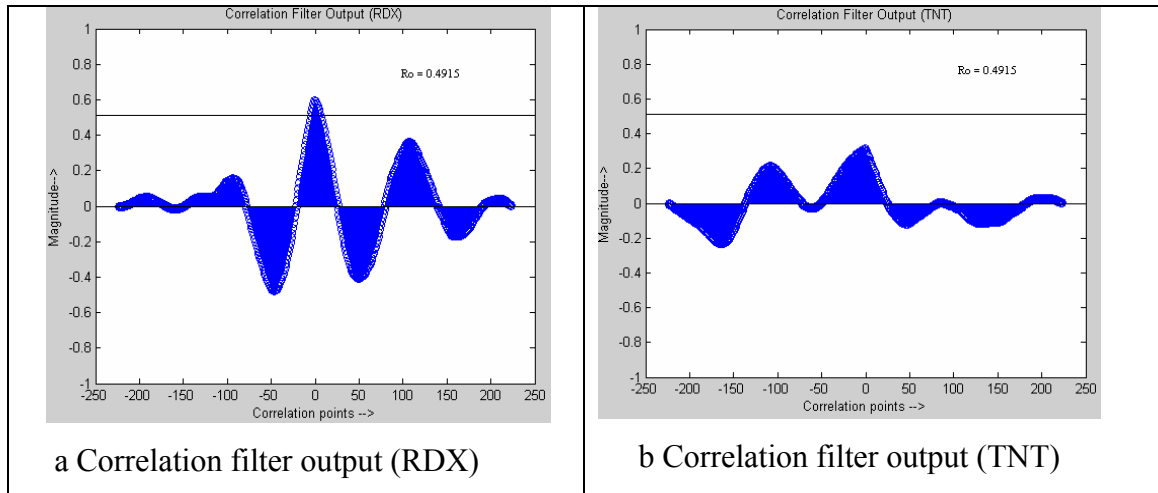
Figure 5.54. Correlation filter output

It can be seen from the Figure 5.54 that the correlation filter output for RDX produces a peak exceeding the threshold R_0 while output for TNT has no peaks exceeding the threshold. The algorithm checks for either one of the outputs producing peaks exceeding the threshold. Hence, this data point/ pixel is selected for further processing.

Type-3 pixels

These pixels do not contain spectra for RDX or TNT but contain some other random spectra. Figure 5.55 shows spectrum from a type-3 pixel.
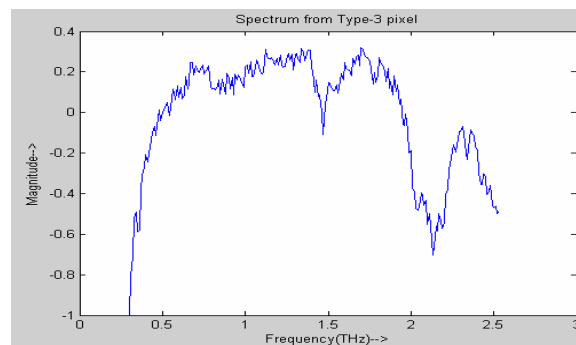
Figure 5.55. Type-3 pixel

The spectrum in Figure 5.55 is correlated with the RDX and TNT spectra to produce a correlation output for each shown in Figure 5.56.

a Correlation filter output (RDX) b Correlation filter output (TNT)
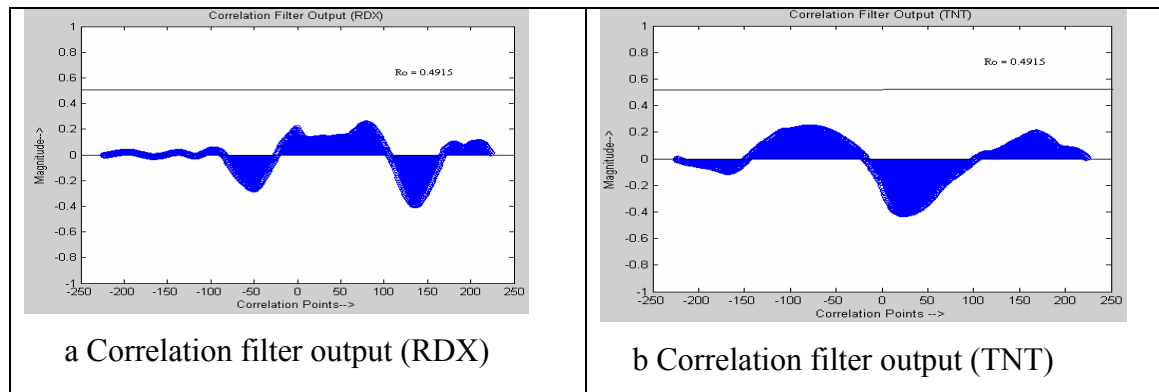
Figure 5.56. Correlation filter output

Thus, it can be seen from Figure 5.56 that none of the correlation output produces a peak exceeding the threshold. Hence, such data points/pixels are discarded. The above simulations were performed for each of the 100 pixels in Figure 5.50. Figure 5.57 shows the result of the simulations for an error probability of 0.2 corresponding to threshold of 0.4915.
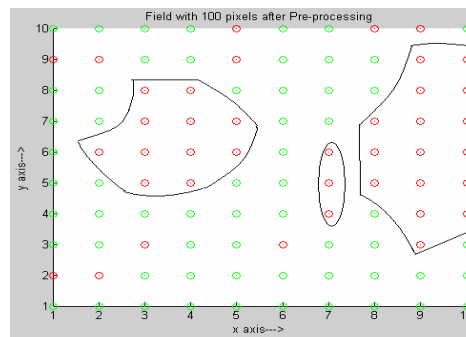
Figure 5.57. Selected pixels after preprocessing

The red dots indicate presence of RDX or TNT and green dot indicates its absence. Thus, the field reduces to hotspots where RDX or TNT could be present. All the pixels/data points within the hotspots are selected for further processing. There are a few false positives i.e. pixels which do not contain the target but are still selected but most of the type-3 pixels are eliminated as they contain no target spectra. Also, there are few false negatives i.e. pixels which have the target spectrum but are not selected but their number can be reduced by reducing the threshold R_0.

Next the error probability of the correlation filters is varied form 0.1 to 0.25 to observe the effects in number of pixels correctly detected number of false negatives and false positives. The results are summarized in Table 5.7.

Table 5.7. Results of preprocessing stage (Method 1) for RDX & TNT spectrum

Error Prob	Pixels	Target present in	Target absent in	False positive	False Negative (Type- 1 pixels)	False Negative (Type- 1 pixels)
0.15	100	25	75	10	0	8
0.16	100	25	75	14	0	7
0.17	100	25	75	17	0	4
0.18	100	25	75	17	0	4
0.19	100	25	75	17	0	4
0.2	100	25	75	17	0	2
0.21	100	25	75	20	0	2
0.25	100	25	75	26	0	1
0.30	100	25	75	27	0	0
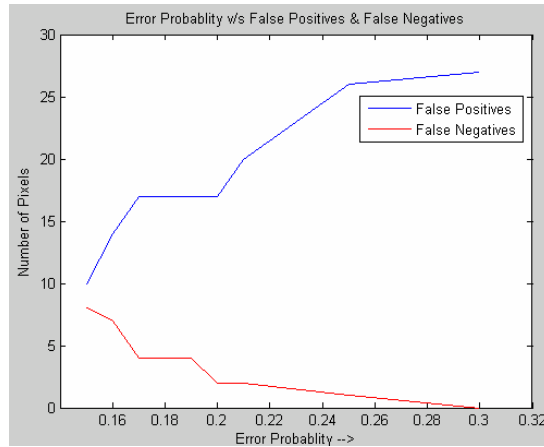
Figure 5.58. Variation of FP & FN with error probability

The Table 5.7 and Figure 5.58 show the variation of the false positives and negatives with the error probability. As the error probability increases the threshold decreases and number of false negatives decreases but at the same time the false positives increases. After the preprocessing stage all pixels/data points (40 out of 100 for case with error probability of 0.2) are selected for further processing as they have significant probability of the target spectrum being present.

5.5.2 Performance of Method 2. In this method RDX or TNT is detected using a characteristic feature in their spectrum like the dominant absorption peak of RDX occurring at 0.8 THz and the dominant absorption peak of TNT around 2 THz. Figure 5.59a shows the spectrum of RDX and the characteristic peak at 0.8 THz is shown in detail in Figure 5.59b. Also, Figure 5.60a shows the spectrum of TNT and the characteristic peak at 2 THz is shown in detail in Figure 5.60b.The occurrence of these peaks at the same frequency in the received spectrum indicates the presence of RDX or TNT in the received spectrum.

a. Complete RDX spectrum   b Characteristic peak of RDX

Figure 5.59. RDX spectrum

a Complete TNT spectrum   b Characteristic peak of TNT
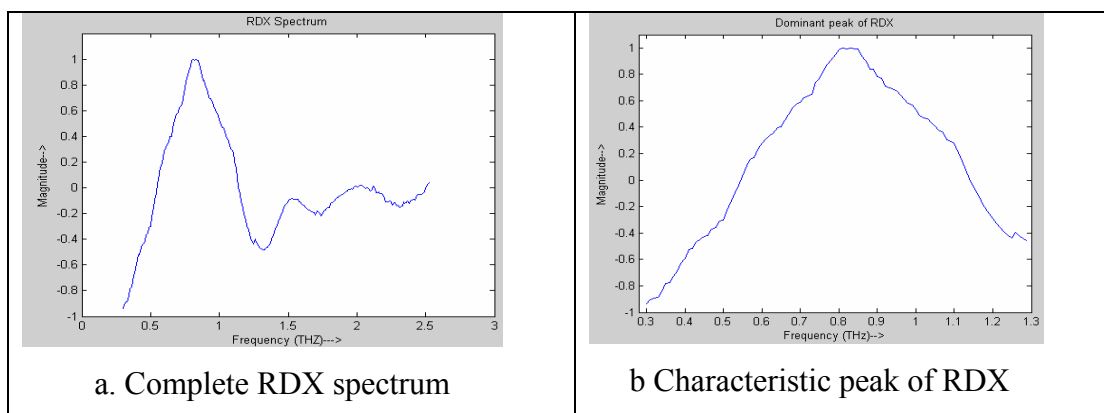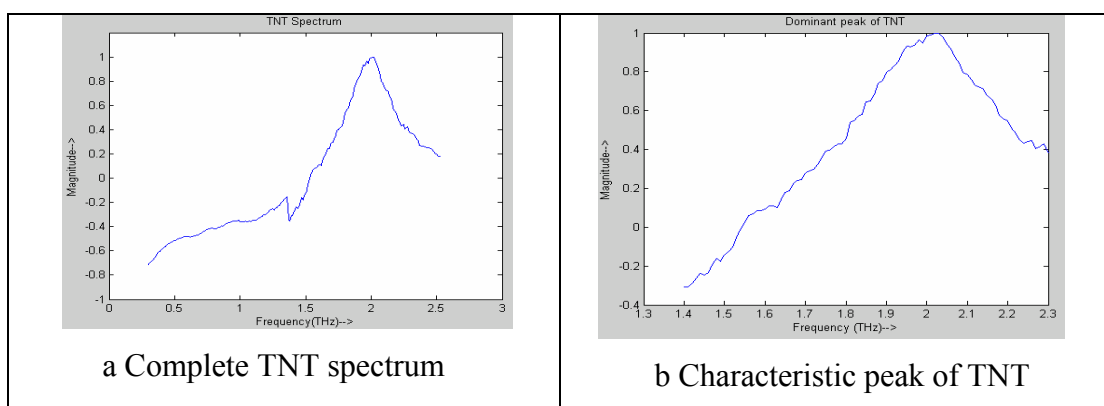
Figure 5.60. TNT spectrum

Similar to the first method consider a field with 100 data points.

Type-1: Pixels in red. These pixels contain a combination of RDX and TNT in randomly varying proportions.

Type-2: Pixels in blue. These pixels contain a combination of RDX, TNT and some other minerals which can be considered as impurities present in the field Again all the spectra are mixed randomly.

Type-3: Pixels in green. These pixels do not contain RDX or TNT but some random spectra of impurities that could be present within the field.
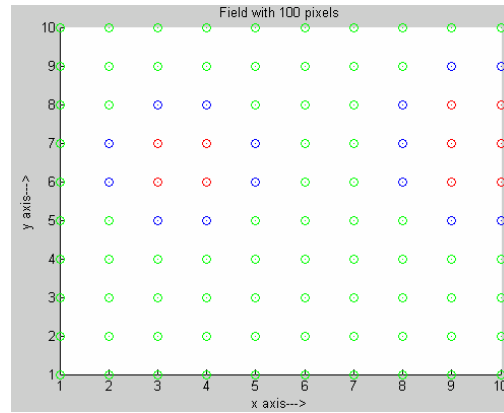
Figure 5.61. Field with 100 pixels

o: Type-1, o:Type-2, o: Type-3

The aim of the preprocessing stage is to select all data samples/pixels that have a significant probability of either RDX or TNT to be present. The correlation filters of the preprocessing stage are designed to correlate the dominant feature of the RDX and TNT spectrum with the received spectrum and select a data point/pixel if the feature occurs at the same frequency as in the target spectrum.

Results for Type-1 pixels

Type-1 pixels contain a combination of RDX and TNT spectrum (Figure 5.63). The spectrum in Figure 5.62 is correlated with the dominant features of the RDX and TNT spectrum i.e. the peaks shown in Figure 5.59b and 5.60b, respectively. The correlation filter output for each of these correlations is shown in Figure 5.63a and 5.63b, respectively. From Figure 5.63 it is seen that the correlation filter output for RDX produces a peak exceeding the threshold ($R_0 = 0.4915$) around the frequency of 0.8 THz while the correlation filter output for TNT produces a similar peak at around 2 THz. Thus, this data point/pixel is selected for further processing. The condition for selecting a pixel is that the correlation filter output must have a peak exceeding the threshold and it must

occur at the same frequency as in the original target spectrum. Also, this condition must be satisfied for any one of the correlation filter outputs.
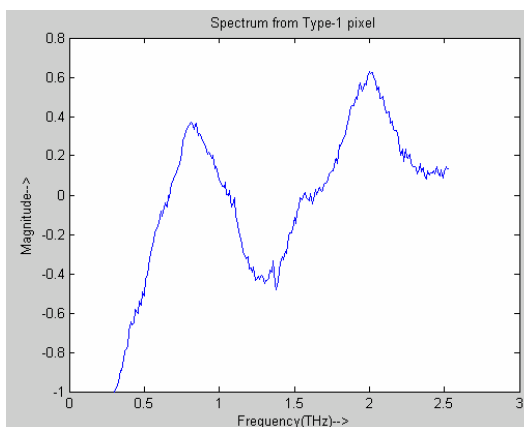
Figure 5.62. Type-1 pixel spectrum

a Correlation filter output (RDX)

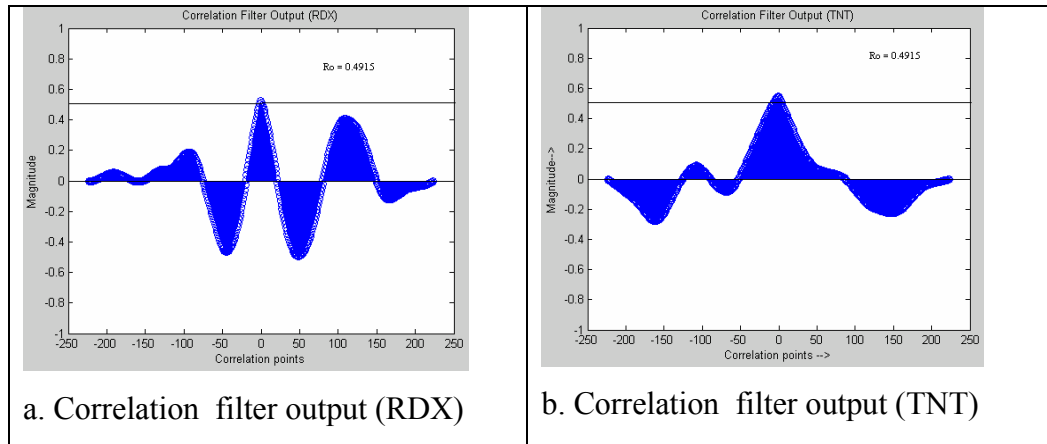b Correlation filter output (TNT)
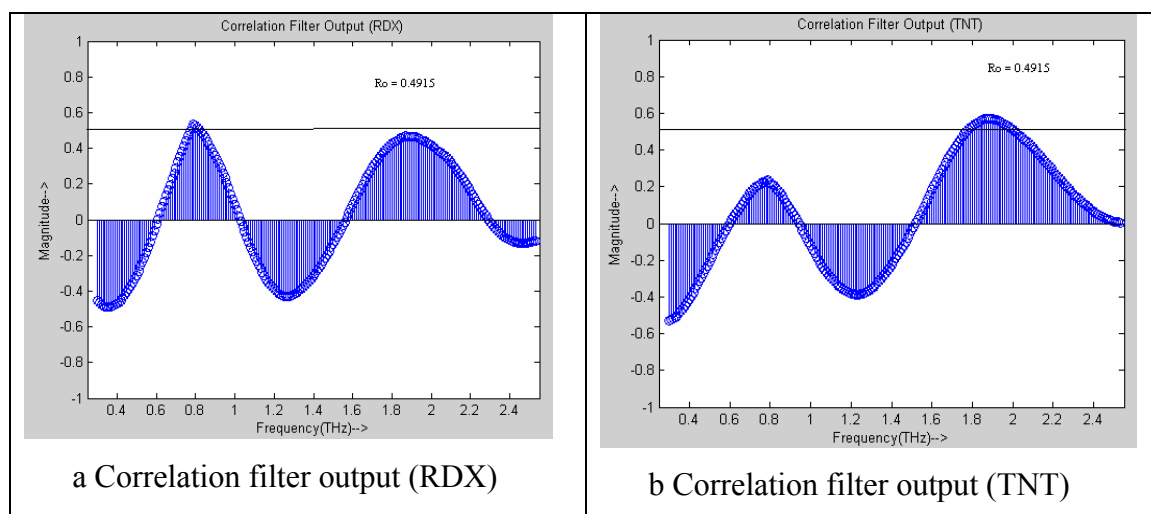
Figure 5.63. Correlation filter output (Type-1 Pixel)

Results for Type-2 pixels

These pixels contain some other spectra along with the RDX and TNT spectra. Figure 5.64 shows a spectrum from a type-2 pixel. The spectrum in Figure 5.64 is given

to the correlation filters which correlate this spectrum with the dominant features of the RDX and TNT spectrum i.e. the peaks shown in Figure 5.59b and 5.60b, respectively.
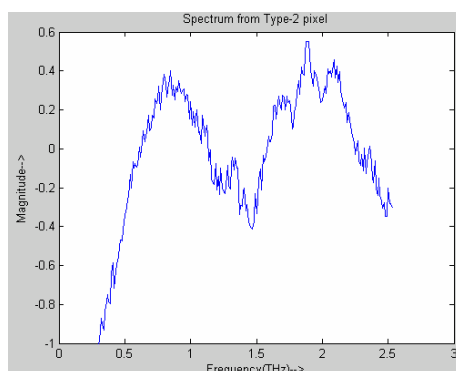
Figure 5.64. Type-2 pixel spectrum

The output of the correlation filters for each case is shown in Figure 5.65a and 5.65b, respectively.

| a Correlation filter output (RDX) | b Correlation filter output (TNT) |
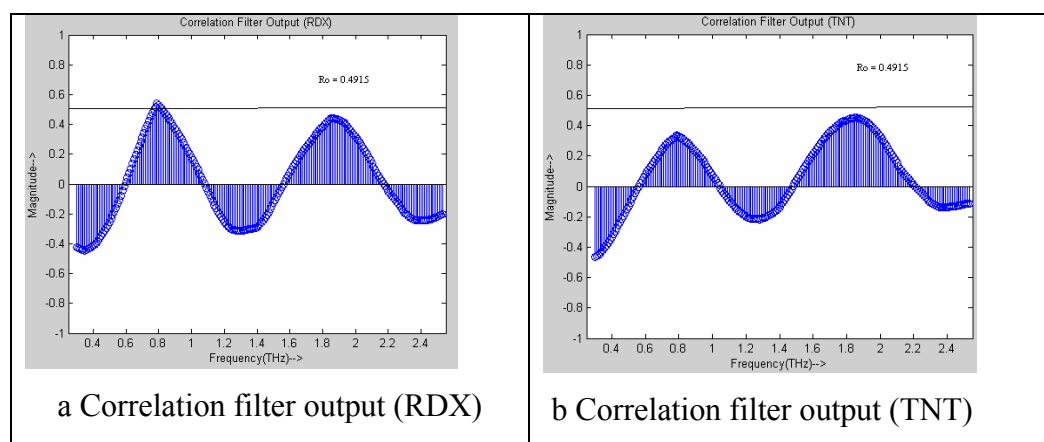
Figure 5.65. Correlation filter output (Type-2 Pixel)

As seen in Figure above only correlation filter output of RDX produces a peak exceeding the threshold at 0.8 THz while the peaks of correlation filter output for TNT are below the threshold. The condition that any one of the correlation filters must produce an output with peak exceeding the threshold and at the proper frequency is satisfied hence this pixel is selected for further processing.

Results for Type-3 pixels

These pixels do not contain spectra for RDX or TNT but contain some other random spectra. Figure 5.66 shows spectrum from a type-3 pixel.
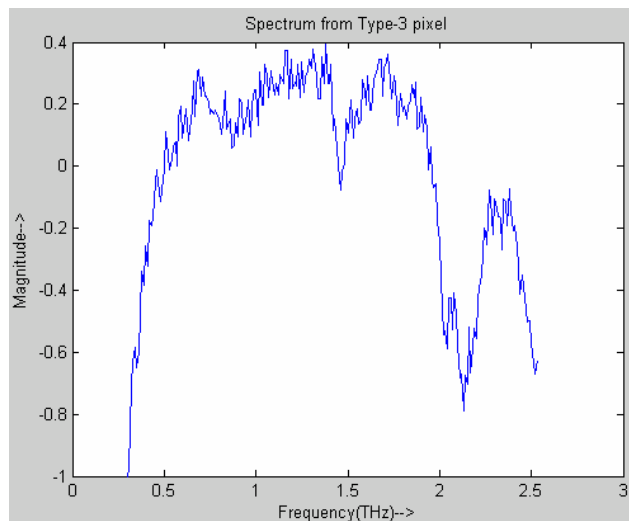
Figure 5.66 Type-3 pixel spectrum

The correlation filter outputs for this pixel are shown in Figure 5.67a and 5.67b. Thus, it is seen from figure above that none of the peaks in the correlation filter output exceed the threshold. Hence, such pixels are discarded. The above simulations were performed for each of the 100 pixels in Figure 5.61. Figure 5.68 shows the result of the simulations for correlation filters with an error probability of 0.2 corresponding to a

threshold of R_0 = 0.4915. Simulations for other value of error probability were also performed and results plotted.

a. Correlation filter output (RDX)

b Correlation filter output (TNT)
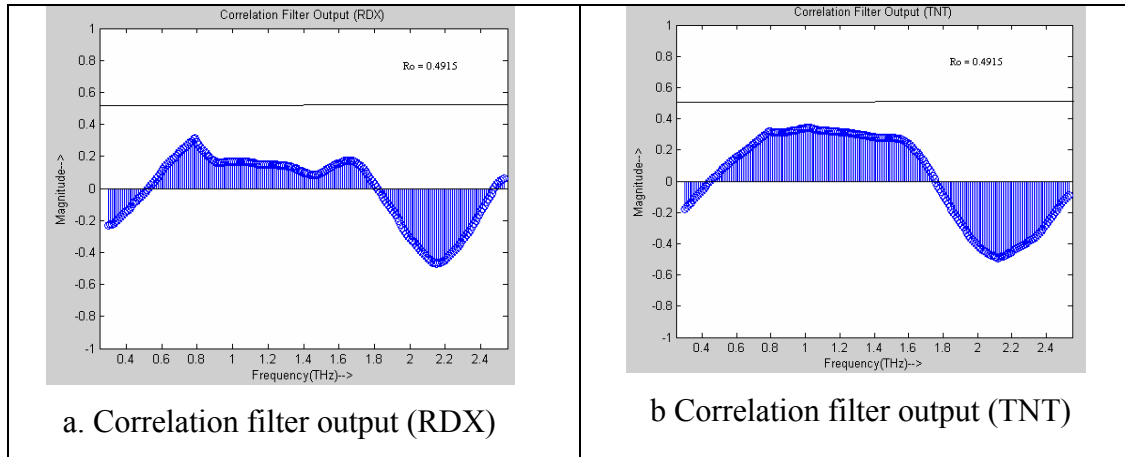
Figure 5.67. Correlation filter output (Type-3 Pixel)

Red dots indicate presence of IED and green dot indicates its absence. The field reduces to hotspots (areas with red pixels) and all pixels within these areas have a significant probability of the target spectrum to be present.
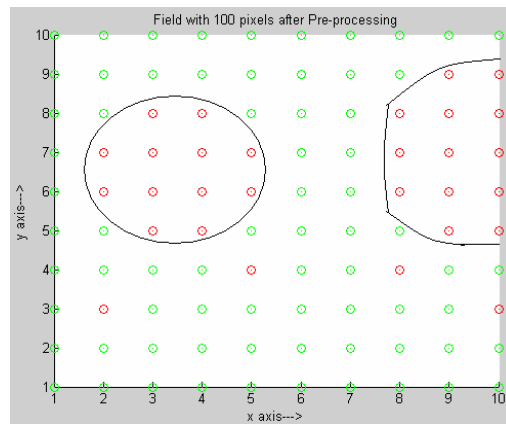
Figure 5.68. Field with selected pixels after preprocessing

Further simulations were performed by varying the error probability from 0.1 to 0.35 to observe the number of pixels correctly detected number of false negatives and false positives. The results are summarized in Table 5.8 and plotted in Figure 5.69.

Table 5.8. Results of preprocessing stage (Method 2) for RDX & TNT spectrum

Error Prob	Pixels	Target present in	Target absent in	False positive	False Negative (Type-1 pixels)	False Negative (Type-2 pixels)
0.14	100	25	75	4	0	2
0.15	100	25	75	3	0	2
0.16	100	25	75	1	0	2
0.17	100	25	75	4	0	0
0.2	100	25	75	4	0	0
0.25	100	25	75	8	0	0
0.35	100	25	75	14	0	0
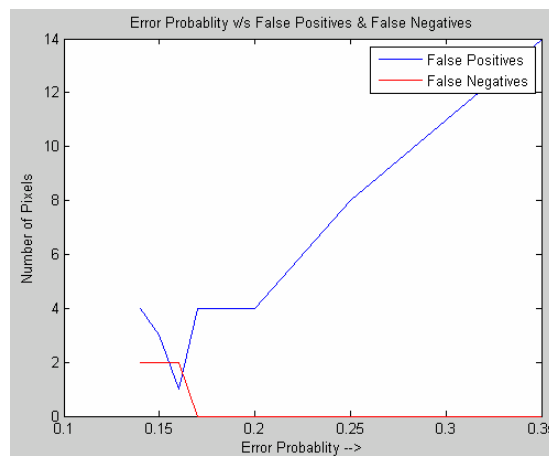
Figure 5.69 Variation of FP & FN with error probability

Thus, from Table 5.8 and Figure 5.69 the variations in the number of false negatives and false positives can be seen. As the error probability is increased the threshold decreases and the number of false negatives reduce but at the same time number of false positives increases. Comparing Table 5.8 with Table 5.7 it can be seen that in the second case the number of false negatives is less. This is because in the second method a characteristic peak as well as the frequency at which it occurs is considered. Thus, the method two is suitable for substances of explosives having a characteristic feature occurring in a certain frequency range.

5.6 UNMIXING STAGE FOR A MIXTURE OF RDX AND TNT

In the previous section simulation of the preprocessing stage is done when two target spectra i.e. RDX and TNT are present.In this section unmixing of all the pixels selected by the preprocessing stage is performed. These pixels have a significant probability of RDX or TNT to be present within them. The stage of unmixing by the improved ICA algorithm is used to ascertain which pixels have the target present and which do not with maximum accuracy hence eliminating all the false positives. The unmixing algorithm used is the improved ICA algorithm discussed in Section 4.2 and it separates only the required spectra. The unmixing algorithm is done for both types of filters of the preprocessing stage i.e. ones which use the entire target spectrum and ones which use a characteristic feature. The entire RDX or TNT spectrum or a characteristic feature in RDX or TNT spectra is given as reference to the improved ICA algorithm. The improved ICA algorithm separates two spectra, one corresponding to RDX and one corresponding to TNT. The separated spectra form each of the pixels is given to a final correlation filtering stage consisting of two correlation filters designed to detect RDX or TNT with maximum accuracy.

5.6.1 Unmixing of Data from Filters of Method 1. These filters discussed in Section 4.1.2 correlate the entire target spectrum. Figure 5.70 shows the actual location of the target i.e. type-1, type-2 and type-3 pixels within the field and Figure 5.71 shows the hotspots in the field separated by the pre-processing stage with filters that detect the entire target spectrum. These hotspots contain pixels that have significant probability of

RDX or TNT to be present within them and spectrum from these pixels has to be unmixed in this stage.
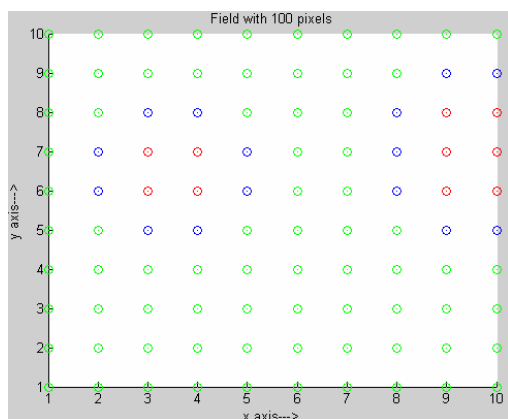
Figure 5.70. Field with 100 pixels   Figure 5.71. Field after preprocessing
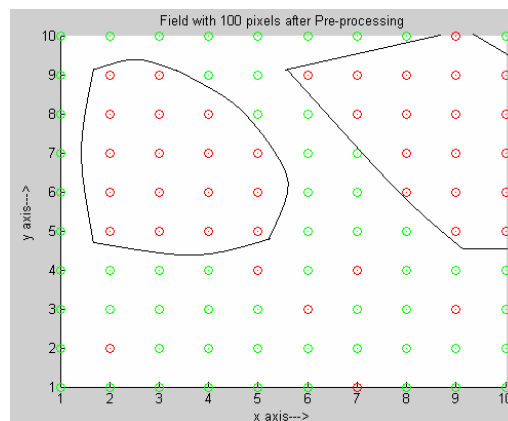
The RDX and TNT spectra (Figure 5.72a and Figure 5.72b) acts as a reference input to the ICA algorithm and spectra from all the pixels marked in red in Figure 5.71 are given as an input to the improved ICA algorithm. Spectra from one pixel of each type are shown in Figure 5.73.

a. RDX spectrum   b. TNT spectrum
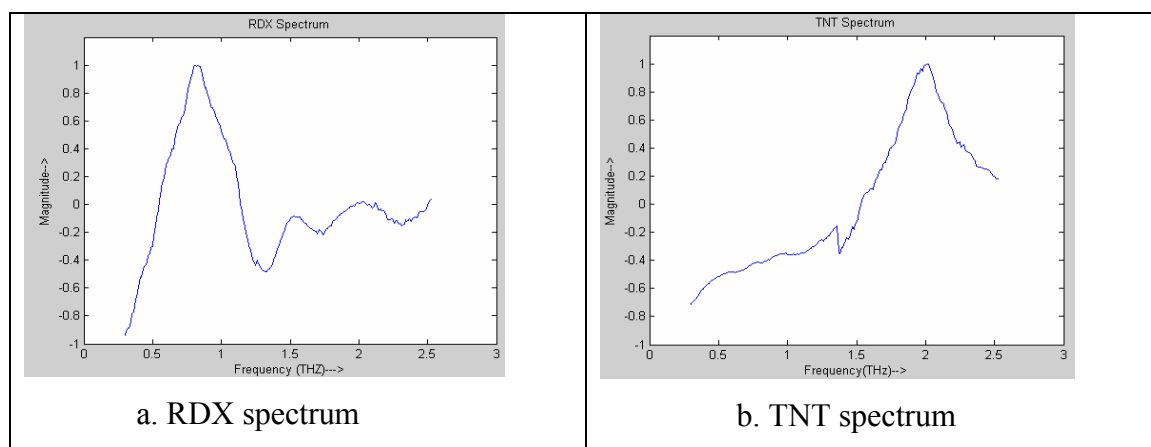
Figure 5.72. Explosive spectra

For each composite spectrum given to it, the improved ICA algorithm separates two spectra, one corresponding to RDX and one for TNT. Figure 5.74 shows the separated spectrum from each type of pixel corresponding to the RDX reference and Figure 5.75 shows separated spectra corresponding to the TNT reference. It can be seen from this figure that spectra from type-1 and type-2 pixels closely resembles the RDX or TNT spectra while the separated spectrum from type-3 pixels is some arbitrary spectrum having no resemblance to either RDX or TNT spectra.

a. Type-1 Pixel Spectrum   b. Type-2 Pixel Spectrum

c. Type-3 Pixel Spectrum
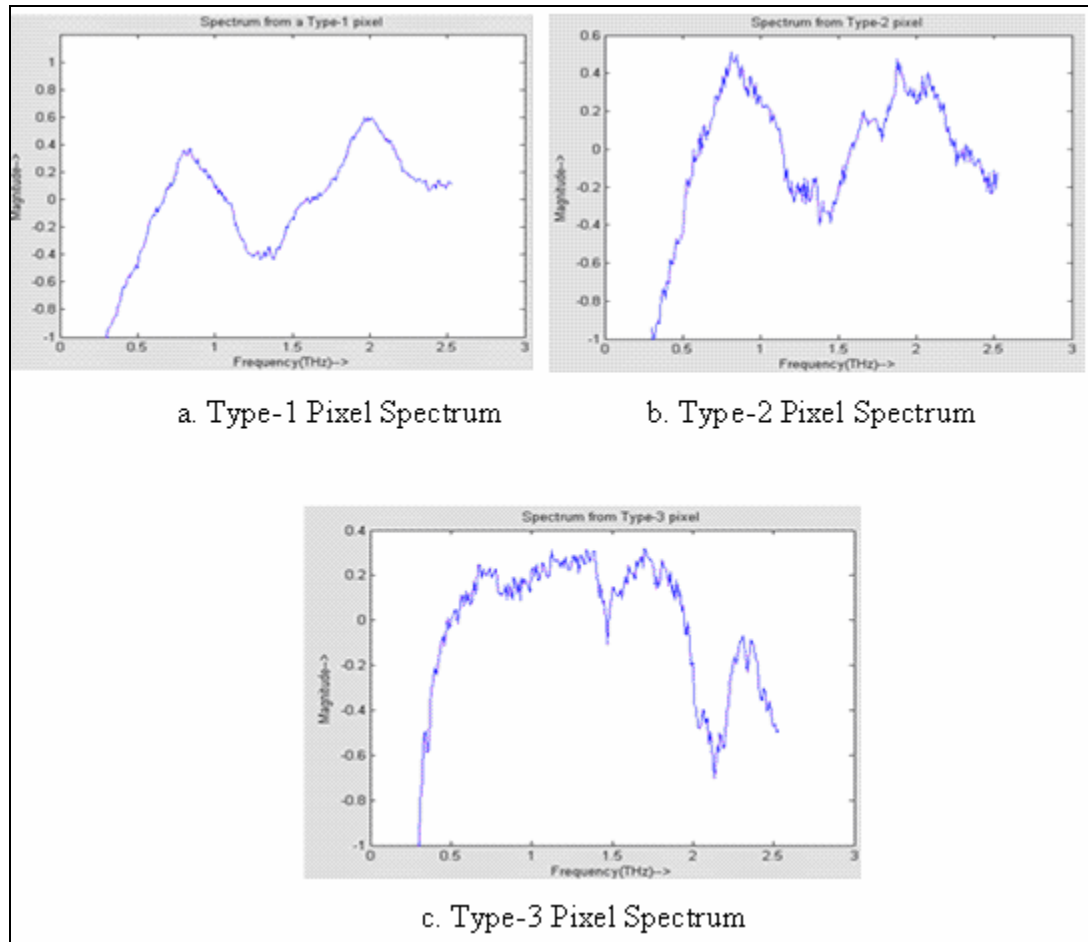
Figure 5.73. Inputs to improved ICA algorithm
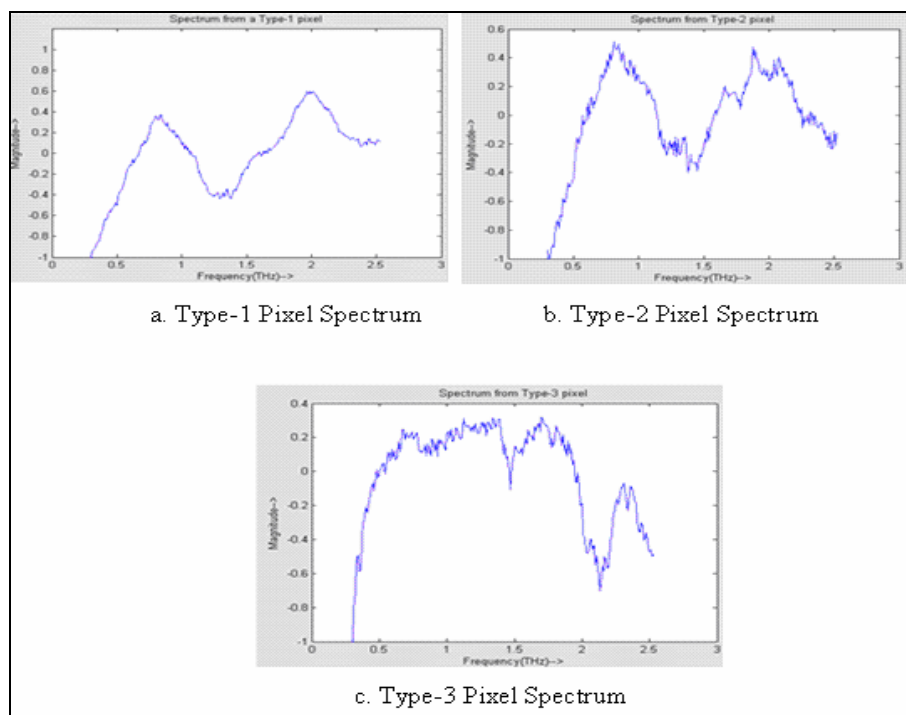
Figure 5.74 Output of the improved ICA with RDX as reference
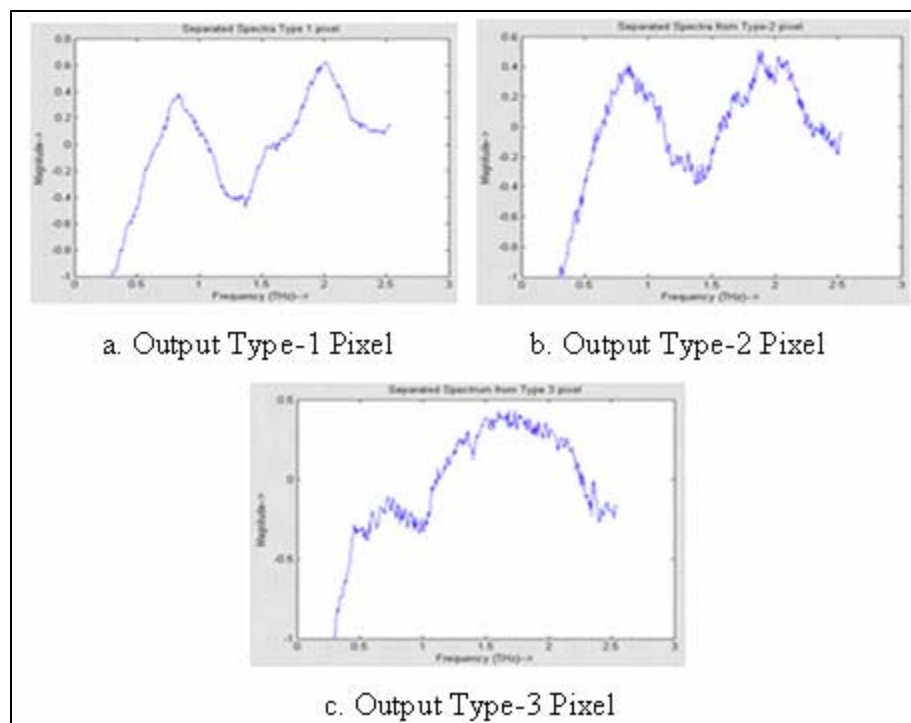
Figure 5.75 Output of the improved ICA with TNT as reference

To make a final decision about which pixels have the target and which do not, the separated spectra with RDX as reference are given to a correlation filter designed to detect the RDX spectrum and those with TNT as reference are given to a correlation filter designed to detect the TNT spectrum. Correlation filter outputs are shown in Figure 5.76 and Figure 5.77.

a. Filter Output (Type-1 pixel)   a. Filter Output (Type-1 pixel)

b. Filter Output (Type-2 pixel)   b. Filter Output (Type-2 pixel)

c. Filter Output (Type-2 pixel)   c. Filter Output (Type-2 pixel)
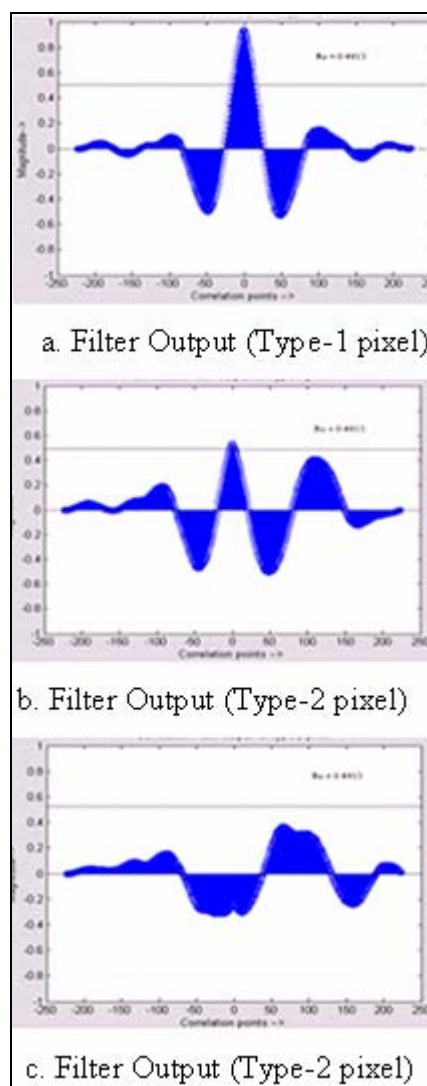
Figure 5.76   Figure 5.77

Correlation filter output (RDX reference)   Correlation filter output (TNT reference)

Figure 5.76 shows the correlation filter output for each separated spectrum having RDX as its reference and Figure 5.77 shows the correlation filter output with for spectra having TNT as reference. It can be seen that type-1 and 2 pixels have a high correlation peak which is above the threshold for this filter while peaks of the type-3 pixels are below the threshold. Figure 5.78a shows the pixels selected after preprocessing and the detected pixels after the unmixing stage are shown in Figure 5.78b. It can be seen that false positives have been eliminated and the false negatives i.e. the pixels which were missed in the preprocessing stage are same as before.

| a Pixels after preprocessing | b: Detected pixels after unmixing |
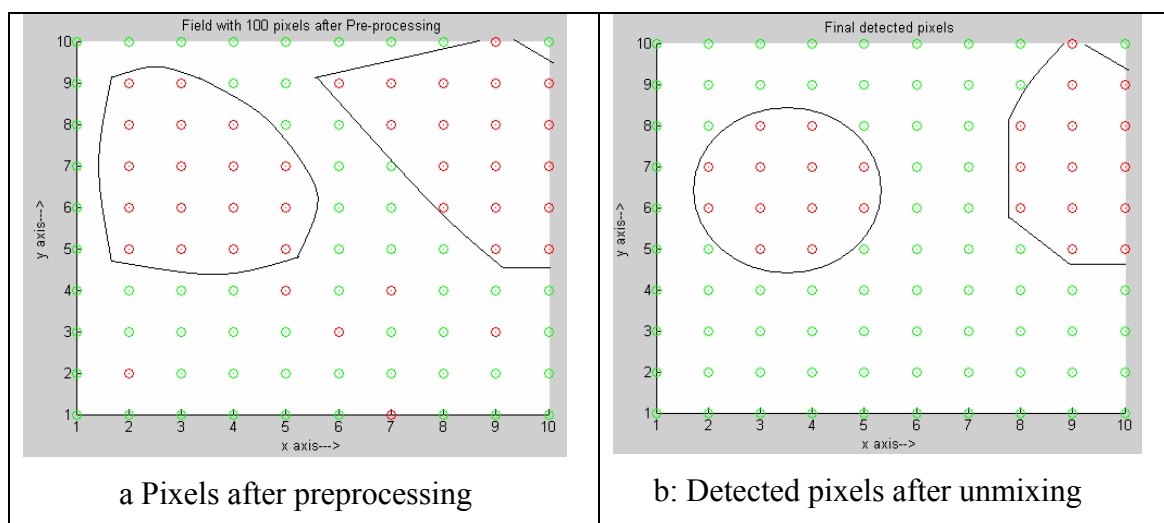
Figure 5.78. Field before and after unmixing

Thus, the unmixing algorithm gives an accurate detection of the RDX and TNT in the field. The accuracy of the algorithm can be adjusted by changing the error probability of the correlation filters.

5.6.2 Unmixing of Data from Filters of Method 2. This is the second type of filter of the preprocessing stage which correlates a characteristic feature of the target spectrum like a peak or valley. Performance of the unmixing algorithm for data from this

type of filter is demonstrated here. Figure 5.79b shows the field with the hotspots after the preprocessing stage with this type of filters. For this type of filters the false positive rate is very low as they detect a characteristic feature and also check the frequency at which it occurs.

| a Actual target locations | b Selected pixels after preprocessing |
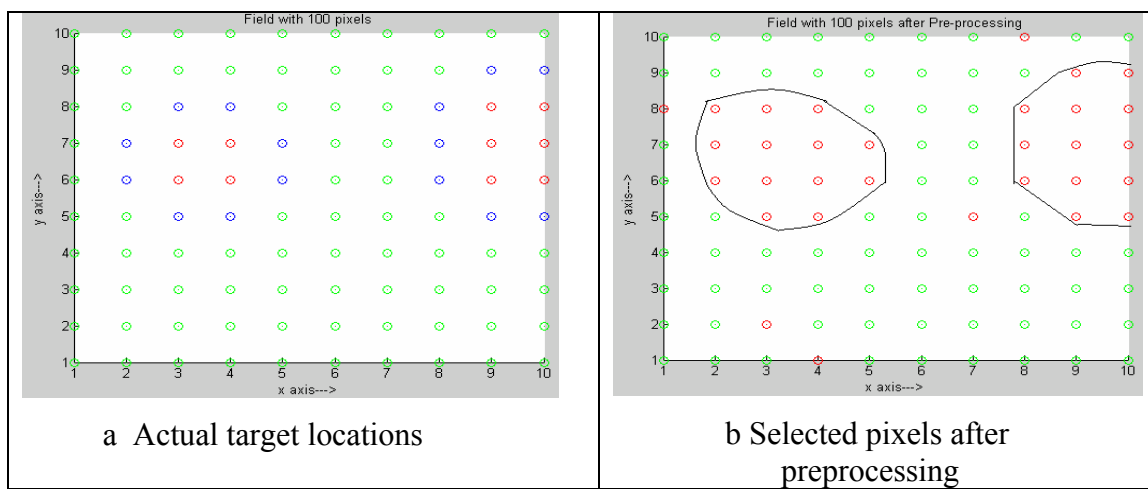
Figure 5.79. Field before and after preprocessing

The spectra corresponding to each selected pixel is given to the unmixing stage. The unmixing stage uses the improved ICA algorithm to compute two spectra, one corresponding to RDX and another corresponding to TNT. These unmixed spectra are given to the final correlation filtering stage. The final filtering stage is similar to the preprocessing stage and has correlation filters to RDX and TNT spectra. If the filter output for any filters exceeds the threshold then that pixel contains the target. The detected pixels at the end of this stage are shown in Figure 5.80.
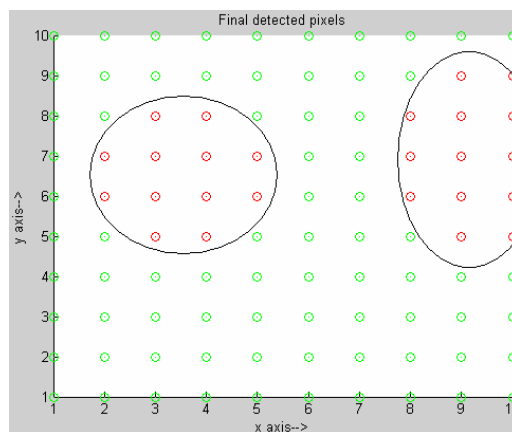
Figure 5.80. Final detected pixels

Thus, the unmixing stage eliminates all the false positives and accurately detects all the pixels containing RDX or TNT.

6: SIMULATIONS OF ALGORITHM WITH MINERAL DATA

In Section 5 simulations of the detection algorithm were done using THz data of RDX and TNT. But this data was not actual laboratory data but was taken from published papers. Also, the RDX and TNT spectra are quiet simple in the sense that both have only one significant peak in them. Hence, the advantages of the unmixing stage are not very obvious with this data. In order to demonstrate the significance of the unmixing stage, in this section simulations of the detection algorithm discussed in Section 4 are done using mineral data from the cuprite library. The cuprite library provides frequency spectra of naturally occurring minerals like calcite, alunite, ect. This library contains varied spectra which are more complex as compared to the spectra considered in Section 5.

6.1 PREPROCESSING STAGE FOR RANDOM CONTENT OF TARGET

The preprocessing of THz data using correlation filters for reduction of processing load on the further processing stages is described in Section 4.1. In order to demonstrate the effectiveness of the proposed pre-processing stage, a performance measurement of this stage is presented in this section using mineral data. The threshold of the correlation filters is calculated in a similar way as in Section 5.

Two methods of correlation filtering were proposed for the preprocessing stage in Section 4.1.2. In Method 1 the filters correlate the entire target spectrum covering the entire frequency range. In Method 2 a characteristic feature of the target spectrum like a peak or valley that occur at specific frequencies are correlated. To demonstrate the performance of the correlation filters consider a field with a 100 evenly spread data points or pixels as shown in Figure 6.1. The THz spectrum from these pixels has to be processed to determine if any of them contain the target spectra. The field consists of three kinds of pixels:

Type-1: Pixels in red. These pixels contain a combination of varying proportion of Mineral A (target spectrum) and noise.

Type-2: Pixels in blue. These pixels contain a combination of mineral A, mineral B and mineral C mixed in varying proportions with noise.

Type-3: Pixels in green. These pixels do not contain the target spectrum of mineral A, instead it contains varying combination of three other minerals with noise.
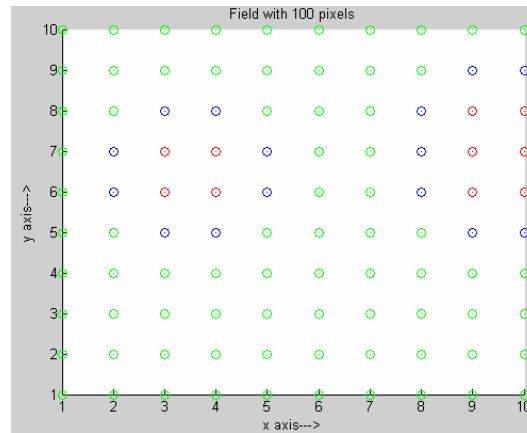
Figure 6.1. Field with 100 pixels

o: Type-1, o:Type-2, o: Type-3

The objective of the preprocessing stage is to detect and select for further processing all type-1 and type-2 pixels which contain the target spectrum for further processing.

6.1.1 Method 1. Here the correlation filters are built to correlate the entire target spectrum covering its entire frequency range of 0.1 THz to 2.4 THz. Figure 6.2 shows the target spectrum to be detected. Correlation filter output is computed for each pixel as in Section 5.1 and all pixels/data points for which the correlation filter output exceeds the pre-chosen threshold are selected for further processing. Results similar to the pre-processing stage for RDX (Section 5.1) are observed. Figure 6.3 shows the selected pixels after the pre-processing stage where the correlation filters have an error probability of 0.2 i.e. threshold R_0 is 0.4915.
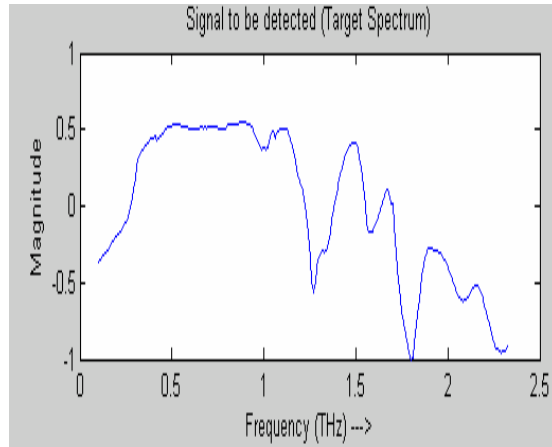
Figure 6.2. Target spectrum
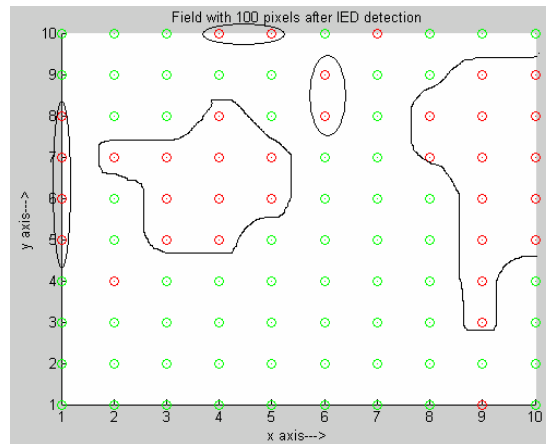
Figure 6.3. Selected pixels after preprocessing

Red dots indicate presence of the target and green dot indicates its absence. Thus, the field reduces to hotspots where the target could be present. All the pixels/data points within the hotspots are selected for further processing. It can be seen that most of the type-1 and type-2 pixels are selected and type-3 pixels are eliminated as they do not contain the target spectrum. However there are a few false positives i.e. pixels which do not contain the target but are still selected. Also, there are few false negatives i.e. pixels

which have the target spectrum but are not selected. The number of false positives and negatives can be reduced by choosing a proper threshold value (R_0). Hence, the error probability of the correlation filters is varied form 0.1 to 0.25 to observe the effects in number of pixels correctly detected number of false negatives and false positives. The results are summarized in Table 6.1.

Table 6.1. Results of preprocessing stage (Method 1) for target spectrum

Error Prob	Pixels	Target present in	Target absent in	False positive	False Negative (Type-1 pixels)	False Negative (Type-2 pixels)
0.05	100	25	75	0	0	6
0.10	100	25	75	1	0	3
0.15	100	25	75	15	0	3
0.20	100	25	75	16	0	2
0.25	100	25	75	23	0	2
0.30	100	25	75	23	0	0
0.35	100	25	75	27	0	0
0.45	100	25	75	55	0	0

Figure 6.4 shows the variation of the false positives and negatives when the error probability was varied from 0.05 to 0.45. As the error probability is increased the threshold for detection decreases and more pixels are selected.
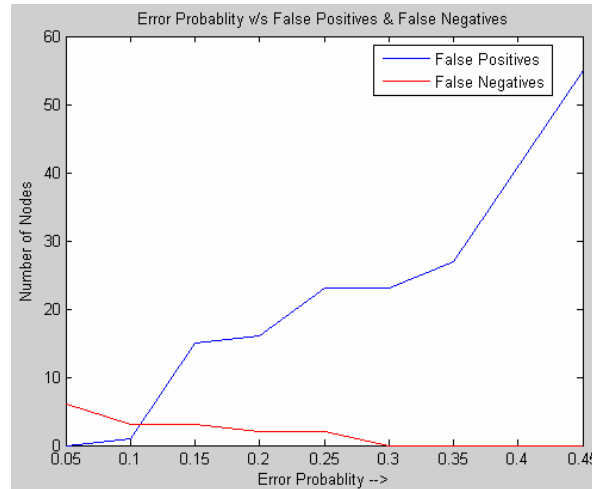
Figure 6.4. Variation of FP & FN with error probability

As the error probability increases the threshold decreases and number of false negatives decreases but at the same time the false positives increase sharply. After the preprocessing stage all pixels/data points marked in red in Figure 6.3 are selected for further processing as they have significant probability of the target spectrum being present.

6.1.2 Method 2. In the following simulations the target spectrum is detected using its characteristic feature like a peak or valley occurring in a particular frequency range instead of detecting the entire spectrum. Consider the target spectrum shown in Figure 6.5 and a characteristic peak in this spectrum is shown in Figure 6.6. The occurrence of this peak at the same frequency in the received spectrum indicates the presence of the target in the received spectrum.

Similar to Method 1, consider a field as in Figure 6.1 with three types of pixels. Simulations similar to Section 5.1.3 were performed for each of the 100 pixels in Figure 6.1. Figure 6.7 shows the result of the simulations for correlation filters with an error probability of 0.2 corresponding to a threshold of $R_0 = 0.4915$. Red dots indicate presence of the target spectrum and green dot indicates its absence. The field reduces to two hotspots and all pixels within these areas have a significant probability of the target spectrum to be present.
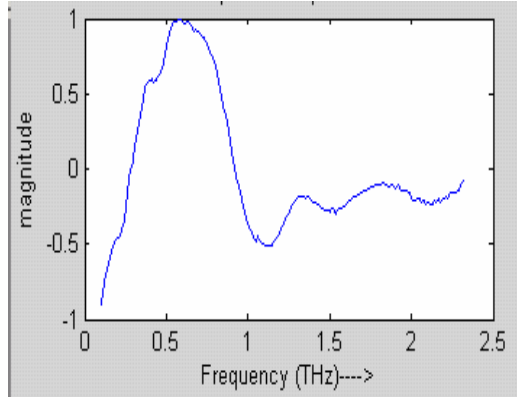
Figure 6.5. Target spectrum   Figure 6.6. Characteristic peak
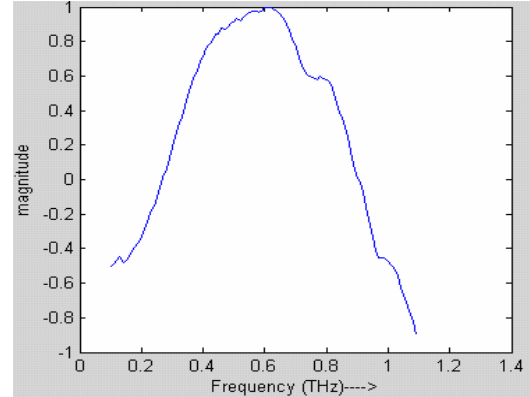
Figure 6.7. Detected pixels after preprocessing

The error probability of the correlation filters was varied from 0.1 to 0.25 to evaluate the performance of the preprocessing stage. The results are summarized in Table 6.2 and plotted in Figure 6.8

Table 6.2. Results of preprocessing stage (Method 2) for target spectrum

Error Prob	Pixels	Target present in	Target absent in	False positive	False Negative (Type-1 pixels)	False Negative (Type-2 pixels)
0.05	100	25	75	0	0	3
0.10	100	25	75	0	0	3
0.15	100	25	75	0	0	3
0.20	100	25	75	14	0	1
0.25	100	25	75	22	0	0
0.30	100	25	75	34	0	0
0.35	100	25	75	41	0	0
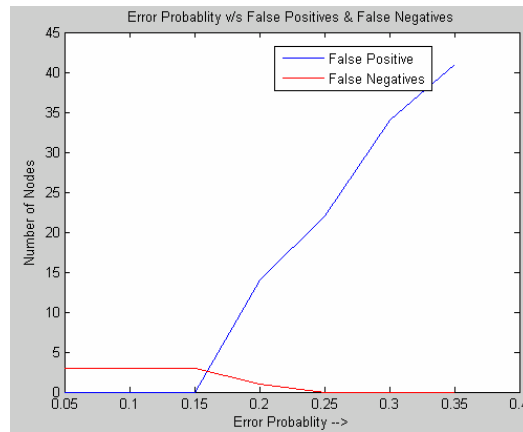
Figure 6.8. Variation of FP & FN with error probability

After the preprocessing stage with correlation filters having error probability 0.2 only 33 (all red dots) out of the 100 pixels are selected for further processing as they have

some probability of the target spectrum being present. Table 6.2 along with Figure 6.8 shows the variation of the false positives and negatives with the error probability. It is seen that as the error probability increases the threshold for detection will decrease. Hence, the number of false negatives decreases but at the same time false positives increase sharply.

Thus, results for the preprocessing stage are similar to the pre-processing stage with the RDX spectrum shown in Section 5.1.

6.2 UNMIXING STAGE WITH RANDOM CONTENT OF TARGET

The improved ICA algorithm described in Section 4.3 separates out the desired independent components and discards all unnecessary components. The separated components depend on the reference spectra given to the algorithm. All components that resemble the reference spectra are separated and the remaining components are ignored. The reference spectra given to the algorithm are those of the target materials that are to be searched in the scene. The simulation of the improved ICA algorithm for unmixing of THz data is done in this section using the cuprite data from the cuprite library. The hotspots or the separated pixels from the preprocessing stage form the input to the improved ICA algorithm. These pixels have a significant probability of mineral A (target) to be present within them. The stage of unmixing by the improved ICA algorithm is used to ascertain which pixels have the target present and which do not with maximum accuracy. The spectrum of mineral A (target spectrum) available form the spectral library is given as a reference to the improved ICA algorithm. The improved ICA algorithm separates the spectrum of the target i.e. mineral A if present in a pixel for each of the pixels separated by the preprocessing stage. The separated spectra form each of the pixels is given to a final correlation filtering stage designed to detect the target with maximum accuracy. Analysis of data from both method 1 and method 2 correlation filters mentioned in Section 4.2 is performed.

6.2.1 Unmixing of Data from Filters of Method 1. These filters discussed in Section 4.1.2 correlate the entire target spectrum. Figure 6.9 shows the actual location of the target i.e. type-1, type-2 and type-3 pixels within the field and Figure 6.10 shows the hotspots in the field separated by the pre-processing stage with filters that correlate the

entire target spectrum. These hotspots contain pixels that have significant probability of the target to be present within them and spectra from these pixels have to be unmixed in this stage.
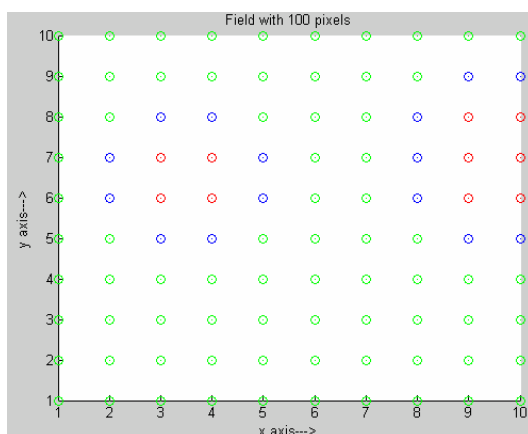
Figure 6.9. Field with 100 pixels

o: Type-1, o:Type-2, o: Type-3
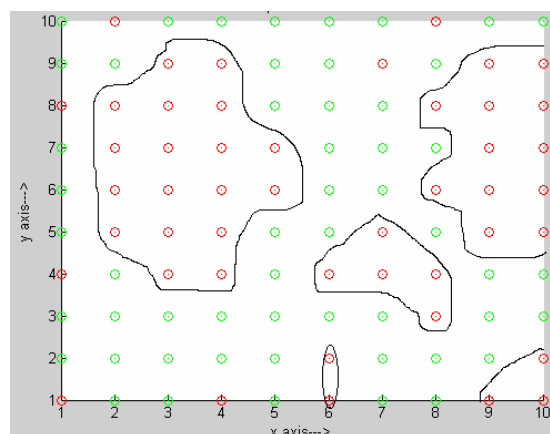
Figure 6.10. Separated hotspots in the field

The target spectra (Figure 6.11) acts as a reference input to the ICA algorithm and spectra from all the pixels marked in red in Figure 6.10 are given as an input to the improved ICA algorithm. Spectra from one pixel of each type are shown in Figure 6.12. For each composite spectrum given to it, the improved ICA algorithm separates outs a spectrum which is as close as possible to the target spectrum. If the algorithm does not find a spectrum close to the reference it stops computation after 200 iterations. It tries to minimize the closeness measure which is the covariance between the reference and the computed output. Also in this case the target spectrum is complex in nature as compared to the RDX and TNT spectra considered earlier. The target spectrum has many peaks and valleys at different frequencies.
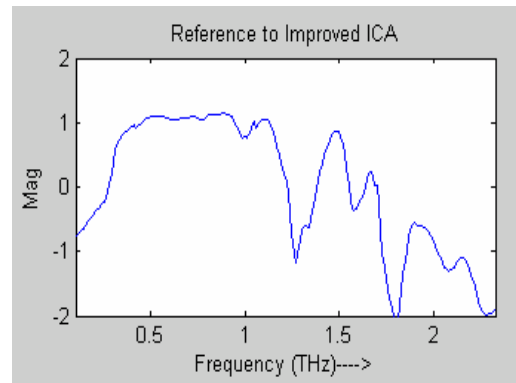
Figure 6.11. Reference to improved ICA (target spectrum)

a. Type-1 Pixel Spectrum

b. Type-2 Pixel Spectrum

c. Type-3 Pixel Spectrum
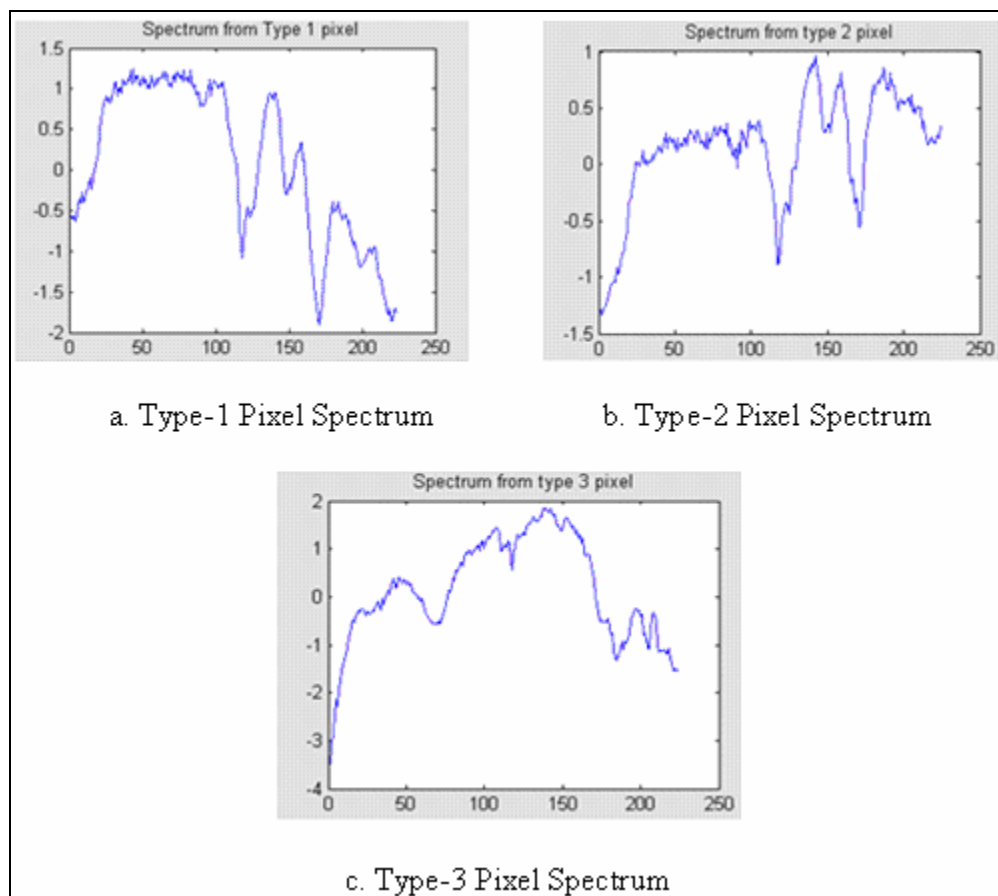
Figure 6.12. Inputs to improved ICA algorithm

The separated spectrum from each type of pixel is shown in Figure 6.13. It can be seen from this figure that spectra from type-1 and type-2 pixels closely resembles the target spectrum while the separated spectrum from type-3 pixels is some arbitrary spectrum having no resemblance to the target.

a. Output Type-1 Pixel

b. Output Type-2 Pixel

c. Output Type-3 Pixel
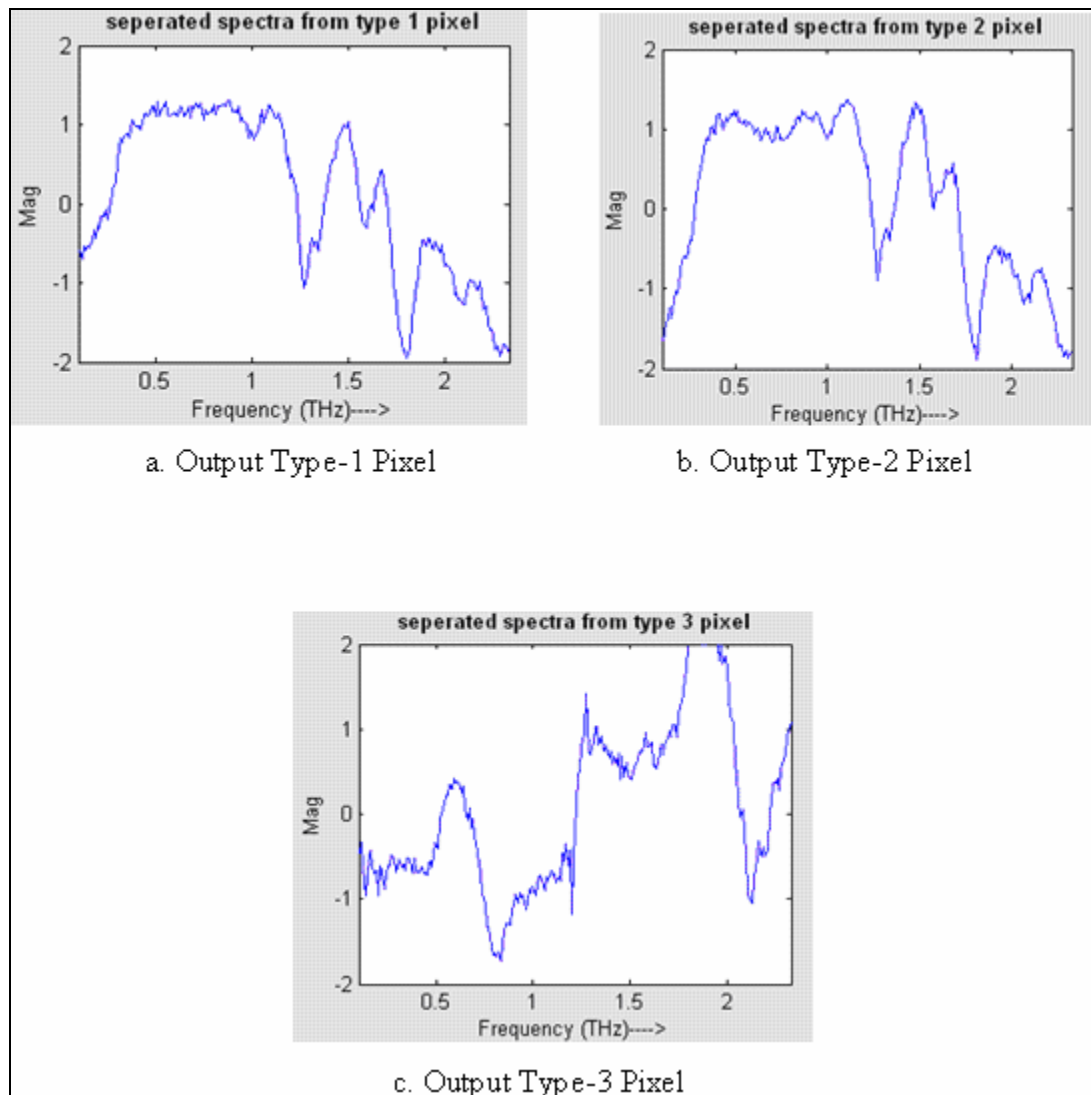
Figure 6.13. Outputs of improved ICA

To make a final decision about which pixels have the target and which do not, the separated spectrum from each pixel is given to a correlation filter designed to detect the target spectrum. Figure 6.14 shows the correlation filter output for each pixel type. It can be seen that type-1 and 2 pixels have a high correlation peak which is above the threshold for this filter while peaks of the type-3 pixels are below the threshold.
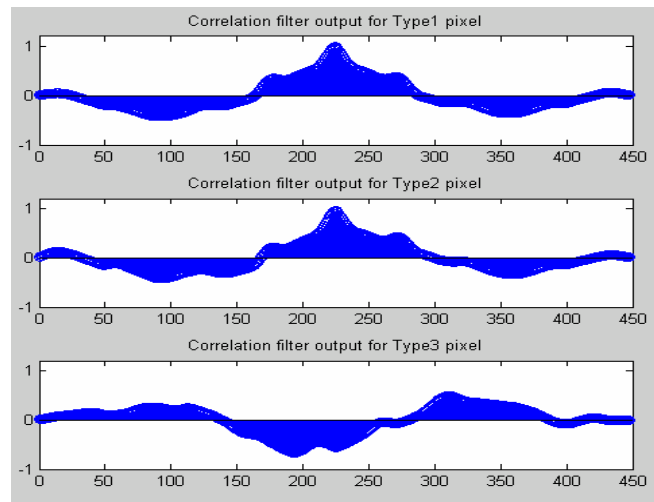
Figure 6.14. Correlation filter output

The final detected pixels for which the correlation peak is above the threshold are shown in Figure 6.15b. Also, shown in the figure is the actual location of the target pixels. It can be seen that nearly all of the false positives have been eliminated and the false negatives i.e. the pixels which were missed in the preprocessing stage are same as before. The unmixing stage accurately detects the pixels that contain the target spectra thus eliminating all the false positives incurred in the preprocessing stage. Thus the exact location of the IEDs in the field can be determined.

| a Actual target locations | b Final detected pixels |
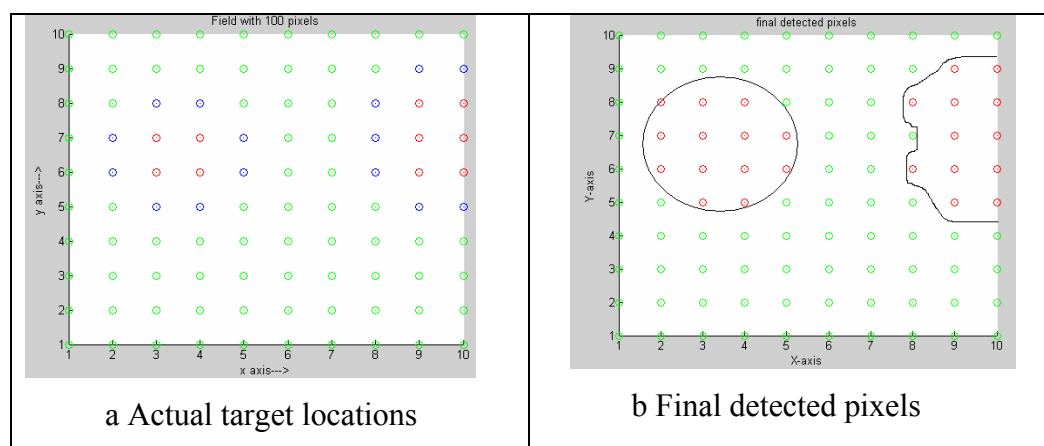
Figure 6.15. Field before and after detection

6.2.2 Unmixing of Data from Filters of Method 2. This is the second type of filter which correlates a characteristic feature of the target spectrum like a peak or valley. Performance of the unmixing algorithm for data from this type of filter was measured. Figure 6.16b shows the field with the hotspots after the preprocessing stage with this type of filters. For this type of filters the false positive rate is very low as they detect a characteristic feature and also check the frequency at which it occurs. From the figure it can be seen that there are no false positives.

| a Actual target locations | b Selected pixels after preprocessing |
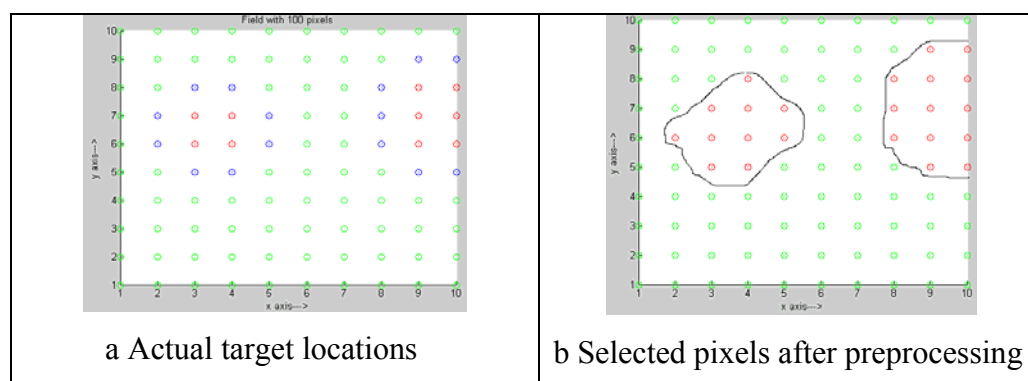
Figure 6.16. Field before and after preprocessing

Although it is seen that there are no false positives by this method, unmixing is performed so that it can be confirmed that all selected pixels have the target spectrum present within them. The unmixing stage performs a more accurate analysis as compared to the preprocessing stage hence it would be beneficial in a real life scenario where the location of the targets is not known. Figure 6.17b shows the detected pixels after the unmixing and final correlation filtering.

a Actual target locations   b Final detected pixels
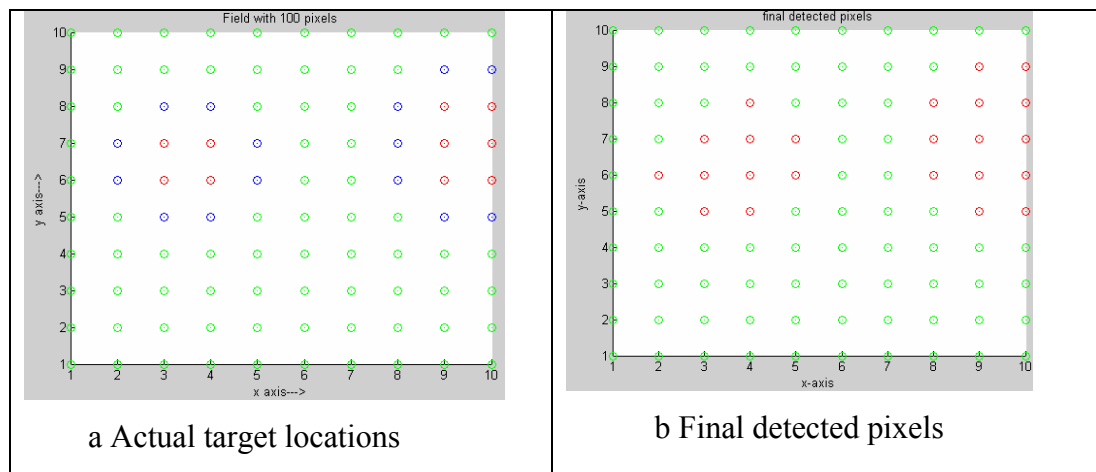
Figure 6.17. Field before and after detection

Thus, similar results are seen after the preprocessing stage and after unmixing by improved ICA for this type of filters. But after this stage it can be said with 100% surety that the selected pixels contain the target.

6.3 PREPROCESSING STAGE WITH DETERMINISTIC TARGET CONTENT

In the simulations of Section 6.1 the content of the target spectrum within a pixel is varied in a random fashion for the hundred pixels. To demonstrate the performance of the preprocessing correlation filters with a deterministic content of the target, the content of the target mineral in the type-2 pixels is varied from less than one percent to 50 percent. As the content of the target is varied the threshold R_0 of the correlation filter has

to be adjusted accordingly for efficient detection. Thus, the user can choose the threshold depending on the circumstance and desired accuracy of the system. For each chosen value of the threshold i.e. at each error probability value there is a minimum limit of the target that can be detected. Only the content of the type-2 pixels is made deterministic whereas the content of the type-1 and type-3 pixels is still varied randomly.

6.3.1 Performance of Method 1. Consider a field similar to Figure 6.18 with 100 pixels of type-1, type-2 and type-3. The type-1 and type-3 pixels are same as described in Section 6.1. The type-2 pixels contain a combination of target mineral, mineral B and mineral C. The proportion of these minerals is varied to determine the minimum detectable content of the target for each value of threshold and corresponding error probability. Figure 6.18 shows the target spectrum which is to be detected.
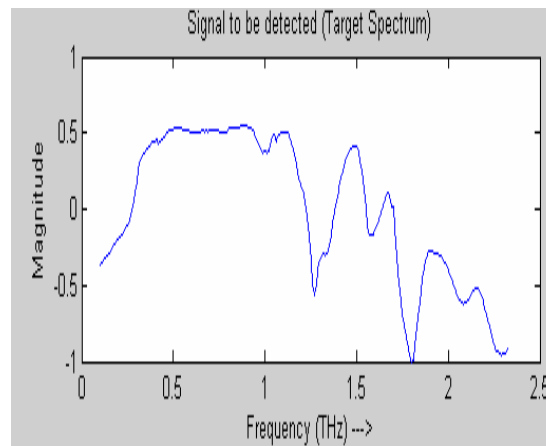
Figure 6.18 Target spectrum

The results are summarized in Table 6.3. The table gives the minimum value of the target to be present within a pixel for each probability of error. It also gives the false positives for each value of error probability.

Table 6.3.Results of preprocessing stage (Method 1) with deterministic content of target

Error Probability (Threshold R_0)	Minimum % of Target that can be detected	False Positives
0.01 (0.8605)	80	0
0.05 (0.7152)	60	0
0.1 (0.6172)	32	1
0.15 (0.5472)	25	9
0.2 (0.4915)	15	14
0.25 (0.4447)	10	26
0.3 (0.4043)	<5	30

It can be seen that as the percentage of the target reduces, a filter with a lower threshold and higher error probability is needed to detect it. Thus, the user can set the threshold depending on the desired accuracy. Also, as the error probability increases the number of false positives (pixels that do not contain the target but are detected) increase thus increasing the number of pixels selected for further processing.

6.3.2 Performance of Method 2. Similar simulations were performed for the method 2 where the filters detect a characteristic feature in the target spectrum instead of the entire target spectrum.

| a Complete target spectrum | b. Characteristic peak |
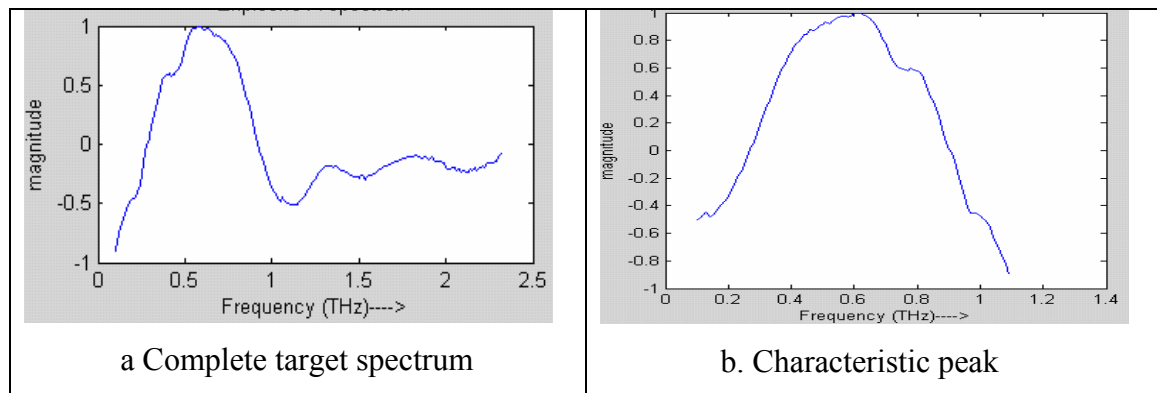
Figure 6.19. Target spectrum

Figure 6.19a shows the target spectrum and Figure 6.19b shows its characteristic peak which is to be detected. The results for this case are summarized in Table 6.4

Table 6.4. Results of preprocessing stage (Method 2) with deterministic content of target

Error Probability (Threshold R_0)	Minimum % of Target that can be detected	False positives
0.01 (0.8605)	54	0
0.05 (0.7152)	35	0
0.1 (0.6172)	20	0
0.15 (0.5472)	14	0
0.2 (0.4915)	13	0
0.25 (0.4447)	12	0
0.3 (0.4043)	11	0
0.35 (0.3686)	9	0
0.4 (0.3367)	<5	1

Thus, from the above table it can be seen that the performance for feature (peak or valley) correlation is better as compared to the correlation of entire spectra. This kind of correlation filters can detect lesser percentage of the target at a given threshold or error probability. The reason for this is that these filters detect the feature as well as the frequency at which it occurs leading to more accurate results. It can also be seen that there are nearly zero false positives for this type of filters. Thus, if the target spectrum has prominent features occurring in certain frequency ranges it is recommended to use this type of filters.

6.4 UNMIXING STAGE WITH DETERMINISTIC CONTENT OF TARGET

In Section 6.3 an evaluation of the pre-processing stage for deterministic content of the target was done. It was found that for a given error probability or threshold value the filters can detect a sample data/pixel only if it contains a minimum percentage of the target. In this section an evaluation of the unmixing stage is done with deterministic

content of the target. The percentage of target in the sample data/pixel is varied from 1 percent to 50 percent and the pixel is given to the unmixing algorithm. The unmixing algorithm i.e. the improved ICA algorithm finds a spectrum resembling the reference. The similarity of this spectrum to the reference depends on the content of target present in the sample. Thus, as the content of the target reduces the threshold of the output correlation filters has to be lowered to detect the separated spectrum.

6.4.1 Unmixing of Data from Filters of Method 1. These filters discussed in Section 4.1.2 correlate the entire target spectrum with the spectrum from the sample/pixel. The composite spectra from the selected pixels are given to the unmixing stage where the improved ICA algorithm separates a spectrum similar to the reference provided to it. The content of the target spectra in the composite spectra is varied from one percent to around 50 percent and the separated spectrum is observed. Also, the threshold or error probability of the output correlation filters is computed so that these filters can detect if the separated spectrum is the target spectrum or not. Figure 6.20 shows the target spectrum to be detected. This spectrum also forms the reference input to the improved ICA algorithm.
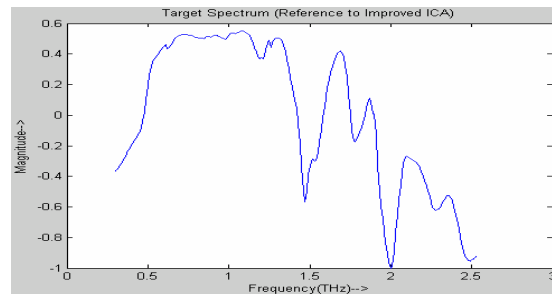
Figure 6.20. Target spectrum

Table 6.5 shows the error probability of the final correlation filters depending on the percentage of target present in the composite spectra. It can be seen that as the

percentage of the target increases the peak value of correlation output also increases and a filter with lower error probability can be used to detect the separated spectrum.

Table 6.5. Results of unmixing stage (Method 1) with deterministic content of Target

Target content (%)	Maximum value of Correlation peak of the output Correlation Filter	Error probability of the output Correlation filters
1	0.3502	0.3783
5	0.3816	0.3312
10	0.4233	0.2757
15	0.4678	0.2244
20	0.5307	0.1639
25	0.5827	0.1230
50	0.9725	0.0003

Figures 6.21-6.25 show the separated target spectrum for each percentage of target content and the correlation output for each.

a Type-2 pixel. target content = 1%   b Final correlation output
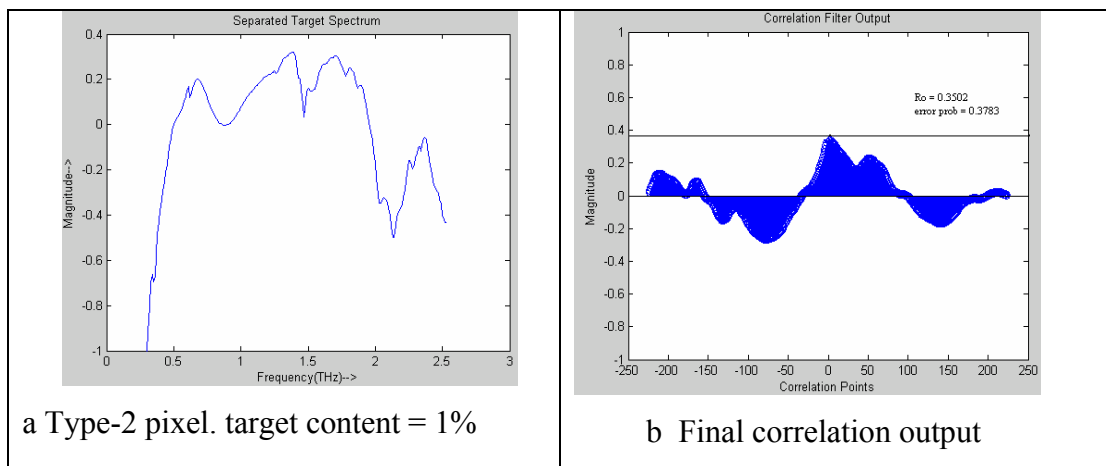
Figure 6.21. Spectrum (1%) after unmixing and filter output

a. Type-2 pixel. target content = 5%   b Final correlation output
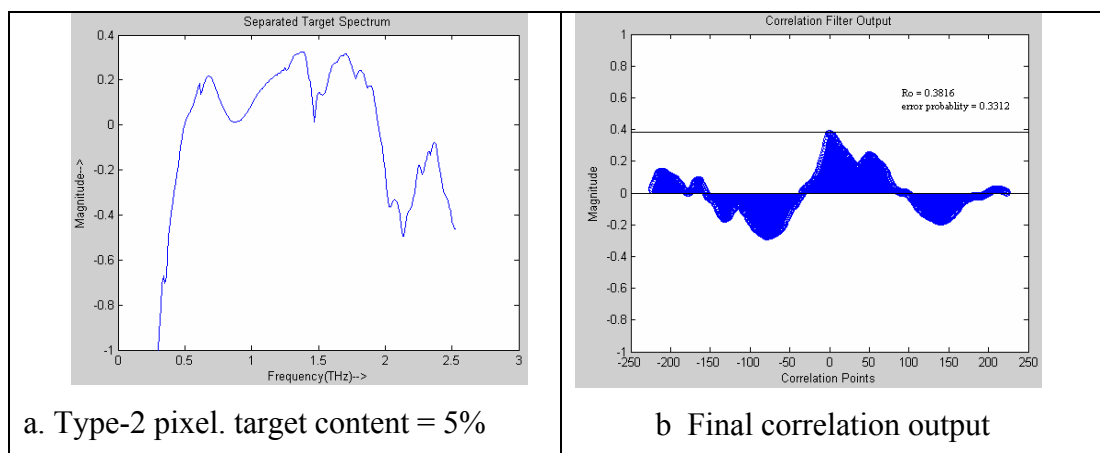
Figure 6.22. Spectrum (5%) after unmixing and filter output

a. Type-2 pixel. target content = 10%   b Final correlation output
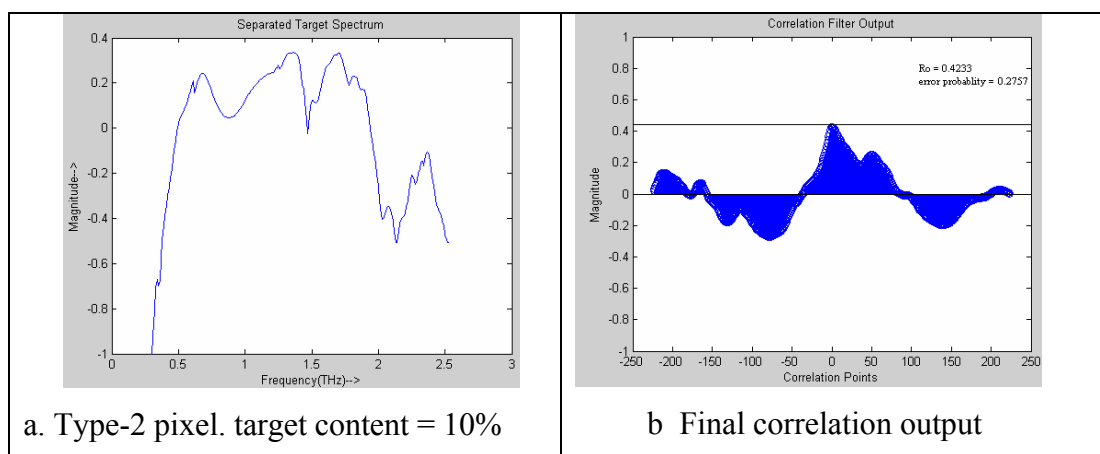
Figure 6.23. Spectrum (10%) after unmixing and filter output

a. Type-2 pixel. target content = 25%   b Final correlation output
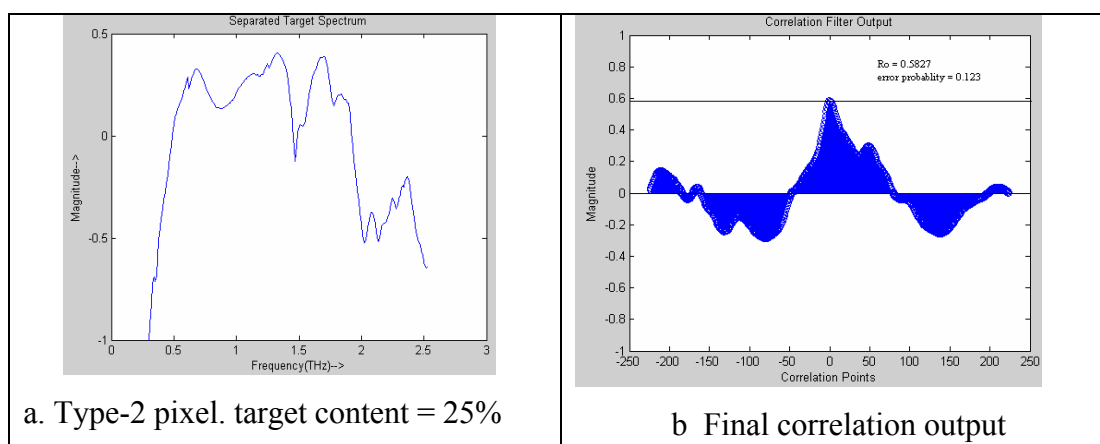
Figure 6.24. Spectrum (25%) after unmixing and filter output

a. Type-2 pixel. target content = 50%

b Final correlation output
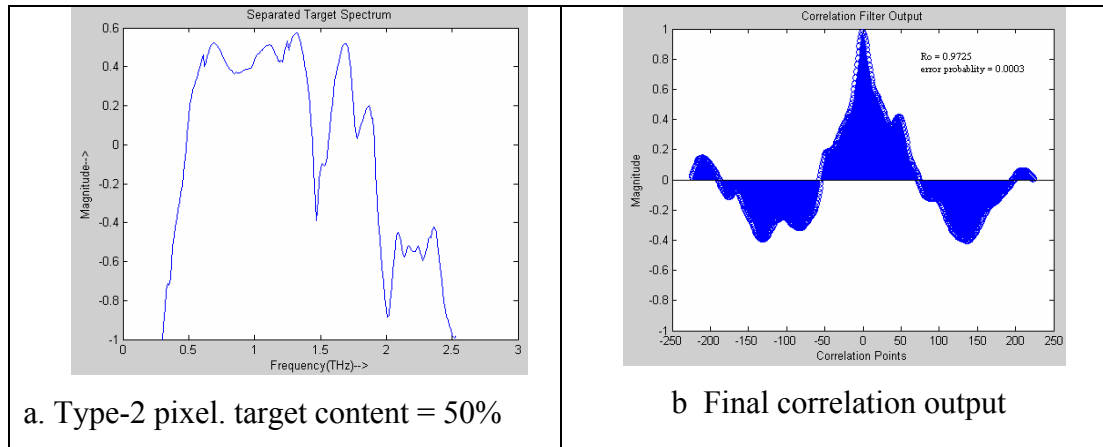
Figure 6.25. Spectrum (50%) after unmixing and filter output

From Figures 6.21 – 6.25 it can be seen that as the percentage of the target spectrum in the composite sample given to the unmixing stage increases the separated spectrum looks more and more similar to the target spectrum. Also, the final correlation filters which do a correlation of this separated spectrum with the target spectrum produces an output with higher peaks thus lowering the error probability of the correlation filters required to detect them.

6.4.2 Unmixing of Data from Filters of Method 2. These filters discussed in Section 4.1.2 correlate a characteristic feature of the target spectrum like the dominant peak or valley occurring in a certain frequency range with the received spectrum from the sample/pixel. Figure 6.26a shows the target spectrum and Figure 6.26b shows the dominant peak in it. Similar simulations are performed wherein the percentage of target spectrum in the sample/pixel is varied from one percent to 50 percent and the unmixed target spectrum is computed by the improved ICA algorithm. This unmixed target spectrum has to be detected by the final correlation stage. The error probability of the final correlation filters is found so that they can accurately detect the unmixed target spectrum. Results are summarized in Table 6.6.

| a Complete target spectrum | b. Characteristic peak |
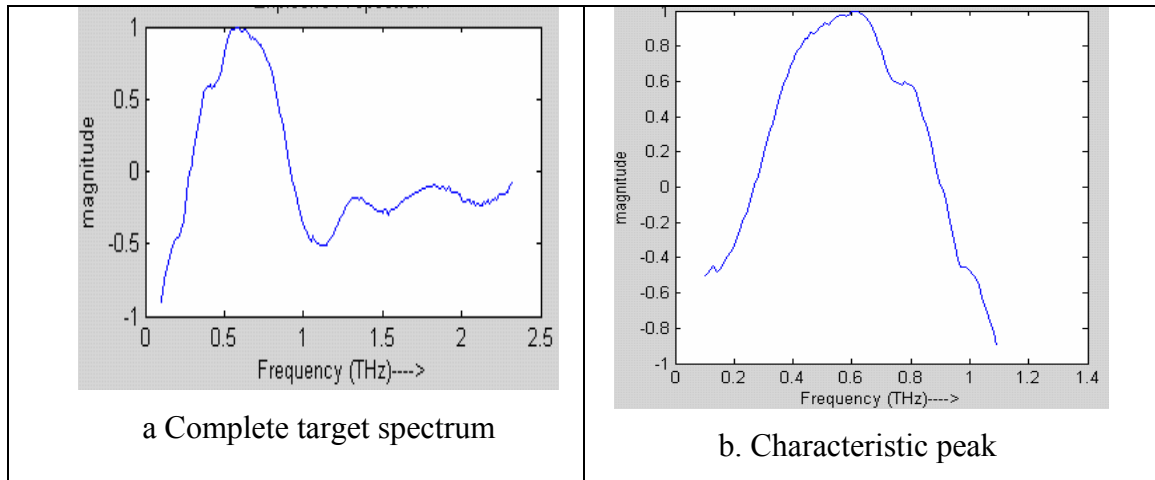
Figure 6.26. Target spectrum

Table 6.6 Results of unmixing stage (Method 2) with deterministic content of Target

Target content (%)	Maximum value of Correlation peak of the output Correlation Filter	Error probability of the output Correlation filters
1	0.2467	0.5742
5	0.3878	0.3224
10	0.4040	0.3004
15	0.4691	0.2230
20	0.6187	0.0991
25	0.6561	0.0776
50	0.8434	0.0129

The results in the table show that as the percentage of the target increases the maximum value of the correlation peak also increases. Hence, filters with lesser error probability are needed to detect the target spectrum.

7: FUTURE WORK

In this section a practical detection system for detection of IEDs and similar threats is proposed. The problem of detection of IED and other explosives is a complex one. Critical issues like standoff, real time and wide area detection have to be dealt with. Various detection strategies for detection of IEDs and explosives have been explored with each of these techniques having some strengths and potential disadvantages. For an efficient solution to the IED problem a system is needed which utilizes the capabilities of multiple detection strategies to come up with a system which has a higher overall performance as compared to the individual detection strategies.

Explosives detection techniques usually focus on either bulk explosives or traces of explosives. Detection of bulk explosives is carried out either by imaging characteristics of the explosive device or by detection of the explosive itself. Trace detection utilizes either emitted vapors from the explosive or explosive particles deposited on surfaces. Various techniques for bulk detection of explosives are X-rays, infrared, terahertz, microwaves, neutrons, gamma rays, magnetic resonance and magnetic fields. Some techniques for trace detection are Optical absorption, Optical fluorescence, Bio sensors, etc. None of these techniques can single handedly detect IEDs satisfying the constrains of standoff, real time and wide area detection. Hence, a system which uses multiple orthogonal sensors for IED detection is proposed here.

An Orthogonal Detection System

As pointed earlier detection of IED has constrains of standoff distance, time of detection and wide area coverage. This means that the system must provide the detection over a safe standoff distance, the detection must take minimum time so that there is enough time to disarm the IED and the detection system must cover a large area. An orthogonal system can be defined as a system in which detection methods are mutually independent i.e. they detect independent characteristics of the explosive device. For example an IED contains an explosive material and an electronic triggering mechanism. Hence, a system that detects the explosive by using a method like THz imaging and detects the electronic circuitry by stray electromagnetic radiations can be called an

orthogonal system. A system can also be partially orthogonal for example a system using THz imaging and THz spectroscopy. Successful standoff detection of an explosive when an explosive is present and very few indications of an explosive when there is no explosive is the intent of a system of orthogonal detectors. This system could contain an array of different type of sensors using different type of devices and technologies.

The advantages of a system of orthogonal detection technologies using an array of sensors over a system dependent on one technology are the following:

- It has a higher probability of detecting the presence of an explosive device over a large area and at a standoff distance.
- It has an ability to obtain spatial and temporal information about the explosive device.
- It is more difficult for a potential bomber to avoid, confuse, or defeat the system.
- It can be more effective in detecting explosive devices than any single technology.

Distributed arrays can be fixed in one location with multiple sensors or distributed over a geographical area. The most likely design for an IED detection application, especially for wide-area surveillance, would be a set of spatially and geographically distributed arrays of orthogonal and/or partially orthogonal sensors. Although distributed arrays provide the advantage of broad coverage and increased standoff capability, they present some substantial technical challenges. The following are among the most significant:

- Communications between sensors, arrays, and decision makers
- Sensor sampling and refresh approaches and rates
- Effective data transfer, integration, and assessment within an array
- Fusion of information from different sensor or detection technology types
- Sensor fault detection and isolation to maintain array data integrity
- Operationally acceptable times to sense, analyze, and identify the explosive device
- Intelligent aggregation of information for detection decision making
- Ease of deployment, maintenance, and operation

These challenges can be dealt with by designing a system utilizing data fusion from the orthogonal sensors. Figure 7.1 shows a system utilizing orthogonal sensors and data fusion.
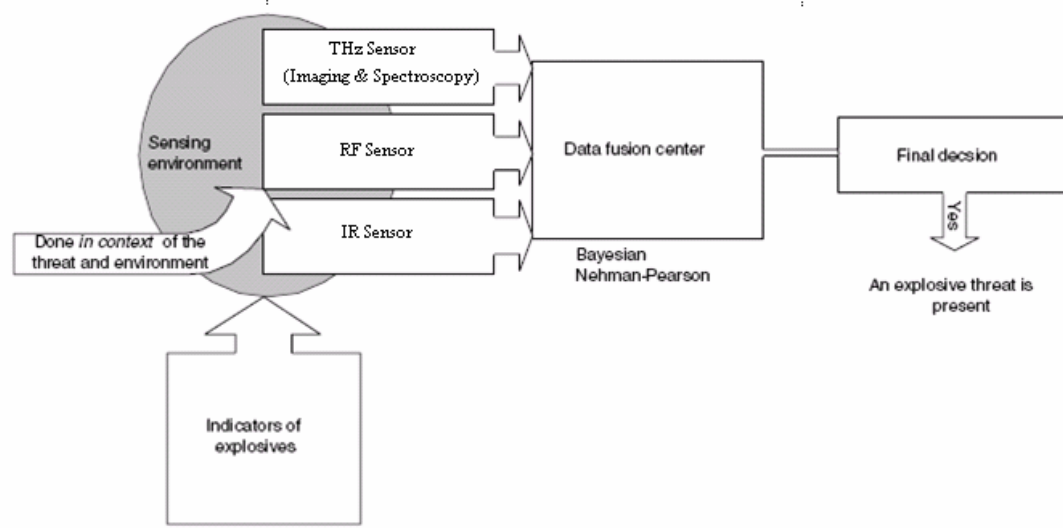
Figure 7.1: An IED detection system

The goal of decision fusion is the combination of input from multiple sensors or detectors. Decision fusion can be made using the Bayesian decision theory or Nehman-Pearson results. Under the Bayesian decision theory for a set of conditionally independent sensors or detectors, the optimal fused decision is the weighted sum of the individual results. The weights depend on the sensitivity and specificity of individual tests or sensor system behaviors.

Research efforts are needed on the integration of information from distributed orthogonal sensors to achieve real-time conflict resolution and decision making with high system effectiveness, and on integration tools based on data fusion and decision fusion. In addition, research coupling parallel sensors via decision fusion with sequential sensor systems may provide valuable insights.

8: CONCLUSIONS

In this thesis an effort was made to develop signal processing algorithms for processing terahertz data to detect IEDs at a standoff distance and in real time over a wide area. The developed algorithm has two stages with stage one as the preprocessing stage and stage two as the unmixing stage. The preprocessing stage utilizes correlation filters for selecting data points/ pixels that could have some explosive spectrum present within it. It was seen that this stage discards most of the data points/ pixels which do not have any explosive content. Due to this number of data points/pixels given to the unmixing stage is reduced considerably, causing a reduction in computation required in the second stage. Two types of correlation filters were proposed, one which uses the entire target spectrum and another which uses characteristic features in the target spectrum. It was seen that the filters which use a characteristic feature in the target spectrum perform better as compared to the filters that use entire target spectrum. But this is true only when that target spectrum has a notable characteristic feature like a peak or valley occurring a certain frequency. If the target spectrum does not have any characteristic features then using the entire spectrum would produce better results. Also, the threshold of the correlation filters in the preprocessing stage can be adjusted to reduce the number of false negatives and false positives. Decreasing the threshold increases the probability of error causing reduction in the false negatives i.e. most of the pixels having the target are detected. But at the same time this causes increase in the number of false positives i.e. pixels which do not have the target but are still selected. Thus, depending on the need of the user the desired accuracy can be obtained but at the cost of increased processing in the second stage.

The second stage does an unmixing of the spectrum in each pixel using a variant of the Independent Component Analysis (ICA) algorithm. This algorithm takes the required target spectra as reference and separates out spectra which are as close as possible to the target spectra. Thus, the algorithm avoids computation of all constituent spectra in the composite spectrum. After the required spectra are separated they are given to a final correlation filtering stage for determining if the separated spectra are of the target or not. All the false positives present in the preprocessing stage are removed in this

stage. Thus, the second stage accurately detects all the pixels that have the target present in them.

The simulations for both the stages were done using THz data of explosives like RDX and TNT and also with mineral data. The THz data was taken from published papers as actual laboratory data was not available. The importance of the unmixing stage was not clearly evident when the explosive data was used as the spectrum of RDX and TNT are not very complex in nature. Hence, to demonstrate the significance of the unmixing stage mineral data was used which provided spectra of various minerals. The spectrum of the target mineral considered was more complex, meaning it consisted of several peaks and valleys. With this data the importance of the unmixing stage becomes evident. Thus, the simulation results show that the detection algorithm can detect IEDs at a standoff distance and in real time over a wide area.

APPENDIX A

OPTIMIZATION THEORY

The cICA algorithm does an optimization of the ICA contrast function under some constrains. To better understand the process, consider the following optimization theory.

Optimization is finding a value that satisfies the maxima or minima of that function. Consider a problem where it is needed to maximize or minimize a function

$$f(x_1, x_2)$$

Subject to the constrain

$$g(x_1, x_2) = 0$$

The procedure followed is called method of Lagrange multipliers. The first step is to define a new function, the Lagrange function:

$$F(x_1, x_2, \lambda) = f(x_1, x_2) + \lambda g(x_1, x_2) \tag{1}$$

where λ is some constant, known as Lagrange multiplier. Now the necessary conditions for maximization or minimization of equation (1) with respect to x_1, x_2 and λ are

$$\frac{\partial F}{\partial x_1} = \frac{\partial f}{\partial x_1} + \lambda \frac{\partial g}{\partial x_1} = 0$$

$$\frac{\partial F}{\partial x_2} = \frac{\partial f}{\partial x_2} + \lambda \frac{\partial g}{\partial x_2} = 0 \tag{2}$$

$$\frac{\partial F}{\partial \lambda} = g(x_1, x_2) = 0$$

If these three equations are solved simultaneously then $F(x_1, x_2, \lambda)$ is maximized or minimized with respect to x_1, x_2 and λ. The third equation ensures that the constrain is also satisfied. This implies that $f(x_1, x_2)$ has been maximized or minimized since the second term on the right side of equation (2) is zero.

Inequality Constrains: Consider a problem where it is needed to maximize or minimize a function

$$f(x)$$

subject to the constrain $\qquad\qquad g(x) \leq b$

The approach of this kind of problem is to introduce a new variable called slack variable to convert the inequality to an equality. Hence,

$$g(x) + \upsilon^2 = b \qquad (3)$$

Now the problem can be solved similar to the case of equality constrain. The Lagrange function is

$$F(x, \lambda, \upsilon) = f(x) + \lambda[g(x) + \upsilon^2 - b] \qquad (4)$$

The Lagrange function is now differentiated with respect to x, λ, υ and result equated to zero.

$$\frac{\partial F}{\partial x} = \frac{\partial f}{\partial x} + \lambda \frac{\partial g}{\partial x} = 0$$

$$\frac{\partial x}{\partial \upsilon} = 2\lambda\upsilon = 0 \qquad (5)$$

$$\upsilon^2 = b - g(x)$$

The above three equations must be met for the solution of the optimization problem with inequality constraints.

APPENDIX B

MATLAB CODES

```
%MAIN CODE%
%This Code is for the Simulation of mixture of RDX and TNT
%Other Simulations can be done in the same way
clear, close all
dB=10;
counter = 0;
pixel_1 = [];
pixel = zeros(5,10);
selected_pixel=zeros(100,224);
seperated_signal_rdx=zeros(100,224);
seperated_signal_tnt=zeros(100,224);
false_negative= 0;
false_positive = 0;
false_negative_final= 0;
false_positive_final = 0;


%Computation of Threshold
error_prob = 0.25;
R0 = 1-exp(((erfcinv(error_prob/2))^2)/(-2))


%Explosive and Mineral Spectra
rdx =[0.24372    0.24911 0.2516   0.25251 0.25949 0.26937 0.2712   0.27908
0.28591 0.29592 0.30201 0.31367 0.31419 0.32277 0.32736 0.32962 0.33101
0.33979 0.34193 0.34977 0.35057 0.3637   0.37582 0.38618 0.39547 0.40693
0.42053 0.429127    0.430799    0.44131 0.44973 0.45491 0.45907 0.46224
0.46936 0.4701  0.47906 0.48565 0.49572 0.49945 0.5011   0.50808 0.50946
0.51239 0.52784 0.53135 0.54251 0.54987 0.5556   0.56249 0.56931 0.57135
0.57001 0.5709  0.56972 0.569712    0.56043 0.55482 0.54392 0.54382
0.535   0.53254 0.52209 0.52     0.51963 0.51572 0.51042 0.50552 0.5008
0.49814 0.49175 0.48513 0.48185 0.4807  0.47574 0.47089 0.46645 0.46277
0.45357 0.45199 0.44948 0.43712 0.42692 0.41528 0.40375 0.39367 0.38491
0.37569 0.3675  0.35931 0.35263 0.34695 0.34122 0.33578 0.33145 0.32851
0.33484 0.33026 0.32728 0.32403 0.32156 0.32132 0.32109 0.32109 0.32245
0.32356 0.32636 0.32904 0.33423 0.33895 0.34321 0.34745 0.35212 0.35712
0.36274 0.36663 0.37186 0.37658 0.38018 0.38157 0.3852   0.38676 0.38683
0.38833 0.38714 0.38659 0.38677 0.38732 0.38422 0.38281 0.38088 0.3798
0.3784  0.37648 0.37372 0.37315 0.37184 0.37069 0.3696   0.36957 0.36585
0.37194 0.37116 0.36839 0.3654   0.36896 0.37201 0.37321 0.37461 0.37582
0.37636 0.38103 0.38297 0.38334 0.38587 0.38765 0.38922 0.39107 0.39158
0.3935  0.3935  0.3954  0.39665 0.39812 0.39965 0.4002   0.40089 0.40054
0.40353 0.40452 0.40319 0.40311 0.40547 0.40585 0.4042   0.40321 0.40112
0.40213 0.40253 0.40032 0.39823 0.40019 0.40414 0.40092 0.39584 0.39577
0.39626 0.39494 0.39433 0.39344 0.38816 0.38363 0.38351 0.38358 0.38512
0.38413 0.37971 0.38289 0.38246 0.37839 0.37925 0.37646 0.37678 0.37859
0.38328 0.38107 0.38266 0.38501 0.38131 0.38446 0.38562 0.38687 0.38613
0.38869 0.39217 0.39349 0.39309 0.39315 0.39486 0.39664 0.40267 0.40571
0.40803 0.4098];
tnt
=[0.13277,0.13894,0.14383,0.14696,0.15234,0.15848,0.16417,0.17004,0.174
98,0.17806,0.18300,0.18786,0.19190,0.19524,0.19891,0.20324,0.20482,0.20
736,0.21031,0.21250,0.21397,0.21558,0.21908,0.22063,0.22283,0.22419,0.2
2544,0.22692,0.22721,0.22702,0.22856,0.22849,0.22646,0.22857,0.22809,0.
22964,0.23104,0.23305,0.23327,0.23647,0.23949,0.24243,0.24597,0.24783,0
.25116,0.25156,0.25559,0.25466,0.25606,0.25703,0.25546,0.25380,0.25362,
0.25879,0.25891,0.25978,0.26392,0.26268,0.26808,0.26919,0.27248,0.27409
,0.275903,0.27717,0.27826,0.28085,0.28177,0.28153,0.28072,0.28271,0.278
```

```
59,0.27848,0.27802,0.27891,0.28108,0.27859,0.27921,0.28030,0.27717,0.28
015,0.28226,0.28292,0.28257,0.28472,0.28846,0.29002,0.29299,0.29547,0.3
0052,0.30227,0.30433,0.30846,0.31206,0.31737,0.32107,0.32335,0.31825,0.
32153,0.32543,0.33039,0.333546,0.33888,0.34330,0.34841,0.35328,0.35955,
0.361052,0.28641,0.28156,0.29919,0.30000,0.30726,0.31734,0.32733,0.3235
9,0.32850,0.34624,0.3593,0.3524,0.36681,0.37463,0.382182,0.40288,0.4229
7,0.43522,0.44962,0.45324,0.45939,0.45968,0.46313,0.46940,0.46977,0.465
84,0.48355,0.49837,0.50199,0.51673,0.52350,0.52463,0.53791,0.5435,0.546
82,0.55645,0.56844,0.58496,0.58666,0.59257,0.59909,0.60067,0.61153,0.64
431,0.649183,0.65861,0.66145,0.68855,0.69084,0.70420,0.72692,0.73401,0.
74949,0.75549,0.76518,0.77306,0.79151,0.80611,0.80349,0.80696,0.81906,0
.81159,0.82738,0.82933,0.83294,0.83227,0.82347,0.80932,0.80039,0.780979
,0.77094,0.75057,0.74596,0.73494,0.722951,0.71830,0.71559,0.70193,0.693
29,0.68164,0.66074,0.650963,0.64770,0.63303,0.62240,0.60847,0.60148,0.6
0419,0.60704,0.59033,0.59455,0.59916,0.58044,0.57596,0.57418,0.57559,0.
5683,0.56503,0.55747,0.55093,0.53412,0.53205,0.53289,0.53153,0.53000,0.
52840,0.526904,0.52645,0.5246,0.52371,0.52005,0.51351,0.50530,0.5058,0.
49808,0.49971,0.49480;];
s(1,:) =[0.36697     0.37222 0.3782  0.38436 0.39074 0.39809 0.40674
0.41648 0.42456 0.43171 0.4387  0.44577 0.45358 0.46072 0.46779 0.47649
0.48858 0.50607 0.53107 0.56469 0.60301 0.63464 0.656   0.66975 0.67817
0.68524 0.6913  0.69674 0.70201 0.70743 0.71279 0.7188  0.70567 0.71109
0.71646 0.72237 0.72998 0.73556 0.73991 0.74265 0.7447  0.74673 0.74665
0.74653 0.74566 0.74482 0.74427 0.74311 0.74148 0.73851 0.73714 0.73649
0.73555 0.73629 0.73501 0.73439 0.74025 0.73889 0.73941 0.73878 0.74134
0.74405 0.74353 0.74465 0.74046 0.73878 0.73641 0.73296 0.73278 0.73843
0.74445 0.74972 0.75014 0.74995 0.74843 0.74954 0.75171 0.75328 0.75579
0.75493 0.75272 0.74979 0.74612 0.74316 0.73474 0.72124 0.70728 0.69829
0.68416 0.67836 0.68147 0.67747 0.68599 0.70498 0.72205 0.72991 0.70987
0.72478 0.73194 0.73565 0.73572 0.73526 0.73298 0.72781 0.71554 0.69816
0.67723 0.65181 0.6241  0.60017 0.5812  0.56545 0.54144 0.50042 0.44444
0.37865 0.31268 0.28119 0.31192 0.35716 0.38169 0.39538 0.40107 0.39595
0.39703 0.41812 0.4492  0.48298 0.51554 0.54475 0.5722  0.59903 0.62121
0.64017 0.65582 0.67007 0.68362 0.69338 0.69865 0.69941 0.69537 0.68343
0.65983 0.6261  0.58207 0.52575 0.47817 0.45143 0.44839 0.45427 0.46633
0.47668 0.48766 0.50297 0.52166 0.54413 0.56284 0.56999 0.5594  0.52683
0.52682 0.46756 0.3837  0.31271 0.26998 0.23418 0.201   0.16941 0.13967
0.1149  0.098824    0.10476 0.14375 0.19646 0.24592 0.28832 0.32673
0.36317 0.38909 0.40507 0.40825 0.4056  0.40234 0.39994 0.39772 0.39286
0.39102 0.38655 0.37668 0.36627 0.35308 0.33895 0.32684 0.31155 0.29869
0.28142 0.26702 0.26197 0.25827 0.2614  0.26225 0.26966 0.2831  0.28888
0.29431 0.29971 0.30085 0.29583 0.28627 0.26935 0.24552 0.23448 0.20704
0.18676 0.16649 0.14586 0.13096 0.125   0.11881 0.11819 0.12144 0.12455
0.12793 0.13422];
s(2,:) =[0.219  0.26932 0.33701 0.39495 0.41479 0.40195 0.41552 0.45999
0.49725 0.52205 0.54193 0.56036 0.57649 0.59021 0.60302 0.61451 0.62599
0.63823 0.65139 0.66498 0.67275 0.67759 0.67946 0.68097 0.68295 0.68663
0.69172 0.69835 0.70674 0.71616 0.72716 0.73804 0.71299 0.72346 0.73417
0.74424 0.74938 0.75756 0.76341 0.76849 0.77109 0.77124 0.77074 0.76835
0.76609 0.76286 0.75903 0.75536 0.75075 0.74786 0.745   0.74065 0.73857
0.7348  0.73268 0.73249 0.7303  0.73016 0.73005 0.73059 0.73083 0.73092
0.73198 0.73488 0.73675 0.73895 0.73906 0.74378 0.74688 0.75138 0.75646
0.76101 0.76351 0.76629 0.76875 0.77145 0.77327 0.77538 0.77642 0.77832
0.7811  0.78329 0.78432 0.78606 0.78703 0.78858 0.79006 0.79288 0.79079
0.78867 0.78781 0.7842  0.78193 0.77962 0.77542 0.7803  0.77822 0.77611
0.78274 0.79002 0.796   0.79971 0.80185 0.80252 0.79908 0.79826 0.80195
0.80484 0.8069  0.80285 0.79547 0.7832  0.73489 0.71298 0.72447 0.69601
```

```
0.65688 0.62329 0.68302 0.71798 0.7345  0.73343 0.72515 0.7186  0.7219
0.72611 0.73603 0.74899 0.75944 0.76787 0.77416 0.7769  0.7764  0.7762
0.77772 0.78351 0.78808 0.79209 0.79111 0.79036 0.79496 0.79511 0.791
0.78373 0.7751  0.76378 0.75263 0.73758 0.72959 0.73988 0.75841 0.76913
0.77092 0.76858 0.7665  0.75945 0.75064 0.74519 0.73959 0.73153 0.73153
0.71721 0.70205 0.68965 0.67501 0.66018 0.65011 0.6349  0.61306 0.58254
0.5504  0.5109  0.46586 0.44401 0.44239 0.44887 0.45852 0.45858 0.45465
0.44612 0.43173 0.41073 0.37612 0.34567 0.34726 0.38416 0.4067  0.4106
0.4193  0.42257 0.4342  0.45993 0.47775 0.51434 0.55985 0.58297 0.59477
0.5997  0.60265 0.60724 0.61175 0.60915 0.61238 0.59185 0.56926 0.59049
0.61563 0.62243 0.62147 0.59817 0.56066 0.54811 0.5242  0.50731 0.49397
0.4897  0.49009 0.48778 0.47477 0.46408 0.43292 0.41948 0.41154
0.41753];
s(3,:)
=[0.151528403162956,0.186773627996445,0.226627856492996,0.2491778880357
74,0.263140290975571,0.257041394710541,0.262268424034119,0.314153194427
49,0.34473180770874,0.365987837314606,0.389759480953217,0.4189826548099
52,0.448219895362854,0.477171570062637,0.503706395626068,0.527110338211
06,0.546073377132416,0.558839619159698,0.56877076625824,0.5773610472679
14,0.58626914024353,0.59591943025589,0.604315876960754,0.61253398656845
1,0.621591210365295,0.631901800632477,0.644165992736816,0.6574634909629
82,0.672378480434418,0.687856674194336,0.70128470659256,0.7130383849143
98,0.683329880237579,0.697052896022797,0.708894908428192,0.719779849052
429,0.728134393692017,0.735950350761414,0.741059303283691,0.74513167142
868,0.747349441051483,0.748551547527313,0.746141910552978,0.74210506677
6276,0.735716462135315,0.725956797599792,0.715826869010925,0.7058167457
58057,0.695137023925781,0.684300482273102,0.676128804683685,0.670778334
140778,0.669138252735138,0.669188261032104,0.669800817966461,0.67455828
1898498,0.680572211742401,0.692793726921082,0.695845603942871,0.7036471
96292877,0.715304732322693,0.727616131305695,0.7370485663414,0.74903881
5498352,0.760584115982056,0.768897891044617,0.777783930301666,0.7846566
43867493,0.79430764913559,0.799533426761627,0.806056439876556,0.8119293
4513092,0.818959653377533,0.82276576757431,0.825433313846588,0.83154815
4354096,0.835500419139862,0.841075778007507,0.843075394630432,0.8465119
60029602,0.851393759250641,0.854023218154907,0.856058716773987,0.860429
346561432,0.860164999961853,0.863771617412567,0.86671382188797,0.868816
554546356,0.869144082069397,0.87220823764801,0.873466491699219,0.874281
346797943,0.876217544078827,0.875829517841339,0.878814518451691,0.87995
7318305969,0.876460015773773,0.879452228546143,0.880107760429382,0.8813
64226341248,0.88067215681076,0.881947338581085,0.882022559642792,0.8822
88851556778,0.882650196552277,0.883319318294525,0.883171319961548,0.8841
31252765656,0.882969737052918,0.88113409280777,0.874953746795654,0.8577
87609100342,0.829309344291687,0.831071615219116,0.85113650560379,0.8693
41731071472,0.883332073688507,0.891374409198761,0.895400166511536,0.898
151755332947,0.90006697177887,0.900960683822632,0.901291608810425,0.902
116298675537,0.904342830181122,0.904658854007721,0.905926167964935,0.90
8310651779175,0.908747315406799,0.909371554851532,0.909456133842468,0.9
08731162548065,0.909639775753021,0.909053862094879,0.909161984920502,0.
909794986248016,0.909438192844391,0.908489108085632,0.906717419624329,0
.908217012882233,0.908402323722839,0.907345771789551,0.908324182033539,
0.907659232616425,0.905171036720276,0.906576931476593,0.908191382884979
,0.908828794956207,0.909371078014374,0.909613192081451,0.91219055652618
4,0.909939765930176,0.907119274139404,0.906511843204498,0.9077848196029
66,0.906517565250397,0.905733823776245,0.906186699867248,0.901911497116
089,0.90077394247055,0.900773882865906,0.90012925863266,0.8994402289390
56,0.89705753326416,0.893292486667633,0.892928242683411,0.8940395116806
03,0.891984939575195,0.893203914165497,0.894339799880981,0.893694758415
```

```
222,0.893323123455048,0.893109381198883,0.898133158683777,0.89724057912
8265,0.899571597576141,0.899079263210297,0.896217107772827,0.8999733328
81928,0.89739179611206,0.894350945949554,0.897117137908936,0.8969291448
59314,0.891966223716736,0.896610796451569,0.896818935871124,0.891588747
501373,0.886509776115418,0.880887150764465,0.875161230564117,0.85721486
8068695,0.841388523578644,0.833127021789551,0.812981843948364,0.7957339
2868042,0.784738540649414,0.773671567440033,0.776192009449005,0.7819138
76533508,0.785303235054016,0.784914076328278,0.788185179233551,0.792932
629585266,0.787080109119415,0.788558661937714,0.795879781246185,0.79585
0813388824,0.786288201808929,0.768426239490509,0.74762237071991,0.71573
2932090759,0.699293851852417,0.687243103981018,0.692490935325623,0.6998
50022792816,0.705065548419952,0.704658925533295,0.701828956604004,0.693
299651145935,0.689226984977722,0.683233261108398,0.680951237678528,0.67
8235411643982,0.669941186904907;];
s(4,:) =[0.38026    0.39333 0.40343 0.41544 0.4292  0.44264 0.4488
0.45838 0.47147 0.48498 0.49992 0.51168 0.52198 0.53046 0.53756 0.53889
0.53715 0.53403 0.53076 0.52508 0.51828 0.5105  0.50218 0.49408 0.48643
0.48045 0.47554 0.47327 0.47197 0.4721  0.47453 0.47728 0.47191 0.47325
0.47673 0.47754 0.48129 0.48643 0.49218 0.49731 0.50257 0.50904 0.51517
0.52143 0.52823 0.533   0.53654 0.53866 0.53946 0.53878 0.53559 0.53208
0.52932 0.52748 0.51896 0.51426 0.50802 0.4969  0.48544 0.47411 0.46049
0.45057 0.43319 0.4205  0.40688 0.39336 0.38057 0.36958 0.36207 0.36065
0.36077 0.36474 0.37631 0.39231 0.41242 0.43538 0.45962 0.48525 0.50573
0.5245  0.54134 0.55697 0.57028 0.58166 0.5911  0.60108 0.6103  0.61854
0.6271  0.63228 0.64123 0.64781 0.65518 0.66141 0.66952 0.6764  0.66349
0.67187 0.67745 0.68381 0.69     0.69658 0.70368 0.70904 0.71456 0.71979
0.72427 0.72746 0.72511 0.71801 0.62647 0.6688  0.72703 0.74885 0.75688
0.76095 0.76513 0.76762 0.77076 0.77367 0.77644 0.77974 0.78108 0.78335
0.7854  0.7883  0.79017 0.79311 0.79229 0.79675 0.79706 0.79669 0.79902
0.80057 0.80125 0.80388 0.80251 0.80372 0.80573 0.80328 0.80875 0.80873
0.80955 0.80669 0.80709 0.80309 0.80638 0.80591 0.80345 0.80146 0.80499
0.80071 0.8011  0.79683 0.79264 0.79316 0.78962 0.78338 0.78349 0.78258
0.78257 0.77685 0.77394 0.77087 0.76584 0.76501 0.76145 0.75666 0.75626
0.75386 0.74736 0.74053 0.73572 0.73304 0.73065 0.72624 0.72184 0.71869
0.71464 0.70793 0.69975 0.69837 0.69352 0.68209 0.67551 0.67134 0.67364
0.6698  0.66542 0.66355 0.65545 0.64929 0.64621 0.64154 0.63434 0.62985
0.61318 0.59746 0.59665 0.57638 0.54954 0.51112 0.4773  0.45784 0.46952
0.527   0.5628  0.56536 0.5609  0.53835 0.49977 0.49192 0.52073 0.53844
0.54719 0.55043 0.54895 0.54714 0.54367 0.54285 0.54481 0.54727 0.55027
0.55699];


%Energy Normalization
s(1,:)=normalize(s(1,:));
s(2,:)=normalize(s(2,:));
s(3,:)=normalize(s(3,:));
s(4,:)=normalize(s(4,:));
rdx=normalize(rdx);
tnt=normalize(tnt);

%Number of pixels in the field
num_pixels = 100;


%Formation of the Type-1,2,3 pixels
for i=1:100
```

```
    %Type 3
    if((i>=1 && i<=40)||(i>=91 && i<=100)||(i==41)||(i==42)||(i>=45 &&
i<=48)||(i==51)||(i>=56 && i<=57)||(i==61)...
            ||(i>=66 && i<=67)||(i>=71 && i<=72)||(i>=75 &&
i<=77)||(i>=81 && i<=88))
        for j=1:3;
            P(j,:)= s(ceil(1 + (4-1).*rand(1,1)),:) ;
        end
         n= 0.1*rand(1,length(s));
         S(i,:) = P(1,:)*rand(1,1) + P(2,:)*rand(1,1) +n; %+
P(3,:)*rand(1,1)+n ;
         S(i,:) = normalize(S(i,:));


    %Type 2 Pixels
    elseif((i>=43 && i<=44)||i==52||i==55||i==62||i==65||(i>=73 &&
i<=74)||(i>=49 && i<=50)||i==58||i==68||i==78||(i>=89 && i<=90))

         n= 0.2*rand(1,length(s));
         S(i,:) = rdx*rand(1,1) + tnt*rand(1,1) + s(1,:)*rand(1,1)+n ;
         S(i,:) = normalize(S(i,:));


%-----------------------For Deterministic Content -------------------%
%          num1 = ceil(1 + (4-1).*rand(1,1))
%          num2 = ceil(1 + (4-1).*rand(1,1))
%          %num1 = 10;
%          %num2 = 7;
%          S(43,:) = rdx*0.05 + s(num1,:)*0.55 + s(num2,:)*0.4 ;
S(43,:)=normalize(S(43,:));
%          S(44,:) = rdx*0.06 + s(num1,:)*0.45 +
s(num2,:)*0.49 ;S(44,:)=normalize(S(44,:));
%          S(52,:) = rdx*0.07 + s(num1,:)*0.46 +
s(num2,:)*0.47 ;S(52,:)=normalize(S(52,:));
%          S(55,:) = rdx*0.08 + s(num1,:)*0.46+ s(num2,:)*0.46 ;
S(55,:)=normalize(S(55,:));
%          S(62,:) = rdx*0.1 + s(num1,:)*0.45 + s(num2,:)*0.45 ;
S(62,:)=normalize(S(62,:));
%          S(65,:) = rdx*0.2 + s(num1,:)*0.4 + s(num2,:)*0.4 ;
S(65,:)=normalize(S(65,:));
%          S(73,:) = rdx*0.3 + s(num1,:)*0.35 + s(num2,:)*0.35 ;
S(73,:)=normalize(S(73,:));
%          S(74,:) = rdx*0.4 + s(num1,:)*0.3 + s(num2,:)*0.3;
S(74,:)=normalize(S(74,:));
%          S(49,:) = rdx*0.5 + s(num1,:)*0.251 +
s(num2,:)*0.251;S(49,:)=normalize(S(49,:));
%          S(50,:) = rdx*0.6 + s(num1,:)*0.2 + s(num2,:)*0.2;
S(50,:)=normalize(S(50,:));
%          S(58,:) = rdx*0.2 + s(num1,:)*0.4 + s(num2,:)*0.4 ;
S(58,:)=normalize(S(58,:));
%          S(68,:) = rdx*0.3 + s(num1,:)*0.35 + s(num2,:)*0.35 ;
S(68,:)=normalize(S(68,:));
%          S(78,:) = rdx*0.4 + s(num1,:)*0.3 + s(num2,:)*0.3;
S(78,:)=normalize(S(78,:));
%          S(89,:) = rdx*0.5 + s(num1,:)*0.251 +
s(num2,:)*0.251;S(89,:)=normalize(S(89,:));
%          S(90,:) = rdx*0.6 + s(num1,:)*0.2 + s(num2,:)*0.2;
S(90,:)=normalize(S(90,:));
```

```
%-----------------------------------------------------------------%
    else
    %Type 1 Pixels
            n= 0.1*rand(1,length(s));
            S(i,:) = rdx + tnt + n;
            S(i,:) = normalize(S(i,:));

    end
end

% Correlation Filters

H= fliplr(rdx);
%--------Used for Method 1-----------%
s_detected_rdx = rdx;
s_detected_tnt = tnt;
%----------------------------------%


%-------Used for Method 2------------%
%s_detected_rdx = rdx(1:100);
%s_detected_tnt = tnt(110:200);
%----------------------------------%


% Correlation Filter Output
correlation_s1 = xcorr(s_detected_rdx,rdx);
correlation_s2 = xcorr(s_detected_tnt,tnt);
N = length(s)-length(s_detected_rdx)+floor(length(s_detected_rdx)/2);

for i=1:num_pixels
    correlation_rdx(i,:) = xcorr(S(i,:),s_detected_rdx);
    correlation_tnt(i,:) = xcorr(S(i,:),s_detected_tnt);
    correlation_rdx(i,:) =
normalize_wrt_s1(correlation_rdx(i,:),correlation_s1);
    correlation_tnt(i,:) =
normalize_wrt_s1(correlation_tnt(i,:),correlation_s2);

    %---------------For Method 2--------------------%
%    correlatio = correlation_rdx(i,N+1:N+length(s));
%    new_correlation_rdx(i,:)=correlatio;
%    correlatio = correlation_tnt(i,N+1:N+length(s));
%    new_correlation_tnt(i,:)=correlatio;
    %-------------------------------------------%

    [max_corr_rdx pos1]=max(correlation_rdx(i,:));
    [max_corr_tnt pos2]=max(correlation_tnt(i,:));
    %if (max_corr_rdx >R0 && (pos1>=200 && pos1<=250))||(max_corr_tnt
>R0 && (pos2>=300 && pos1<=375))                    % For Method 2
    if (max_corr_rdx >R0 || max_corr_tnt
>R0 )                         % For Method 1
        selected_pixel(i,:)=S(i,:);
        counter = counter+1;
        pixel_1(i) = 1;
    else
        pixel_1(i) = 0;
        selected_pixel(i,:)=0;
```

```
        end
end

t = -length(correlation_rdx)/2:(length(correlation_rdx)/2)-1;

%Plotting the field having 100 pixels
figure;
for y=1:10
    for x=1:10
        i=(y*10)-10+x;

            %Type 3
            if((i>=1 && i<=40)||(i>=91 && i<=100)||i==41||i==42||(i>=45
&& i<=48)||i==51||(i>=56 && i<=57)...
                         ||i==61||(i>=66 && i<=67)||(i>=71 && i<=72)||(i>=75
&& i<=77)||(i>=81 && i<=88))
                    hold;plot(x,y,'go:');hold;
            elseif ((i>=43 &&
i<=44)||i==52||i==55||i==62||i==65||(i>=73 && i<=74)||(i>=49 &&
i<=50)||i==58||i==68||i==78||(i>=89 && i<=90))
                    hold;plot(x,y,'bo:');hold;
            elseif ((i>=53 && i<=54)||(i>=63 && i<=64)||(i>=59 &&
i<=60)||(i>=69 && i<=70)||(i>=79 && i<=80))
                    hold;plot(x,y,'ro:');hold;
            end

    end
end
title('Field with 100 pixels');
xlabel('x axis--->');
ylabel('y axis--->');

%Plotting the Field after Preprocessing
figure;
i=1;
for k = 1:10
    for j = 1:10
        if pixel_1(i) == 1
            hold;plot(j,k,'ro-');hold;
        else
            hold;plot(j,k,'go-');hold;
        end
        i=i+1;
    end

end
title('Field with 100 pixels after Pre-processing');
xlabel('x axis--->');
ylabel('y axis--->');

%Results
for i=1:100
    if((i>=43 && i<=44)||i==52||i==55||i==62||i==65||(i>=73 &&
i<=74)||(i>=49 && i<=50)||i==68||i==78||(i>=89 && i<=90)||...
```

```
            (i>=53 && i<=54)||(i>=63 && i<=64)||(i>=59 &&
i<=60)||(i>=69 && i<=70)||(i>=79 && i<=80))...
            && (max(correlation_rdx (i,:))<R0)&& (max(correlation_tnt
(i,:))<R0)
            false_negative = false_negative +1;
    elseif  ((i>=1 && i<=40)||(i>=91 &&
i<=100)||(i==41)||(i==42)||(i>=45 && i<=48)||(i==51)||(i>=56 &&
i<=58)||(i==61)...
            ||(i>=66 && i<=67)||(i>=71 && i<=72)||(i>=75 &&
i<=77)||(i>=81 && i<=88))&& ...
            (max(correlation_rdx (i,:))>R0 || max(correlation_tnt
(i,:))>R0)
            false_positive = false_positive + 1;
    end
end


%------------------------------------------------------------------------%
%------------------End Of Pre-Processing-----------------------------%
%-----------------Unmixing using Improved ICA------------------------%
mu0 = 1;
lambda0 = 1;
gamma = 1;
learningRate = 1;
OverValue=0.000001;  maxIter = 200;
threshold = 1.75;
ref1=rdx;
ref2=tnt;
num_selected_pixels=0;
for i=1:100
    if( selected_pixel(i,:)~=0)
        num_selected_pixels = num_selected_pixels+1;
        X= selected_pixel(i,:);
        [X,V] = whiten(X);          % whitening
        w = rand(size(X,1),1);w=w/norm(w);
        [y1, w] = cICA(X, ref1, threshold, w, learningRate, mu0,
lambda0, gamma, maxIter, OverValue);
        [y2, w] = cICA(X, ref2, threshold, w, learningRate, mu0,
lambda0, gamma, maxIter, OverValue);
        seperated_signal_rdx(i,:) = y1;
        seperated_signal_tnt(i,:) = y2;
        seperated_signal_rdx(i,:) =
normalize(seperated_signal_rdx(i,:));
        seperated_signal_tnt(i,:) =
normalize(seperated_signal_tnt(i,:));
    else
        seperated_signal_rdx(i,:)=0;
        seperated_signal_tnt(i,:)=0;
    end
end




%------------------------------------------------------------------------%
%------------------------End of Unmixing-----------------------------%
%--------------------Final Conformation of location of IED-----------%
```

```
%Computation of Threshold
error_prob = 0.25;
R0_final = 1-exp(((erfcinv(error_prob/2))^2)/(-2));


%Final Correlation Filtering for Conformation
for i=1:num_pixels
    correlation_final_rdx(i,:) =
xcorr(seperated_signal_rdx(i,:),s_detected_rdx);
    correlation_final_rdx(i,:) =
normalize_wrt_s1(correlation_final_rdx(i,:),correlation_s1);
    correlation_final_tnt(i,:) =
xcorr(seperated_signal_tnt(i,:),s_detected_tnt);
    correlation_final_tnt(i,:) =
normalize_wrt_s1(correlation_final_tnt(i,:),correlation_s1);
    %correlation_final(i,:) = correlation_final(i,:);
    [max_corr_final_rdx ,pos1] = max(correlation_final_rdx(i,:));
    [max_corr_final_tnt ,pos2] = max(correlation_final_tnt(i,:));


    %Method 1
    if (((max_corr_final_rdx > R0_final)&& (pos1>=200 &&
pos1<=250))||((max_corr_final_tnt>R0_final)&& (pos2>=200 &&
pos2<=250)))
    %Method 2
    %if (((max_corr_final_rdx > R0_final)&& (pos1>=200 &&
pos1<=250))||((max_corr_final_tnt>R0_final)&& (pos2>=300 &&
pos2<=375))) %&& (pos>=200 && pos<=250))
        counter = counter+1;
        pixel_2(i) = 1;
    else
        pixel_2(i) = 0;
    end
end


%Plotting the final hotspots in the field
figure;
i=1;
for k = 1:10
    for j = 1:10
        if pixel_2(i) == 1
            hold;plot(j,k,'ro-');hold;
        else
            hold;plot(j,k,'go-');hold;
        end
        i=i+1;
    end

end
title('Final detected pixels');xlabel('x axis-->');ylabel('y axis-->');

%Results after unmixing
%Results
for i=1:100
    if((i>=43 && i<=44)||i==52||i==55||i==62||i==65||(i>=73 &&
i<=74)||(i>=49 && i<=50)||i==68||i==78||(i>=89 && i<=90)||...
```

```
                (i>=53 && i<=54)||(i>=63 && i<=64)||(i>=59 &&
i<=60)||(i>=69 && i<=70)||(i>=79 && i<=80))...
               && (max(correlation_final_rdx (i,:))<R0_final)&&
(max(correlation_final_tnt (i,:))<R0_final)
               false_negative_final = false_negative_final +1;
       elseif ((i>=1 && i<=40)||(i>=91 &&
i<=100)||(i==41)||(i==42)||(i>=45 && i<=48)||(i==51)||(i>=56 &&
i<=58)||(i==61)...
               ||(i>=66 && i<=67)||(i>=71 && i<=72)||(i>=75 &&
i<=77)||(i>=81 && i<=88))...
               && (max(correlation_final_rdx (i,:))>R0_final) ||
(max(correlation_final_tnt (i,:))>R0_final)
               false_positive_final = false_positive_final + 1;
       end
end


%FUNCTION FOR ICA with REFERENCE

function [y, w] = cICA(X, ref, threshold, w0, learningRate, mu0,
lambda0, gamma, maxIter, OverValue)

fprintf('Starting cICA for extracting the desired source signal ..\n');
[ICnum, IClen]=size(X);

w = w0;
oldw = w;

mu = mu0;
lambda = lambda0;

flag = 1;
loop = 1;

% compute the autocorrelation matrix Rxx
Rxx = X(:,[1:end]) * X(:,[1:end])' / IClen;

while (flag == 1)

    % output at current iteration
    y = w' * X;

    % calculate the first order deviation of the Lagarange function
    std_y = std(y);                          % standard deviation
    v_Gaus = normrnd(0, std_y, 1, IClen);    % Gaussian signal with the
same mean and variance
    rou = mean( log(cosh(y)) - log(cosh(v_Gaus)) );
    L1 = sign(rou) * ( X * tanh(y)')/IClen - mu * ( X * (y -
ref)')/IClen ...
         - lambda * ( X * y')/IClen;

    % related to the second order deviation of the Lagarange function
    Sw = sign(rou) * mean(1-tanh(y).^2) - mu - lambda;

    % update of the weight vector
```

```
    w = w - learningRate * inv(Rxx) * L1 / Sw;
%   w = w - learningRate * L1 / Sw;
    w = w/norm(w);

    % update of the parameter mu
    thr = threshold * (1-exp(-loop));
    thr = threshold;
    g = mean( (y-ref).^2 ) - thr;    % corresponds to the inequality
constraint
    mu = max(0, mu + gamma * g);

    % update of the parameter lambda
    h = mean(y.^2) - 1;                    % corresponds to the
equality constraint
    lambda = lambda + gamma * h;


    % decide whether the algorithm has converged or not
    wchange = 1-abs(w'*oldw);
    fprintf('No.%d iteration: change in w is %g\n',loop, wchange);
    if wchange < OverValue
        fprintf('Converged after %d iteration\n',loop);
        flag = 0;
    end

    if loop >= maxIter
        fprintf('After %d iteration, still cannot convergent.\n',loop);
        flag = 0;
    end

    oldw = w;
    loop = loop + 1;

end

% output
y = w'* X;

fprintf('End of cICA algorithm !\n');

% Function that Returns the whitend signals and the whitening matrix.

function varargout = whiten(X,m)

[n,T] = size(X);
if nargin == 1
    m = n;        % default value
end

if m < n   % assumes white noise
    [U,D]   = eig((X*X')/T);
    [puiss,k] = sort(diag(D));
    ibl = sqrt(puiss(n-m+1:n)-mean(puiss(1:n-m)));  % subspace of
signals and noise - that of noise
```

```
    bl   = ones(m,1) ./ ibl ;
    W    = diag(bl)*U(1:n,k(n-m+1:n))';
    IW   = U(1:n,k(n-m+1:n))*diag(ibl);

    fprintf('whitening...Lost %g%% energy\n',100*sum(puiss(1:n-
m))/(sum(diag(D))));
else      % assumes no noise
    IW   = sqrtm((X*X')/T);
    W    = inv(IW);
end;


Y = W * X;


varargout{1} = Y;
varargout{2} = W;



% FUNCTION for Normalizing a Signal

function t1 = normalize(t1);

t1 = (t1 - mean(t1)) / max(abs((t1 - mean(t1))));
```

BIBLIOGRAPHY

[1]   B. Fischer, M. Homan, H. Helm, G. Modjesch, and P. U. Jepsen, "Chemical recognition in terahertz time-domain spectroscopy and imaging," 2005 Semicond.Sci.Technol., vol. 20, pp. S246S253.

[2]   U.S. Department of Homeland Security, Office for Domestic Preparedness, "Explosive Devices," Awareness Level WMD Training., http://cdp.dhs.gov/pdfs/agert/Explosive_Devices.pdf.

[3]   Albert Eisele, "Improved Explosives Becoming More Deadly in Iraq," 2005 The Hill,Mar.28,http://www.hillnews.com/thehill/export/TheHill/News/Iraq/explosiv es1.html, March 2007.

[4]   http://www.globalsecurity.org/military/intro/ied.htm. Definition from Global Security.org, March 2007.

[5]   http://www.washingtonpost.com/wpdyn/content/article/2005/10/25/AR2005102 01987.html, "fusion94.org/.../improvised-explosive-devices/," Pictures of IEDs March 2007.

[6]   G.L. Carr, M.C. Martin, W.R. McKinney, G.R. Neil, K. Jordan and G.P. Williams. "High Power Terahertz Radiation from Relativistic Electrons," Nature, 420: 153 (2002).

[7]   F. Wang, D. Cheever, M. Farkhondeh, W. Franklin, E. Ihlo, J. van der Laan, B.McAllister, R. Milner, C. Tschalaer, D. Wang, D. F. Wang, A. Zolfaghari, T. Zwart, G. Carr, B. Podobedov, and F. Sannibale, "Coherent THz synchrotron radiation from a storage ring with high frequency RF system," Phys. Rev. Lett., vol. 96, p. 064801, 2006.

[8]   G. L. Carr, M. C. Martin, W. R. McKinney, K. Jordan, G. R. Neil, and G. P. Williams, "High-power terahertz radiation from relativistic electrons," Nature, vol. 420, pp. 153{156, 2002.

[9]   R. J. Bell, Introductory Fourier Transform Spectroscopy. Academic, New York, 1972.

[10]   K. M. Evenson, D. A. Jennings, K. R. Leopold, and L. R. Zink in Laser Spectroscopy VII. Papers from the Seventh International Conference on Laser Spectroscopy (T. W. H. andY. R. Shen, ed.), Springer, Berlin, 1985.

[11]   B. Xu, Q. Hu, and M. R. Melloch, "Electrically pumped tunable terahertz emitter based on intersubband transition," Appl. Phys. Lett., vol. 71, pp. 440{442, 1997.

[12]   D. Turchinovich, "Study of ultrafast polarization and carrier dynamics in semicon-ductor nanostructures: A THz spectroscopy approach," PhD thesis, University of Freiburg, 2004.

[13]   D. H. Auston, "Subpicosecond electro optic shock waves," Appl. Phys. Lett., vol. 43, pp. 713{715, 1983.

[14]   Leitensotorfer, et al. "Detectors and Sources for Ultrabroadband electro-optic Sampling," 1999 Experiment and Theory, Applied Physics Letters 74, 1516-1518.

[15]   Q.Wu and X.-C.Zhang, "Free-Space Electro-Optic Sampling of Terahertz Beams," Applied Physics Letters 67, 3523-3525 (1995)

[16]   C. Winniwisser, et all, "Electro-optic detection of THz radiation in LiTaO3, LiNbO3 and ZnTe," Applied Physics Letters 70, 3069-3071 (1997).

[17]   Pickett H.M, Poynter R.L and Cohen E.A, "Submillimeter, millimeter and microwave spectral line catalog," 2003, http://spec.jpl.nasa.gov.

[18]   Pickett M, Poynter R.L, Cohen E.A, Delitsky M. L, Pearson J.C and Muller H.S.P. "Submillimeter, millimeter and microwave spectral line catalog," 1998, Journal of Quantitative Spectroscopy and Radiation transfer, 60, pp.883-890.

[19]   Siegel P.H "Terahertz technology," 2002, IEEE Transactions on Microwave Theory and Techniques, 50(3), pp, 910-928.

[20]   Mann C.M, De Maagt. P, McBride.G, Van-De-Water.F, Castiglione.D, McCalden.A, Deias.L, O'Neill.J, Laisne.A Vallinas.J, Ederra.I, and Haskett.D,"Microfabrication of 3D terahertz circuitry," 2003, IEEE MTT-S International Microwave Symposium Digest, Vol 2, Piscataway, NJ, pp 739-742.

[21]   Malykh.N.I, Nagornyi. A.G and Yampolskii.E.S "Submillimeter wave imagery, Instruments and Experimental Techniques," 1975

[22]   Hartwick. T.S, Hodges D.T, Barker.D.H and Foote.F.B "Far infrared imagery," 1976 Applied Optics, 15(8), pp 1919-1922.

[23]   Lash. A.A, and Yundev.D.N "Visualization of submillimeter laser radiations with pyroelectric television camera, Instruments and Experimental Techniques," 1984

[24]   Hu.B.B and Nuss.M.C, "Imaging with Terahertz Waves," 1995 Optics letters, 20(16), pp. 1716-1718.

[25]   Wu.Q and Zhang.X.C, "Free space electro-optic sampling of terahertz beams," 1995, Applied Physics Letters, 67(24), pp.3523-3525.

[26]   Wu.Q, Hewitt.T.D, Zhang.X.C, "Two dimensional electro-optic imaging of terahertz beams," 1996, Applied Physics Letters, 69(8), pp 1026-1028.

[27]   Jiang.Z and Zhang.X.C, "Electro-optic measurement of THz field pulses with a chirped optical beam," 1998, Applied Physics Letters, 72(16), pp 1945-1947

[28]   O'Hara and Grischkowsky.D "Quasi-optic terahertz imaging," 2001 Optic Letters, 26(23), pp.1918-1920.

[29]   O'Hara and Grischkowsky.D "Synthetic phased array terahertz imaging," 2002, Optic Letters, 27(12), pp1070-1072.

[30]   O'Hara and Grischkowsky.D "Quasi-optic synthetic phased array terahertz imaging," 2004, Journal of the Optical Society of America B: Optical Physics, 21(6), pp 1178-1191.

[31]   Jiang.Z and Zhang.X.C, "Electro-optic measurement of THz field pulses with a chirped optical beam," 1998, Applied Physics Letters, 72(16), pp 1945-1947

[32]   F. G. Sun, Zhiping Jiang and X.-C. Zhang, "Analysis of terahertz pulse measurement with a chirped probe beam," 1998, Applied Physics Letters Volume 73, Number 16

[33]   Michael Herrmann, Masahika Tani, Kiyomi Sakai, Masayoshi Watanabe, "Multichannel Signal Recording with Photoconductive Antennas for THz Imaging," Terahertz Electronics Proceedings, 2002. IEEE Tenth International Conference

[34]   John O'Hara and D. Grischkowsky, "Quasi-optic synthetic phased-array terahertz imaging," Optic Letters 26(23), pp 1918-1920.

[35]   J. E. Parrneter, "The challenge of standoff explosives detection," Proceedings. IEEE 38th Annual 2004 International Carnahan Conference on Security Technology , 355-358 (2004).

[36]   J. C. Carter, S. M. Angel, M. Lawrence-Snyder, J. Scaffidi, R. E. Whipple, J. G. Reynolds, "Standoff Detection of High Explosive Materials at 50 Meters in Ambient Light Conditions Using a Small Raman Instrument," Applied Spectroscopy, 59, 769-775 (2005).

[37]   B. B. Hu and M. C. Nuss, Opt. Lett. 20, 1716-1718 1995.

[38]   D. M. Mittleman, S. Hunsche, L. Boivin, and M. C. Nuss, Opt. Lett. 22, 904 (1997).

[39]   J.O'Hara and D. Grischkowsky, "Synthetic phased-array terahertz imaging," Opt. Lett. 27, 1070 (2002).

[40]   J. O'Hara and D. Grischkowsky, "Quasi-optic synthetic phased-array terahertz imaging," J. Opt. Soc. Am. B 21, 1178-1191 2004.

[41]   John F. Federici, Brian Schulkin, Feng Huang, Dale Gary, Robert Barat, Filipe Oliveira, and David Zimdars, 'THz Imaging and Sensing for Security Applications - Explosives, Weapons, and Drugs," Semiconductor Science and Technology (in press).

[42]   J. F. Federici, D. Gary, R. Barat, D. Zimdars, "Terahertz imaging using an interferometric array," (to be published) Proc. SPIE 5790, (2005).

[43]   K. P. Walsh, B. Schulkin, D. Gary, J. F. Federici, R. Barat, D. Zimdars, 'Terahertz near-field interferometric and synthetic aperture imaging," Proc. SPIE 5411, (2004).

[44]   J. F. Federici, D. Gary, B. Schulkin, F. Huang, H. Altan, R. Barat, and D. Zimdars, "Terahertz imaging using an interferometric array," Appl. Phys. Lett. 83, 2477 (2003).

[45]   R. Thompson, J. M. Moran, and G. W. Swenson, "Interferomtetry and Synthesis in Radio Astronomy," 2nd Edition, Wiley Interscience, NY 2001.

[46]   T. Yuan, H. Liu, J. Xu, F. Al-Douseri, Y. Hu, and X. Zhang, Proceedings of SPIE 5070, 28 (2003).

[47]   B. B. Hu and M. C. Nuss, "Imaging with terahertz waves," Opt. Lett. 20, 1716 (1995).

[48]   B. S. Ferguson, S. H. Wang, D. Gray, D. Abbort and X.-C. Zhang, "T-ray computed tomography," Opt Lett., 27, 1312 (2002).

[49]   K. McClatchey, M.T. Reiten and R.A. Cheville, "Time resolved synthetic aperture terahertz impulse imaging," Appl. Phys. Lett., 79, 4485 (2001).

[50]   T. Dorney, W. W. Symes, R. G. Baraniuk and D. Mittleman, "Terahertz multistatic reflection imaging," J. Opt. Soc. Am. A, 19, 1432 (2002).

[51]   Jason C. Dickinson, Thomas M. Goyette, Andrew J. Gatesman, Cecil S. Joseph, Zachary G. Root, Robert H. Giles, Jerry Waldman, and William E. Nixon, "Terahertz imaging of subjects with concealed weapons," Proceedings of SPIE 2006, Terahertz for Military and Security Applications IV volume 6212.

[52] Jason C. Dickinson, Thomas M. Goyette, Jerry Waldman, "High Resolution Imaging using 325GHz and 1.5THz Transceivers," in Session 9: Systems, G. Narayananan, Editor, Proceedings of the Fifteenth International Symposium on Space Terahertz Technology (STT2004), 373-380, 2004.

[53] Hua Zhong, Nick Karpowicz, Jason Partridge, Xu Xie, Jingzhou Xu and X. -C. Zhang, "Terahertz Wave Imaging for Landmine Detection," Proceedings of the SPIE, Volume 5411, pp. 33-44 (2004).

[54] Colin Baker, William R. Tribe, Bryan E. Cole, Michael C. Kemp, "Developments in people screening using terahertz technology," Proceedings of the SPIE, Volume 5616, pp. 61-68 (2004)

[55] Colin Baker; William R. Tribe; Thomas Lo; Bryan E. Cole; Simon Chandler; Michael C. Kemp, "People screening using terahertz technology," Proceedings of the SPIE, Volume 5790, (2005)

[56] Michael C. Kemp; Antony Glauser; Colin Baker, "Recent developments in people screening using terahertz technology: seeing the world through terahertz eyes," Proceedings of the SPIE, Volume 6212, (2006)

[57] M. C. Kemp, P. F. Taday, B. E. Cole, J. A. Cluff, A. J. Fitzgerald and W. R. Tribe," Security applications of terahertz technology," in Terahertz for Military and Security Applications, R. J. Hwu and D. L. Woolard, eds, Proc. SPIE 5070, 44-52 (2003).

[58] Y. Chen, H. Liu, Y. Deng, D. Veksler, M. Shur, X. -C. Zhang, D. Schauki, M. J. Fitch and R. Osiander, "Spectroscopic characterization of explosives in the far infrared region," in Terahertz for Military and Security Applications II, R. J. Hwu and D. L. Woolard, eds, Proc. SPIE 5411, 1-8 (2004).

[59] K. Yamamoto, M. Yamaguchi, F. Miyamaru, M. Tani, M. Hangyo, T. Ikeda, A. Matsushita, K. Koide, M. Tatsuno and Y. Minami, "Noninvasive inspection of C-4 explosive in mails by terahertz time-domain spectroscopy," Jpn. J. Appl. Phys. 43, 414-417 (2004).

[60] F. Huang, B. Schulkin, H. Altan; J. F. Federici, D. Gary, R. Barat, D. Zimdars, M. Chen and D. B. Tanner, "Terahertz study of 1,3,5-trinitro-s-triazine by time-domain and Fourier transform infrared spectroscopy," Appl. Phys. Lett. 85, 5535-5537 (2004).

[61] William R. Tribe, David A. Newnham, Philip F. Taday, and Michael C. Kemp, "Hidden object detection: security applications of terahertz technology," Proceedings of SPIE Volume 5354

[62] Cook D J, Decker B K, Maislin G and Allen M G " Through container THz sensing: applications for explosive screening," 2004 Proc. SPIE 5354 55

[63] Fitch M J, Schauki D, Kelly C A and Osiander R, "Terahertz imaging and spectroscopy for landmine detection," 2004 Proc. SPIE 5354 45

[64] Osiander R, Miragliotta J A, Jiang Z, Xu J and Zhang X C, "Mine field detection and identification using THz spectroscopic imaging," 2003 Proc. SPIE 5070

[65] Huang F, Schulkin B, Altan H, Federici J, Gary D, Barat R, Zimdars D, Chen M, Tanner D B, "Terahertz study of 1,3,5-trinitro-s-triazine (RDX) by time domain spectroscopy and FTIR," 2003 Appl. Phys. Lett. 83 2477

[66] Campbell M B and Heilweil E J, "Noninvasive detection of weapons of mass destruction using THz radiation," 2003 Proc. SPIE 5070 38

[67] Yunqing Chen, Haibo Liu, Michel J. Fitch, Robert Osiander, James B. Spicer, Michael Shur, X.-C. Zhang, "THz Diffuse Reflectance Spectra of Selected Explosives and Related Compounds," 2005 Proceedings of SPIE Vol. 5790

[68] Ferguson B and Abbott. D,"Wavelet De-noising of optical terahertz pulse imaging data," Journal of Fluctuation and Noise Letters, 1(2), pp L65-L 69.

[69] Dorney. T. D, Baraniuk.R.G and Mittleman.D.M, "Material parameter estimation with terahertz time domain spectroscopy," 2001 Journal of the Optical Society of America: 18(7), pp 1562-1571.

[70] Hadjiloucas. S, Galvao.R.K.H and Bowen.J.W, "Analysis os spectroscopic measurements of leaf water content at terahertz frequencies using linear transforms," 2002, Journal of the Optical Society of America:(Optics & Vision), 19(12), pp 2495-2509.

[71] Bradley Ferguson and Derek Abbot, "Signal Processing for T-ray Biosensor Syatems," 2000, Proceedings of SPIE Smart Electronics and MEMS II, vol 4236, pp 157-169.

[72] Heinz Daniel C., Student Member, IEEE, and Chang Chein-I, Senior Member, IEEE. 2001 "Fully Constrained Least Squares Linear Spectral Mixture Analysis Method for Material Quantification in Hyperspectral Imagery," IEEE Transactions On Geoscience And Remote Sensing, Vol. 39, No. 3, March 2001

[73] Almeida T. I. R. and De Souza C. R. Filho 2004 "Principal component analysis applied to feature-oriented band ratios of hyperspectral data: a tool for vegetation studies," INT. J. Remote Sensing, 20 November, 2004, Vol. 25, No. 22, 5005–5023

[74] Hyvärinen Aapo and Oja Erkki. 2000 "Independent Component Analysis: Algorithms and Applications," Neural Networks, 13(4-5):411-430, 2000

[75] Hyvarinen Aapo and Oja Erkki, 1997 "A Fast Fixed Point Algorithm for Independent Component Analysis," Helsinki University of Technology, Neural Computations 9:1483-1492, 1997.

[76] Jos´e M. P. Nascimento, Student Member, IEEE, and Jos´e M. B. Dias, Member, IEEE. 2000 "Does Independent Component Analysis Play a Role in Unmixing Hyperspectral Data?," Project POSI/34071/CPS/2000.

[77] Keshava Nirmal. 2003 "A Survey of Spectral Unmixing Algorithms," Volume 14, Number 1, 2003 Lincoln Laboratory Journal.

[78] Bayliss Jessica, Gualtieri Anthony J, Cromp Robert F. 1998 "Analyzing Hyperspectral data with Independent Component Analysis," Proc. SPIE, vol. 3240, pp. 133-143 , 1998

[79] Hsuan Ren, Member, IEEE National Central University Taiwan CHEIN-I CHANG, Senior Member, IEEE University of Maryland Baltimore County. 2003 "Automatic Spectral Target Recognition in Hyperspectral Imagery," IEEE Log No. T-AES/39/4/821711 October 4, 2003.

[80] Chein-I Chang, Senior Member IEEE, Clark Brumbley. 1997 "Kalman Filterinlg Approach to Multispectral/Hyperspectral Image Classification," IEEE Log NO. T-AES/35/1/01509. November 22, 1997.

[81] Chein-I Chang, Senior Member, IEEE, and Clark M. Brumbley. 1999 "A Kalman Filtering Approach to Multispectral Image Classification and Detection of Changes in Signature Abundance," IEEE TRANSACTIONS ON GEOSCIENCE AND REMOTE SENSING, VOL. 37, NO. 1, JANUARY 1999

[82] Wei Lu, Jagath C. Rajapakse "ICA with Reference," Neurocomputing 69 (2006) 2244–2257

[83] Wei Lu, Jagath C. Rajapakse "Eliminating indeterminacy in ICA," Neurocomputing 50 (2003) 271 – 290

[84] Wei Lu, Jagath C. Rajapakse "Approach and Applications of Constrained ICA," IEEE Transactions On Neural Networks, Vol. 16, No. 1, January 2005

[85] Theodore F. Elbert "Estimation and Control of Systems," Appendix B: Optimization Theory (pages 563-606)

[86] D. P. Bertsekas, "Constrained Optimization and Lagrange Multiplier Methods," New York: Academic, 1982.

VITA

      Amit Shah was born on April 1th, 1982 in Mumbai, India. He graduated from R. Ruia Junior College, Mumbai, India in May 2000. He did his undergraduate degree in Electronics and Telecommunications from St. Francis Institute of Technology in Mumbai University. He graduated with a Bachelor of Engineering in Electronics and Telecommunications in May 2004. He enrolled for his master's in Computer Engineering at University of Missouri – Rolla in August 2005. He received his Master of Science degree in Computer Engineering in December 2007.